

# **A CRACK DETECTION AND DIAGNOSIS METHODOLOGY FOR AUTOMATED PAVEMENT CONDITION EVALUATION**

A Ph.D. Dissertation  
Presented to  
The Academic Faculty

By

Chenglong Jiang

In Partial Fulfillment  
Of the Requirements for the Degree  
Doctor of Philosophy in the  
School of Civil and Environmental Engineering

Georgia Institute of Technology  
August 2015

Copyright © 2015 by Chenglong Jiang

# **A CRACK DETECTION AND DIAGNOSIS METHODOLOGY FOR AUTOMATED PAVEMENT CONDITION EVALUATION**

Approved by:

Dr. Yi-Chang Tsai, Advisor  
School of Civil and Environmental  
Engineering  
*Georgia Institute of Technology*

Dr. James Lai  
School of Civil and Environmental  
Engineering  
*Georgia Institute of Technology*

Dr. Zhaohua Wang  
College of Architecture  
*Georgia Institute of Technology*

Dr. Adjo A. Amekudzi-Kennedy  
School of Civil and Environmental  
Engineering  
*Georgia Institute of Technology*

Dr. Michael D. Meyer  
Private Company

Dr. Anthony J. Yezzi  
School of Electrical and Computer  
Engineering  
*Georgia Institute of Technology*

Date Approved: June 5<sup>th</sup>, 2015

*To my mom and dad,  
for their constant well-wishing and unconditional love.  
I love you dearly!*

## ACKNOWLEDGEMENTS

I would like to express my deepest gratitude to my advisor, Dr. Yi-Chang Tsai. His constant support, continuous encouragement, and invaluable guidance has made this journey not only possible but enjoyable. I am deeply in debt to him for the time and effort he has dedicated to mentoring my research.

I would also like express my appreciation to Dr. Adjo Amekudzi-Kennedy, Dr. James Lai, Dr. Michael Meyer, Dr. Zhaohua Wang, and Dr. Anthony Yezzi for serving as my committee members and providing feedbacks on this dissertation, especially to Dr. Zhaohua Wang, whose patient help and insightful guidance are greatly appreciated.

I have been fortunate enough to be in an excellent research group. I would like to express my thanks to all my colleagues for their company and help, Chengbo Ai, Chieh Wang, YiChing Wu, Feng Li, Yipu Zhao, Zhengbo Li, Jinqi Fang, Bruno PopStefanov, Arnaud Golinviaux, Josephine Simon, Daniel Luh, Zach Lewis and Yuchun Huang.

I will always be grateful to my family and friends, who have always been there whenever needed. This would not have been possible without their support and encouragement.

## TABLE OF CONTENTS

ACKNOWLEDGEMENTS .....	iv
LIST OF TABLES .....	ix
LIST OF FIGURES .....	x
SUMMARY .....	xv
CHAPTER 1. INTRODUCTION .....	1
1.1 Background .....	1
1.2 Research Objective.....	3
1.3 Proposal Organization .....	4
CHAPTER 2. LITERATURE REVIEW .....	5
2.1 Major Research in the Field .....	5
2.2 Development of Data Acquisition Techniques .....	8
2.3 Literature Review on Crack Detection.....	12
2.3.1 Major Crack Detection Methods.....	12
2.3.2 Performance Evaluation.....	20
2.3.3 Summary .....	21
2.4 Literature Review on Crack Classification .....	23
2.4.1 Crack Definitions in Federal and State Agency’s Protocols.....	24
2.4.2 Automatic Classification Outcomes .....	27
2.4.3 Physical Crack Characteristics for Classification .....	28
2.4.4 Common Methods for Feature Interpretation .....	29
2.4.5 Performance Evaluation.....	31

2.4.6 Summary .....	32
CHAPTER 3. PROPOSED ALGORITHM FOR CRACK DETECTION .....	34
3.1 Proposed Algorithm for Automatic Crack Detection on Pavement Images .....	34
3.1.1 Algorithm Flowchart.....	34
3.1.2 Image Enhancement through Non-Crack Feature Removal and Profile Rectification .....	36
3.1.3 Crack Potential Map Generation through Adaptive Thresholding and Tensor Voting .....	39
3.1.4 Key Point Identification through Iterative Morphological Thinning and Skeleton Analysis.....	43
3.1.5 Crack Curve Detection Using Minimal Path .....	45
3.1.6 Curve Selection through Statistical Analysis.....	47
3.2 Demonstration of the Proposed Algorithm .....	50
CHAPTER 4. PERFORMANCE EVALUATION OF THE PROPOSED ALGORITHM FOR CRACK DETECTION.....	58
4.1 Demonstration on Synthetic Images .....	58
4.2 Accuracy Evaluation on Real Pavement Images.....	60
4.2.1 Buffered Hausdorff Distance Scoring Method .....	60
4.2.2 Existing Crack Detection Algorithms for Benchmarking.....	62
4.2.3 Performance Evaluation on Different Pavement Surface Textures .....	64
4.2.4 Performance Evaluation on Different Crack Patterns.....	74
4.3 Repeatability Test.....	84

CHAPTER 5. PROPOSED FRAMEWORK FOR PAVEMENT CRACK DIAGNOSIS .....	90
5.1 Overview of the Pavement Crack Diagnosis Framework .....	91
5.2 Multi-scale Crack Representation Using Crack Fundamental Element .....	93
5.2.1 Crack Fundamental Element .....	93
5.2.2 Multi-Scale Topological Crack Representation .....	95
5.3 Crack Classification on AASHTO Provisional Standard PP 67 .....	98
5.4 Crack Classification on GDOT PACES Protocol .....	104
5.4.1 Algorithm Flowchart .....	106
5.4.2 Experimental Tests .....	109
5.4.3 Full-Coverage Pavement Crack Survey .....	116
5.5 Crack Deterioration Analysis: A Pilot Study in Real-world Environment .....	119
CHAPTER 6. CONCLUSIONS AND RECOMMENDATIONS .....	132
6.1 Contributions .....	133
6.2 Findings .....	135
6.3 Recommendations for Future Work .....	140
APPENDIX A. MINIMAL PATH AND ITS APPLICATION ON PAVEMENT CRACK DETECTION .....	143
A.1 Background .....	143
A.2 Theory of Minimal Path Techniques .....	145
A.3 Preliminary Investigation on Crack Detection .....	149
APPENDIX B. TENSOR VOTING AND ITS APPLICATION ON PAVEMENT IMAGES .....	152

B.1	Background .....	152
B.2	Theory of the Tensor Voting Framework .....	154
B.2.1	2D Tensor Representation.....	154
B.2.2	Voting Process .....	156
B.3	Preliminary Investigation on Pavement Images .....	158
APPENDIX C. PROFILE-BASED CRACK WIDTH MEASUREMENT .....		160
C.1	Proposed Crack Width Measurement Method .....	160
C.2	Validation on Synthetic Data .....	164
C.3	Validation through Lab Tests .....	167
REFERENCES .....		169



## LIST OF TABLES

Table 2.1 Comparison between local-based and global-based crack detection.....	19
Table 4.1 Accuracy scores on different pavement surface textures.....	66
Table 4.2 Accuracy scores on different crack patterns .....	76
Table 4.3 Computation time on different crack patterns (unit: second) .....	83
Table 5.1 Data reporting for the example in Figure 5.6.....	102
Table 5.2 Data reporting for the example in Figure 5.7.....	103
Table 5.3 Crack properties extracted from wheelpath and central bands .....	107
Table 5.4 Performance of load cracking classification.....	110
Table 5.5 Performance of B/T cracking classification.....	112
Table 5.6. Site comparison on SR 236 and SR 275 .....	115
Table C.1 Performance of crack width measurement on synthetic data (unit: mm).....	166
Table C.2 Performance of crack width measurement in lab test .....	168

## LIST OF FIGURES

Figure 2.1 Illustration of INO/Pavemetrics LCMS (Laurent et al. 2008).....	11
Figure 2.2 Illustration of load cracking and B/T cracking at different severity levels .....	26
Figure 3.1 Proposed algorithm for automatic crack detection .....	35
Figure 3.2 Example of profile rectification on one transverse profile .....	38
Figure 3.3 Comparison between original range image and rectified range image .....	39
Figure 3.4 Illustration of crack potential map generation .....	42
Figure 3.5 Illustration of crack skeleton extraction .....	44
Figure 3.6 Low contrast nature of pavement images and gamma correction .....	46
Figure 3.7 Crack curve detection using minimal path procedure .....	47
Figure 3.8 Mean and STD of the pixel values along the detected crack curves .....	49
Figure 3.9 Illustration of crack curve selection to remove false positive detections .....	49
Figure 3.10 Algorithm demonstration on Sample Image 1 .....	53
Figure 3.11 Algorithm demonstration on Sample Image 2 .....	54
Figure 3.12 Algorithm demonstration on Sample Image 3 .....	55
Figure 3.13 Algorithm demonstration on Sample Image 4 .....	56
Figure 3.14 Algorithm demonstration on Sample Image 5 .....	57
Figure 4.1 Performance demonstration on synthetic images .....	59
Figure 4.2 Illustration of buffered Hausdorff distance (Kaul et al. 2009) .....	61
Figure 4.3 Performance on asphalt dense graded surface (Image No. 5) (a) range image (b) ground truth crack map (c) proposed algorithm (d) minimal path (user-input points as red dots) (e) dynamic optimization (f) LCMS software (ver. 4.1.1) .....	68

Figure 4.4 Performance on asphalt OGFC surface (Image No. 20) (a) range image (b) ground truth crack map (c) proposed algorithm (d) minimal path (user-input points as red dots) (e) dynamic optimization (f) LCMS software (ver. 4.1.1) .....	70
Figure 4.5 Performance on asphalt OGFC surface (Image No. 11) (a) range image (b) ground truth crack map (c) proposed algorithm (d) minimal path (user-input points as red dots) (e) dynamic optimization (f) LCMS software (ver. 4.1.1) .....	71
Figure 4.6 Performance on concrete surface (Image No. 27) (a) range image (b) ground truth crack map (c) proposed algorithm (d) minimal path (user-input points as red dots) (e) dynamic optimization (f) LCMS software (ver. 4.1.1).....	73
Figure 4.7 Performance on longitudinal cracking (Image No. 39) (a) range image (b) ground truth crack map (c) proposed algorithm (d) minimal path (user-input points as red dots) (e) dynamic optimization (f) LCMS software (ver. 4.1.1) .....	77
Figure 4.8 Performance on transverse cracking (Image No. 43) (a) range image (b) ground truth crack map (c) proposed algorithm (d) minimal path (user-input points as red dots) (e) dynamic optimization (f) LCMS software (ver. 4.1.1).....	78
Figure 4.9 Performance on the combination of longitudinal and transverse cracking (Image No. 48) (a) range image (b) ground truth crack map (c) proposed algorithm (d) minimal path (user-input points as red dots) (e) dynamic optimization (f) LCMS software (ver. 4.1.1) .....	80
Figure 4.10 Performance on alligator cracking (Image No. 53) (a) range image (b) ground truth crack map (c) proposed algorithm (d) minimal path (user-input points as red dots) (e) dynamic optimization (f) LCMS software (ver. 4.1.1).....	81
Figure 4.11 Selected sections for repeatability test .....	86

Figure 4.12 Crack length statistics in five different runs collected on Section 1 .....	87
Figure 4.13 Crack length statistics in five different runs collected on Section 2 .....	88
Figure 4.14 Crack map comparison on the highlighted location on the second section between Run 4 and Run 5 .....	88
Figure 4.15 Similarity scores between the detected crack maps in five different runs ....	89
Figure 5.1 Objectives of pavement crack diagnosis in this study .....	93
Figure 5.2 Illustrations of a crack fundamental elements at initial scale (Tsai et al. 2014) .....	95
Figure 5.3 Multi-scale crack properties from CFE model (Tsai et al. 2014) .....	96
Figure 5.4 Illustration of five measurement zones on a typical 12-ft. road lane .....	99
Figure 5.5 Definition of “a crack” in AASHTO PP 67 .....	101
Figure 5.6 Crack classification based on AASHTO PP67 – Example 1      Longitudinal Cracks — Transverse Crack — Pattern Crack — .....	102
Figure 5.7 Crack classification based on AASHTO PP67 – Example 2      Longitudinal Cracks — Transverse Crack — Pattern Crack — .....	103
Figure 5.8 Examples of PACES crack distresses on actual pavements .....	105
Figure 5.9 Flowchart of automatic crack type and severity level classification for load cracking and B/T cracking (Tsai et al. 2014) .....	106
Figure 5.10 Selected project for crack classification evaluation on GA State Route 236 .....	109
Figure 5.11 Representative load cracking evaluation outcomes, from left to right: range image, crack map on intensity image, load cracking — and B/T cracking —, and evaluation outcomes .....	112



Figure 5.12 Representative B/T cracking evaluation outcomes, from left to right: range image, crack map on intensity image, load cracking  and B/T cracking  , and evaluation outcomes.....	113
Figure 5.13 Crack survey results for all 52 100-ft. sections within one-mile segment following GDOT survey practice.....	118
Figure 5.14 Selected project for crack deterioration analysis on GA State Route 26 ....	119
Figure 5.15 Crack condition comparison on the one-mile segment between Dec. 6, 2011 and Dec. 7, 2013 .....	121
Figure 5.16 Change in total crack length across five different timestamps on the selected 200-ft. section near Milepoint 7.5.....	123
Figure 5.17 Comparison between crack deterioration along longitudinal and other directions on the selected 200-ft. section near Milepoint 7.5 .....	123
Figure 5.18 Illustration of crack deterioration along longitudinal direction on the selected section near Milepoint 7.5.....	124
Figure 5.19 Illustration of crack deterioration along transverse direction.....	125
Figure 5.20 Change in number of crack intersections across five different timestamps on the selected 200-ft. section near Milepoint 7.5 .....	126
Figure 5.21 Illustration of crack branching-out (crack intersections are marked as yellow dots).....	127
Figure 5.22 Change in number of crack polygons across five different timestamps on the selected 200-ft. section near Milepoint 7.5 .....	128
Figure 5.23 Illustration of forming crack polygons .....	129

Figure A.1 Preliminary evaluation of minimal path techniques on pavement crack detection .....	151
Figure B.1 Illustration of 2D tensor and tensor decomposition.....	155
Figure B.2 Illustration of the voting process .....	157
Figure B.3 Examples of tensor voting on the pavement cracks (left: input; right: output) .....	159
Figure C.1 Illustration of the proposed crack width measurement method.....	161
Figure C.2 Example of measuring crack width from transverse profiles .....	162
Figure C.3 Illustration of angle adjustment .....	164
Figure C.4 Examples of synthetic data, including different combinations of crack width and orientation: (a) 2 mm and 90 degrees, (b) 5 mm and 40 degrees, (c) 10 mm and 70 degrees, and (d) 20 mm and 10 degrees.....	165
Figure C.5 Illustration of the experimental setup .....	167
Figure C.6 Example image of the collected lab data .....	168

## SUMMARY

Pavement cracks are one of the most common pavement surface distresses. Traditionally, pavement crack evaluation is conducted manually through a human field survey, which is subjective, labor-intensive, time-consuming, and dangerous to field engineers in the hazardous roadway environment. Methods have been developed to automate this process, including both crack detection and classification. However, none of these methods have been fully automated and implemented.

For crack detection, the active contour based minimal path procedure has demonstrated better performance than other existing algorithms; however, it mathematically requires one or more prior input points for each crack curve and cannot be fully automated, which introduces tedious and subjective manual work in practical use, especially for high-density cracks. In this study, a crack detection algorithm to detect accurate and continuous crack curves in a fully automatic manner is proposed. It consists of five major steps: 1) image enhancement through non-crack feature removal and profile rectification, 2) crack potential map generation through adaptive thresholding and tensor voting, 3) key point identification through iterative morphological thinning and skeleton analysis, 4) crack curve detection between neighboring key points using two-point minimal path procedure, and 5) crack curve selection through statistical analysis to remove false positive artifacts. The proposed algorithm has demonstrated its robust performance with a diverse data set, including the different pavement surface types (asphalt dense graded surface, asphalt open graded friction course surface, and concrete surface), and the different crack patterns (longitudinal, transverse, the combination of

both, and alligator). Also, the proposed algorithm has outperformed the dynamic optimization algorithm, which has had the best accuracy as an automatic algorithm in pertinent literature, and the commonly used commercial crack detection software.

For crack classification, although methods have been developed to classify the primitive crack types (e.g. longitudinal and transverse cracks), it remains a challenge to classify the complicated, real-world crack types and severity levels specified by transportation agencies. In this study, a generalized crack diagnosis framework is proposed to transform detected crack maps into meaningful decision-support information valuable to engineers. The proposed framework features a multi-scale crack representation based on a crack fundamental element model, which extracts rich properties from the detected crack maps, and a supervised classifier calibrated with real pavement data, which interprets the extracted crack properties into crack types and severity levels can be flexibly applied to different distress protocols. The proposed framework has been implemented with real-world distress protocols, including AASHTO standard PP 67 and GDOT's PACES protocol. Experienced pavement engineers have compared the results against manual surveys. The proposed framework has demonstrated over 90 percent crack classification and quantification accuracy.

Overall, the proposed crack detection and diagnosis methodology has made significant progress in developing an automated pavement crack evaluation method.



# **CHAPTER 1. INTRODUCTION**

## **1.1 Background**

According to the American Society of Civil Engineers' (ASCE) report card for America's infrastructure, the United States spends \$91 billion per year to maintain highways; however, the expenditure is well below the estimated \$170 billion needed annually between 2008 to 2028 to substantially improve the nation's highway system (ASCE 2013). To maintain the functionality of the highway network under constrained resources, it is crucial to develop performance-based investment strategies that will ensure that available resources are directed to those projects with the highest performance return on investment. The Moving Ahead for Progress in the 21st Century Act (MAP-21) features a new federal emphasis on performance measures of infrastructure condition. As a major component of highway infrastructure, pavement surface condition assessment becomes critical for making data-driven, informed decisions on cost-effective transportation infrastructure management.

Pavement cracks are one of the most common pavement surface distresses. They are caused by constant overloading, asphalt aging, environmental impacts, and improper structural design, etc. Cracking can weaken pavements and lead to gradual structural failure because it allows water and other foreign objects into the base and accelerates the base deterioration. The proper treatment of pavement cracks at the optimal timing is important for cost-effective pavement maintenance. The importance of pavement cracks in surface condition assessment has been recognized by federal and state agencies. The Federal Highway Administration (FHWA) requires state departments of transportation (DOTs) to report pavement crack data as part of their annual pavement condition data

through the Highway Performance Monitoring System (FHWA 2013). The American Association of State Highway and Transportation Officials' (AASHTO) standing committee for performance management suggests using pavement cracks as one of the pavement performance measures to fulfill the requirements of MAP-21 (AASHTO 2013). State agencies also put significant emphasis on pavement cracks through their pavement condition surveys. Ninety-four percent of all state DOTs monitor cracking data for the National Highway System (NHS) (FHWA 2015). In Georgia DOT's (GDOT) statewide survey for fiscal year 2013, over 80% of the surveyed segments (approximately 1 mile for each segment) on the state highway system had cracking-related distresses.

Traditionally, pavement crack evaluation has been conducted manually through human field surveys. However, this manual survey method has poor repeatability and reproducibility, needs excessive time, consumes great amounts of labor, and puts surveyors in hazardous situations (Goodman 2001). The data collected may vary with different raters due to subjectivity. A study investigated the variability of manual distress data surveyed by seven credit Long-Term Pavement Performance (LTPP) distress raters (Rada et al. 1997). This study found that for any combination of distress types and severity levels, the individual rater variability was large. Lee and Kim (2006) found that for a procedure that involves distress drawing and mapping on a grid paper, the average relative bias between three individual raters were 43, 45, and 41 percent for longitudinal, transverse, and block cracks respectively. In addition, the FHWA (2015) published a Notice of Proposed Rulemaking (NPRM) in the Federal Register to propose performance management regulations related to pavement condition assessment as required by the

MAP-21. This legislation requires state DOTs to collect data on the full extent of Interstate System; this is extremely difficult to accomplish through manual surveys.

To overcome the shortcomings of manual surveys, there have been substantial research efforts to develop automated pavement crack evaluation methods (Tighe et al. 2008). Both the automation equipment for data acquisition and the methods for data analysis have been developed over the past two decades. However, unlike IRI or rutting, whose measurement procedures are clearly defined, crack identification and evaluation usually involve human interpretation of complex crack patterns and are difficult to accomplish fully automatically. Researchers have still had difficulty accurately and reliably extracting useful crack information from sensor data.

## **1.2 Research Objective**

The objective of this study is to develop a methodology for automatic pavement crack detection and diagnosis that utilizes emerging sensing technology to improve the accuracy and reliability of pavement crack evaluation in support of data-driven pavement management decision-making. The outcomes of the proposed methodology will play a key role in advancing state DOTs' existing pavement condition assessment practices. To be specific, the research objectives are to:

- **Develop an accurate and robust algorithm for crack detection.** A fully automatic crack detection algorithm is proposed based on the minimal path procedure with no prior requirements on user inputs. The proposed algorithm is able to detect continuous crack curves and preserve the high-level topological information of the crack pattern, which are critical inputs for the subsequent crack

condition analysis, including automatic crack type and severity level classification.

- **Develop a generalized framework for crack diagnosis to transform the detected crack maps into decision support information.** The framework includes 1) a multi-scale crack representation based on a crack fundamental element (CFE) model to extract meaningful crack properties from the detected crack maps, and 2) an automatic crack classification and quantification method with the focus on real-world pavement distress protocols. In addition, it explores the feasibility of representing and quantifying crack deterioration behaviors on real pavements. The proposed crack diagnosis framework will deliver information that can directly benefit DOTs' current pavement management practices and enhance their decision-making capabilities.

### **1.3 Proposal Organization**

Chapter 1 presents background information on pavement surface condition assessment and crack evaluation, and identifies the research objectives. Chapter 2 presents a literature review of current practices and existing studies in the field. Chapter 3 presents the proposed algorithm for pavement crack detection, followed by a comprehensive evaluation in Chapter 4. Chapter 5 presents the proposed generalized framework for pavement crack diagnosis to transform the detected crack maps into decision support information. Finally, Chapter 6 concludes the study and identifies the contributions.

## **CHAPTER 2. LITERATURE REVIEW**

### **2.1 Major Research in the Field**

As early as 1990, Haas and Hendrickson (1990) presented a general model of pavement surface characteristics that integrated several types of sensor information to explain the concept of automated pavement distress surveys. During the 1990s, the research from Haas's group mainly focused on semi-automated and automated crack sealing. Haas (1996) reviewed the overall development of automated crack sealing techniques and discussed the economic feasibility of crack sealing. As an important step in automated crack sealing, a path-planning algorithm was developed with the assumption that a crack map had been generated already (Kim et al. 1998). Later, a semi-automated crack sealing model (Kim and Haas 2002) presented a man-machine balanced crack mapping and representation process for a road maintenance machine. Overall, their system still required a human operator to manually draw the complete crack map on the image. Although a line-snapping algorithm was used to reduce the human hand-eye coordination errors, the proposed system didn't achieve full automation, which limited the practical implementation. After 2000, Haas's research focus has shifted to the application of range data on infrastructure condition assessment and construction management, including stereo vision technique on pavement surface reconstruction (Ahmed and Haas 2010). The stereo vision technique provided a cheap alternative for collecting 3D pavement surface data, but the precision of the system hasn't been validated.

Since the mid-1990s, Cheng (from Utah State University) started the research with Utah DOT on automated real-time pavement distress analysis using intensity

images. At the beginning, they proposed a pavement crack detection and classification algorithm based on a new data structure to store the skeleton and geometry of cracks (Cheng and Miyojim 1998), but the computation speed was slow and failed to fulfill the objective of real-time processing. They further introduced fuzzy logic (Cheng et al. 1999) and multi-stage processing (Cheng et al. 1999) to improve the computation efficiency. This was one of the earliest real-time systems that have been developed for automated pavement distress analysis. Later, they also explored the application of neural networks (Cheng et al. 2001) and adaptive thresholding (Cheng et al. 2003) on crack detection. The performance of the crack detection was limited by the poor image quality. Furthermore, the crack detection outcomes were disconnected blobs without topological crack pattern information, which was inconvenient for DOTs to use practically in determining the crack type and severity levels.

Wang et al., as a research team from the Oklahoma State University, also developed an automated real-time pavement survey system in the early 2000s. Wang's research team (Wang 2000; Wang and Gong 2002; Wang and Gong 2005) introduced a new automated system capable of collecting and analyzing pavement surface distresses, primarily cracks, in real-time. It featured the use of a high-resolution digital camera and the corresponding image processing algorithms and multi-CPU based parallel computing. Although the system resolution increased dramatically, the crack detection with 2D intensity images was still sensitive to different lighting conditions, shadows, and oil stains on the pavement surface, etc. Realizing these limitations, they started to explore the feasibility of collecting the 3D data of pavement surfaces. Wang et al. started with the stereovision based approach for 3D reconstruction (Hou et al. 2007), for which the

precision of depth measurement was a primary concern. They then switched to a high-resolution line laser imaging technique (Wang 2011), and their data acquisition system is now commercially available. In the meantime, their research team also worked on the development of crack detection algorithms (Wang et al. 2007; Zhang et al. 2013).

Lee (from the University of Iowa) is also one of the earliest researchers in the field of automated distress measurement. Since the early-1990s, he started to work on the standardization of network-level distress measurement (Lee 1992) and explored thresholding-based crack detection (Lee and Oshima 1994). Lee and Lee (Lee and Lee 2004; Lee and Lee 2010) presented one representative study of utilizing neural networks in crack detection and classification. Many other researchers (Bray et al. 2006; Nejad and Zakeri 2011; Salari and Bao 2011) were inspired by their work. However, their studies mostly classify cracks into primitive types, such as longitudinal, transverse, and diagonal cracking, etc., which cannot directly benefit a DOT's decision-making process, since more complicated crack types and severity levels are defined in practical use. Later, Lee developed the crack type index for crack classification (Lee and Kim 2005) and is currently working on promoting it as one of the crack-related standards for the American Society for Testing and Materials (ASTM).

Tsai et al. (from the Georgia Institute of Technology) is one of the active research groups in the field of automated pavement distress analysis. They developed a new performance measure to quantitatively evaluate the accuracy of crack detection (Kaul et al. 2009) and assessed the performance of six existing crack detection methods (Tsai et al. 2010). They are also one of the earliest research teams to assess the performance of using the 3D line laser imaging technique for pavement crack analysis (Tsai and Li

2012). In recent years, they have been actively working on the development of crack detection and classification algorithms (Huang and Tsai 2011; Lettsome et al. 2012; Tsai et al. 2014; Tsai et al. 2014; Tsai et al. 2013).

Overall, despite the continuous research efforts for over the past two decades, none of these systems have been implemented by state DOTs and support their pavement maintenance decision-making in a fully automated manner. The following subsections review data acquisition techniques, crack detection, and crack classification methods separately, and identify research needs.

## **2.2 Development of Data Acquisition Techniques**

In the early 1990s, researchers mostly worked with 2D intensity pavement images on the development of crack detection algorithms. By the late 1990s, Cheng et al. (1999) had developed an automated real-time pavement data collection system that used a video camera mounted on the top of a van that traveled at 50 to 70 mph. Limited by the technology's capabilities, this system still collected 2D intensity images, and the image quality was relatively poor, having a resolution of 320 by 240. Wang and Gong (2005) developed another automated pavement survey system with better data quality; their vehicle also traveled at 100 mph in a parallel environment, and the image resolution significantly improved to 1300 by 1024 at the maximum frame rate of 15 per second. Later, the newer intensity image acquisition system collected pavement data with transverse resolution of 4096 pixels; it was capable of capturing cracks having widths of approximately 1 to 2 mm.

The 2D intensity images have been the major data format used by many studies in the past two decades. However, the limitations of 2D intensity images were discussed in



their early stages. El-Korchi et al. (1991) pointed out the importance of lighting in determining the fraction of distress that went undetected. They researched several lighting methods (controlled, natural, ambient, directional, omni-directional, single-source, and multiple-source), and revealed the limitations of 2D intensity images on distress detection: (1) different lighting conditions led to different levels of distress detection, and (2) there were low-contrast details that could not be detected by an optical system. They also pointed out that ambient light was better for crack detection than direct sunlight, and the lighting design was especially important with poor equipment and crack detection algorithms. Nazef et al. (2006) (from Florida DOT) did a comprehensive evaluation of pavement imaging systems, looking into four different factors of pavement image, including spatial resolution, brightness resolution, optical distortion, and the signal-to-noise ratio, and found that all these factors influenced the performance of distress detection. Some researchers introduced artificial lighting sources to enhance the performance of their pavement imaging systems. Xu (2005) used LED lighting as an extra lighting source; however, the beam width of the LED lighting was 0.5 inch, which was not thin enough to provide sufficient depth resolution. The Laser Road Imaging System (LRIS) from INO/Pavemetrics used high power laser line projectors and line-scan cameras to provide consistent quality under different lighting conditions, but the system cost was relatively high. Su et al. (2013) developed a dual-light inspection approach to reduce the crack detection false alarms caused by shadows. Yao et al. (2015) employed a dual-camera setup to capture and merge over-exposed and under-exposed images simultaneously to make both the sunlit and shadow areas visible.

Realizing the limitations of 2D intensity images, researchers started to explore the feasibility of collecting the 3D data of pavement surface. Hou et al. (2007) assessed the possibility of using 3D pavement stereo images for the automated crack analysis. Ahmed and Haas (2010) used a low-cost photogrammetric system to reconstruct a detailed model of a pavement surface. The accuracy of these stereo vision-based techniques hasn't been comprehensively validated; in addition, the techniques still haven't really overcome the limitations of 2D imaging systems, such as lighting conditions. Jahanshahi et al. (2013) used a RGB-D sensor, which collected additional depth information with an infrared projector, to detect and quantify road defects; however, the performance of the sensor might be seriously impacted by the outdoor environment.

With the advances in sensor technology, another 3D imaging technique has become available. Similar to LRIS, the 3D line laser imaging system also uses high-power laser lights to probe the environment and then uses a camera to look for the location of the laser dot. Depending on how far away the laser strikes a surface, the laser dot appears at different places in the camera's field of view; this technique is called triangulation. This 3D laser system has demonstrated its advantages over the traditional 2D intensity imaging system (Tsai and Li 2012). First, the 3D laser-based system is not sensitive to lighting effects when measuring the range (i.e. elevation) like other laser and light detection and ranging (LiDAR) devices. Second, noise, like oil stains, and poor intensity contrast will not interfere with the crack detection algorithms using the acquired range data. As long as there is a distinguishable elevation difference between a crack and its surrounding background, the segmentation algorithm is able to capture the crack. Increased attention has been drawn to the development of this 3D laser-based data

acquisition system and its potential applications. Researchers from Texas (Li et al. 2010) have developed a research version of the 3D laser system and have demonstrated the system's capability, but the developed system is still in the research stage. The low-resolution data collected from such a system (e.g., it collects only 200 profiles per second and has only 2mm crack depth resolution) limited the system's capability, and it didn't operate at highway speed. INO/Pavemetrics (Laurent et al. 2008) has developed a commercial system using the line laser imaging technique. This Laser Crack Measurement System (LCMS) can achieve a 0.5-mm depth resolution, collect 5600 profiles per second with 2080 points on each profile, and operate at highway speed. The illustration of this system is shown in Figure 2.1.

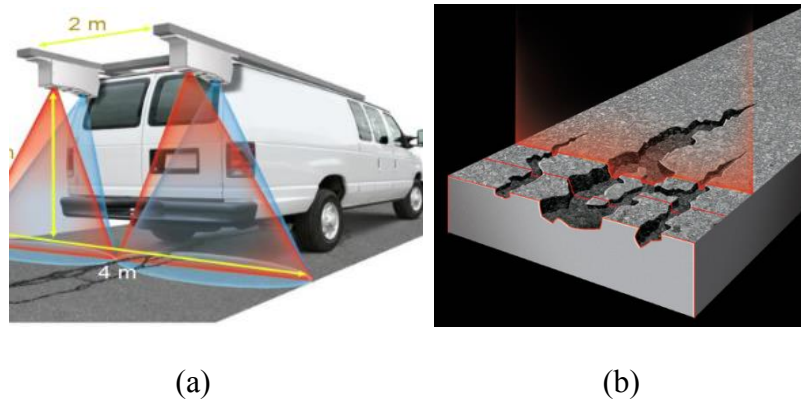


**Figure 2.1 Illustration of INO/Pavemetrics LCMS (Laurent et al. 2008)**

The 3D line laser imaging system can provide pavement range data with much better granularity, and it also has the potential to overcome the long-lasting lighting issue of reliably detecting cracks. However, this technique also has its own limitations. For example, inherent noise exists in the 3D range data; variations of the collected range values are still observed, even on a perfectly flat surface. In addition, since the system collects the range data directly, pavement conditions that lead to elevation change of the pavement surface (e.g. cross-slope, rutting, and scratches) now all become the noise in

crack detection. Overall, the application of this high-speed and high-resolution 3D line laser imaging system on crack detection is still at experimental stage. Detailed validation of the system is still needed to get a better understanding of the characteristics of 3D range data, including noise. Research is needed to develop an accurate and reliable algorithm to take advantage of this emerging technology to improve the crack detection performance.

## **2.3 Literature Review on Crack Detection**

Crack detection refers to the process of extracting objects of interest, i.e. cracks, from the background. For example, in the image-based context, the pixels in the pavement image are segmented as either crack or non-crack pixels. In the literature, this process is also referred to as crack segmentation or crack map generation, and these three terms will be used synonymously in this study. Crack detection is usually the very first step in extracting crack information from the sensor data. This section reviews the existing literature on crack detection. It categorizes and summarizes the major approaches for crack detection and also discusses the performance evaluation of crack detection accuracy from previous studies.

### **2.3.1 Major Crack Detection Methods**

Most existing crack detection algorithms are based on two primary assumptions:

- 1) Crack pixels can be distinguished from their surrounding area, since they usually have a lower intensity/range value; i.e. crack pixels are usually darker/deeper than their neighborhood;
- 2) cracks are usually continuous within a certain neighborhood; that is, crack pixels are connected with each other to form curves instead of being isolated.

These two facts hold true for both 2D intensity images and 3D range images. Starting from

these two primary assumptions, thresholding and edge detection are the two primitive crack segmentation approaches that have been used in the literature (Tsai et al. 2010).

Thresholding-based segmentation methods exploit the fact that cracks are darker/deeper than the background. Kirschke and Velinsky (1992) presented some of the earliest work on automated sensing of cracks in highway pavement using histogram and thresholding. Koutsopoulos et al. (1993) presented a comparative study of different thresholding methods, including the Otsu method, Kittler's method, a relaxation method, and a regression method. They showed that the regression-based method performed the best among these methods. To tackle the challenge of using the regression-based method in the presence of shadows, Oh et al. (1997) proposed an iterated clipping method. This method iteratively used the mean and standard deviation values to eliminate noise while preserving crack pixels. A statistical approach was presented by Koutsopoulos and Downey (1993) to reduce the influence of the imperfections of segmentation on the subsequent crack condition assessment. Instead of direct thresholding based on pixel values, Cheng et al. (1999) proposed a fuzzy logic-based method. According to their analysis, there was inherent vagueness rather than randomness in pavement crack images because of grayness and spatial ambiguity in crack images. Consequently, conventional co-occurrence methods might not work well. Instead, they used fuzzy homogeneity as the criterion, and used fuzzy homogeneity vectors and fuzzy co-occurrence matrices to handle the grayness and spatial uncertainty among pixels. In 2008, Hassani and Tehrani also used a similar fuzzy-logic based system for automatic pavement crack detection. Some researchers (Huang and Xu 2006; Lee and Lee 2004; Oliveira and Correia 2013) introduced image cells/tiles into the crack segmentation. In their studies, crack analysis

was conducted on cells (for example, regions of 8x8 pixels) and each cell was classified as a crack or non-crack cell based on the mean and standard deviation of the pixel values inside. This approach effectively reduced the isolated noises at pixel level, but the selection of cell size could be a tricky problem. In summary, the core logic of thresholding-based methods is to compare each pixel to its neighborhood: if the value of a pixel is significantly lower, then it is determined to be a crack pixel. Considering that only the neighborhood information is used to identify a crack pixel, these methods are usually computationally efficient. However, they are mostly limited in the following aspects. First, pavement images are noisy, which is caused by both the inherent sensor noises and the pavement surface texture. Cracks on the image usually have a low contrast with the pavement background. Therefore, a thresholding-based approach inevitably introduces random false detections from local minima across the image. Researchers have explored different variants of the method (e.g. fuzzy logic approach, cell-based statistical analysis) to tackle this problem; however, the fundamental issue still exists. Second, the diverse characteristics of pavement surface (e.g. different lighting conditions, shadows, oil stains, and surface textures, etc.) make it difficult to select universally applicable parameters, while the performance of the thresholding-based methods directly depends on the selection of parameters. The existing methods are mostly validated on limited datasets, but their performance for practical use on large datasets is questionable. Third, the outcomes of thresholding-based methods are usually discontinuous pixels / blobs, which are difficult to further interpret for the subsequent crack type and severity analysis.

Edge detection is another common image processing technique used for crack segmentation. Over the past 30 years, many simple but useful edge detectors have been

developed and are widely used, such as Roberts, Sobel, Prewitt, and LOG edge detectors (Davis 2005). The representative Canny edge detection (Canny 1986) optimized a performance index that favored true positive, true negative, and accurate localization of detected edges. It has been applied to pavement crack segmentation by multiple studies (Ayenu-Prah and Attoh-Okine 2008; Santhi et al. 2012). Canny's analysis, however, was restricted to a linear shift invariant filter. Motivated by the idea of Canny's edge detection algorithm, Mallat and Zhong (1992) first proposed a decimated fast bi-orthogonal wavelet transform to obtain an image edge representation by computing the local maximum of the gradient of an image. This technique has been widely applied in pavement crack segmentation because of its capability of analyzing information at multiple scales simultaneously (Cuhadar et al. 2002; Zhou et al. 2005; Zhou et al. 2006). Wang et al. (2007) used an "a trous" algorithm-based wavelet edge detection procedure for pavement distress segmentation. This algorithm was an un-decimated wavelet transform executed via a filter bank without sub-sampling. Some researchers used both wavelet and Radon transformation to enhance the crack features for segmentation (Nejad and Zakeri 2011; Zhou et al. 2005). Beamlet transformation has also been explored recently to capture the linear connectivity of cracks (Ouyang and Wang 2012; Ying and Salari 2010). Zalama et al. (2014) used Gabor filter to detect cracks along specific directions. Essentially, the edge detection approach is also a thresholding process: instead of thresholding using pixel values on the image domain directly, it first converts the image into a different domain, such as gradient domain, various frequency domains, etc., where the cracks are expected to be more distinguishable from the rest of the image. Then a thresholding is conducted to select the local minima/maxima depending on the

characteristics of the transformed domain. Clearly, the previously stated issues for thresholding-based approach still exist here. In addition, due to the anisotropic characteristic of techniques such as wavelet transformation, these approaches may not handle well the cracks with high curvature or low continuity (Zou et al. 2012).

Overall, thresholding and edge detection based crack detection belongs to local-based image processing methods, where the detection of crack pixels completely relies on the local information in a small neighborhood. Although in general cracks bear elevations that are lower than the surrounding pavement, the contrast of cracks may be seriously weakened by the background noise, such as pavement surface texture and raveling, etc., possible crack degradations, such as the width and depth change along the cracks, and foreign debris inside the cracks. As a result, local-based crack detection algorithms may have difficulty detecting the full crack curves: they usually detect a set of disconnected crack fragments with many false positives (Zou et al. 2012). Some recent studies (Huang et al. 2014; Zou et al. 2012) employed a “bottom-up” approach, such as the tensor voting framework, to fill in the gaps between disjointed detection results. However, given the nature of such an approach, it can only detect the rough skeleton of the crack pattern rather than the precise crack curves because it blurs out the area around the cracks with a similar effect as image morphological erosion and can potentially lead to the loss of crack meandering patterns at a detailed level.

In order to detect accurate and continuous crack curves, another alternative is to avoid hard decisions to determine crack pixels solely based on local information. In this study, we refer to this as a global-based approach for crack detection. The additional assumption of a global-based algorithm is that the intensity/range along a crack may not



always be lower than the surrounding pavement background. To incorporate this assumption into the detection algorithm, a potential function is first introduced, which indicates the possibility of a pixel being a crack pixel. It is noted that some intermediate results from the local-based algorithms can be used here as a crack potential function. For example, a potential function can simply be the original image, given the assumption that crack pixels are lower than the rest of the image. It can also be a representation of the image from gradient or frequency domains. Then, globally, continuous crack curves are generated by minimizing the potential along the curves. Such an approach is clearly more computationally expensive, since it formulates the crack detection task into an optimization problem. However, with the increase of computational power in recent years, it has become feasible, and more and more researchers have started to explore global-based crack detection algorithms. Alekseychuk (2006) proposed a crack segmentation algorithm based on local probability modeling and global probabilistic dynamic optimization. This algorithm was originally developed for radiography; Tsai et al. (2010) first applied it to pavement crack segmentation, and demonstrated that it outperformed many existing algorithms in terms of accuracy at the cost of computation time. Huang and Tsai (2011) used a grid cell based analysis to speed up the computation by shrinking the search space from the entire image to only the selected grids. However, its computation speed was still a major concern for large-scale pavement survey tasks, and the results sometimes suffered from extensive false positive detections, especially on pavement images with noisy backgrounds. The minimal path approach is a major category of global-based algorithms that have been explored by many studies. Some researchers (Amhaz et al. 2014; Avila et al. 2014; Nguyen et al. 2011) used minimal path

algorithm based on graph theory (e.g. Dijkstra's algorithm); however, the results suffered from digitization bias due to the metrication error and the existence of false positive detections. The minimal path algorithm (Cohen and Kimmel 1997) based on the active contour model, on the other hand, is free from metrication error because it deals with the continuous version as long as possible, and, thus, provides higher accuracy. Kaul et al. (2012) applied it on pavement crack segmentation. Despite its advantages in accuracy, the key limitation of the minimal path approach is that it requires prior user-input points at the beginning to initialize the process. The original study required both end points of the desired curve, and studies have been conducted to relax this requirement. Some studies (Avila et al. 2014; Nguyen et al. 2011) enumerated on every pixel across the image to calculate the minimal path, which was apparently less ideal from the perspective of computational cost. Benmansour and Cohen (2009) proposed a variant of the minimal path approach, which required one end-point as initial input and detected representative key points along the curve using front propagation. The algorithm terminated automatically on closed curves, but for open structures, either all the endpoints or some endpoints plus the length of the curves were still required. Kaul et al. (2012) further improved the algorithm, which only required one arbitrary point along the desired curve with the stopping criteria re-designed to work with both closed and open curves. However, the performance depended on the step-size of the propagation, and the issue of early termination impacted the performance on low-contrast pavement areas and high-density cracks. Overall, research efforts are still needed to further eliminate/minimize the constraint on prior user-input information and improve the crack detection accuracy

under a fully automated scenario. Table 2.1 shows the general comparison between local-based and global-based crack detection algorithms.

**Table 2.1 Comparison between local-based and global-based crack detection**

	Local-based	Global-based
<b>Principle</b>	1) Crack pixels have lower intensity / range values; 2) Cracks are continuous linear features instead of isolated.	1) Cracks are <i>perceptually salient</i> long continuous curves; 2) The intensity/range along a crack may <i>not always</i> be lower.
<b>Main Methods</b>	1) Thresholding 2) Edge detection	1) Potential function and optimization
<b>Pros</b>	1) Faster computation; 2) Fair amount of existing studies from image processing area.	1) Higher accuracy: full continuous crack curves 2) The results naturally contain high-level topological and geometrical features
<b>Cons</b>	1) Low accuracy: disconnected crack fragments with many false positives	1) Slower computation 2) Requirements on prior user inputs

Besides the studies from academic researchers, sensor manufacturers and vendors from the industry have also developed crack detection functions in their systems or solutions. For example, the INO/Pavemetrics, the manufacturer of the LCMS system (Laurent et al. 2008), has provided the crack detection function in their data analysis software. These functions are not published work, so the details of the algorithms cannot be reviewed here. The performance of these functions is later compared with existing published algorithms and the proposed algorithm in this study.

### 2.3.2 Performance Evaluation

It is difficult to compare the performance of the existing crack detection algorithms for the following reasons:

First of all, there is no consistent performance measure to evaluate the accuracy of the algorithms. Many studies conducted a qualitative evaluation to show the superiority of their particular algorithms in comparison with others (Koutsopoulos et al. 1993; Nazef et al. 2006; Wang et al. 2007; Wang et al. 2007). In order to quantitatively demonstrate the performance of crack detection algorithms, specific scoring criteria must be developed. Huang and Xu (2006) and Zhou et al. (2006) measured the performance of their algorithms based on pixel-wise statistical correlation between the ground truth image and detected crack map. Mean square error is another metric that has been widely used. However, these two methods are region-based methods that use the entire image data for image comparison and do not target the crack regions specifically. This can obscure the results, considering the fact that crack pixels are typically only a small percentage of the total image pixels, and these scoring measures are not specifically sensitive to crack information. In addition, information about crack locations is not used in these evaluation methods. This may lead to the error that two segmented crack images having different crack locations are considered the same simply because they have the same number of total crack pixels in an image. Some other quantification methods target the objects of interests only, including Receiver Operator Characteristics (ROC) (Kerekes 2008; Song et al. 2007) and Hausdorff distance (Beauchemin et al. 1998; Wang 2002), but they cannot provide a fair comparison when outliers exist. Kaul et al. (2009) proposed

a buffered Hausdorff distance based scoring method, which provided an effective criterion to quantitatively evaluate the performance of pavement crack segmentation.

Secondly, although there are various performance evaluation criteria available for pavement crack segmentation, a publicly available pavement surface image database shared among researchers is lacking, so it is difficult to fairly compare the achieved results with the published approaches. Many approaches are only demonstrated on selected and limited samples, and the robustness of the algorithms on a diverse dataset is not evaluated. There is a need to establish a consistent pavement image dataset, which covers diverse pavement surface characteristics, crack characteristics, and other factors that may impact the performance of crack segmentation. It will better serve the research community and transportation agencies and further stimulate the development and improvement of crack segmentation algorithms.

Overall, none of these developed algorithms have been implemented by state DOTs and support their pavement maintenance decision-making in a fully automated manner.

### **2.3.3 Summary**

The overview of existing literature reflects that fully automatic, reliable, and robust pavement crack detection still remains a challenge. There are some prominent areas of concern in this field:

- The emerging high-resolution line laser imaging system can provide 2D intensity and 3D range pavement surface data with much better granularity, and it also has the potential to overcome the long-lasting lighting issue of reliably detecting cracks. However, 3D pavement surface data has its own noise for crack detection,

including inherent sensor noise and any pavement conditions involving surface elevation change, e.g. cross-slope, rutting, raveling, grooves, etc. These different types of noise and their impacts on crack detection haven't been thoroughly studied in the existing literature.

- The performance of solely local-based crack detection algorithms is limited. First, these algorithms provide disconnected detection outcomes, which directly limits their use to support practical crack type and severity level analysis. For example, the calculation of crack orientation is limited to several specific directions (such as longitudinal and transverse) without continuous crack curves. Second, the results contains a fair number of false positive detections, given the noisy nature of pavement surfaces.
- The global-based crack detection approach, such as the minimal path procedure, provides preferable crack detection outcomes, given its capability of detecting continuous crack curves and preserving the high-level topological features of the crack patterns, which are critical for the subsequent pavement condition assessment. However, these algorithms mostly require prior user inputs. For example, dynamic optimization requires a predominant searching direction, and minimal path procedures require at least one user-input point. In addition, the accuracy of crack detection is also controlled by the prior user inputs; this has become another concern especially for high-density cracks (e.g. alligator cracking), which requires a lot of user inputs and the accuracy and consistency of these inputs cannot be guaranteed. Research needs to be conducted to minimize / eliminate human intervention for achieving a fully automatic crack detection.

- The computation speed of global-based algorithms needs to be further improved for practical implementation.
- There is a need for a consistent performance evaluation method and a publicly available pavement image dataset for the researchers to improve their crack detection algorithms and for the end-users, such as DOTs, to select the optimal algorithm for their automated condition assessment system.

## **2.4 Literature Review on Crack Classification**

Compared to the significant efforts that have been made on the development of sensing techniques and automatic crack detection algorithms, the related studies on crack classification are limited. In the literature, most crack classification methods are presented in combination with crack detection methods. The difficulty of crack classification directly depends on the expected outcomes. Most studies target classification of pavement cracks into primitive types, such as longitudinal, transverse, and diagonal, etc., which indeed makes classification less challenging. However, federal and state agencies have much more complicated and diverse crack definitions in their pavement distress protocols. This section first reviews several representative pavement distress protocols from federal and state agencies, and then summarizes the existing automatic crack classification studies from the perspectives of classification outcomes, physical crack characteristics used for classification, common methods used for feature interpretation, and performance evaluation.

## **2.4.1 Crack Definitions in Federal and State Agency's Protocols**

### 2.4.1.1 AASHTO Provisional Standard

In 2010, AASHTO developed a provisional standard PP67-10 for crack classification and quantification (AASHTO 2010). A crack is defined as a fissure of the pavement material at the surface with minimum dimensions of 1-mm width and 25-mm length. The inside and outside wheel paths are defined as longitudinal strips of pavement 0.75m wide and centered at 0.875 m from the centerline of the lane on both sides. Five measurement zones are created by the wheel paths and the areas between and outside the wheel paths. Three types of cracks are defined: longitudinal cracks, transverse cracks, and pattern cracks. Longitudinal and transverse crack types are defined according to crack orientation in a particular measurement zone. In current practice, all cracks that are not defined as transverse or longitudinal belong to pattern cracks.

The crack definitions in the AASHTO provisional standard are relatively straightforward and closely tied to its scope. This standard aims to quantify crack distresses at the network level by utilizing automated methods. Therefore, it avoids the complicated crack definitions that are, currently, difficult to model automatically.

### 2.4.1.2 GDOT COPACES Protocol

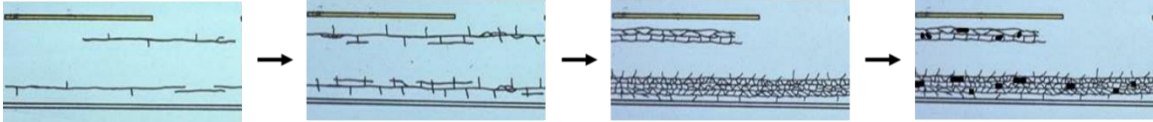
Georgia Department of Transportation' (GDOT) Pavement Condition Evaluation System (PACES) (GDOT 2007) is designed for conducting the annual pavement surface condition survey in Georgia. A total of ten types of distresses have been defined for flexible pavement, including load cracking, block/transverse (B/T) cracking, reflection cracking, edge distress, rutting, raveling, bleeding/flushing, corrugation/pushing, patches and potholes, and loss of section. Both the presence of these distresses and their



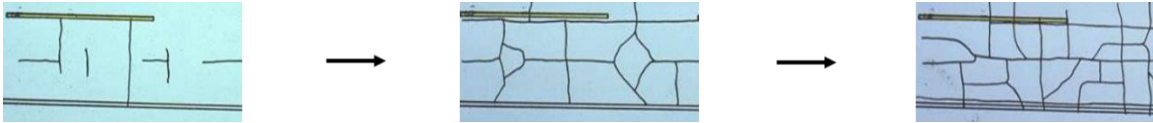
corresponding severity levels must be measured in a field survey. Load cracking and B/T cracking are the two most common pavement surface distresses in Georgia.

Load cracking is caused by repeated heavy loads and always occurs in the wheel paths. Figure 2.2(a) illustrates four different severity levels of load cracking. Severity Level 1 usually starts as a single longitudinal crack in the wheel path. Severity Level 2 has a single or double longitudinal crack with a number of 0-2, foot-long transverse cracks intersecting. The crack width in this severity level is larger than Severity Level 1 cracks. Severity Level 3 shows an increasing number of longitudinal and transverse cracks in the wheel path. This level of cracking is marked by a definite, extensive pattern of small polygons, which are formed by the intersection of these cracks. Severity Level 4 has the definite “alligator hide” pattern but has deteriorated to the point that the small polygons are beginning to pop out.

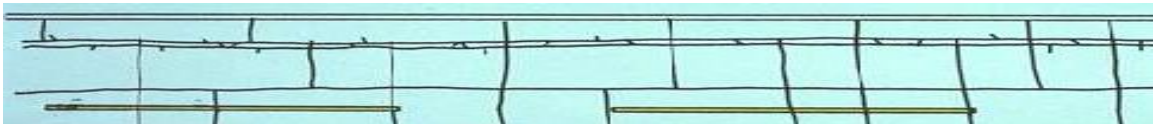
Unlike load cracking, B/T cracking is caused by weathering of the pavement or shrinkage of cement-treated base materials. B/T cracking is not load related, and, therefore, is usually distributed uniformly throughout the roadway. Figure 2.2(b) shows the illustrations of three different severity levels of B/T cracking. Severity Level 1 is made up of transverse, longitudinal, or a combination of both types of cracks, but the block pattern has not developed yet. Severity Level 2 has a definite block pattern, and Severity Level 3 has a very large number of small blocks. It needs to be noted that for both Severity Level 2 and Severity Level 3, some of the cracks may meander into the wheelpaths for short distances but are still considered as B/T cracking.



(a) Load cracking from Severity Levels 1 to 4 (from left to right)



(b) B/T cracking from Severity Levels 1 to 3 (from left to right)



(c) Combination of load cracking and B/T cracking

**Figure 2.2 Illustration of load cracking and B/T cracking at different severity levels**

The crack definitions in the PACES protocol are clearly more sophisticated than the AASHTO provisional standard. The crack types and severity levels are defined based on the combination of multiple factors, including crack location, length, width, orientation, intersections, and polygons, etc. The classification of these crack types and severity levels involves human identification of complex and diverse crack patterns in the field, which is challenging to mimic automatically.

#### 2.4.1.3 SHRP LTPP Protocol

Federal agencies also have their pavement distress protocols. In 1987, the Strategic Highway Research Program began the largest and most comprehensive pavement performance test in history – the Long-Term Pavement Performance (LTPP) program. In this program, highway agencies in the United States and 15 other countries have been collecting data on pavement conditions, climate, and traffic volumes and loads from more than 1,000 pavement test sections. That information will allow pavement

engineers to design better, longer-lasting roads. The distress identification manual (U.S. Department of Transportation Federal Highway Administration 2003) provides a consistent, uniform basis for collecting distress data for the LTPP program.

This LTPP protocol defines six types of crack-related distresses on asphalt concrete surfaces, including fatigue cracking, block cracking, edge cracking, longitudinal cracking (wheel path and non-wheel path), reflection cracking at joints, and transverse cracking. Similar to the GDOT PACES protocol, the LTPP protocol defines both crack types and severity levels based on crack width, orientation, location, and topological pattern, etc. Even at the federal level, these crack definitions are complicated comparing to the primitive types in the AASHTO provisional standard.

#### **2.4.2 Automatic Classification Outcomes**

From the perspective of automatic classification, most existing studies didn't target any real-world pavement distress protocols. Cheng et al. (1999) and Zhou et al. (2006) classified pavement cracks into longitudinal, transverse, and diagonal cracking; these classification outcomes were basically orientation related. Some other studies (Bray et al. 2006; Cheng and Miyojim 1998; Lee and Lee 2004; Li et al. 2011; Saar and Talvik 2010; Salari and Bao 2010; Sun et al. 2009; Zhou et al. 2005) further incorporated block cracking and alligator cracking into their crack type classification. These classification outcomes significantly simplify the crack classification problem, but a clear gap is observed between these outcomes and the crack definitions in most real-world pavement distress protocols. It is difficult for state agencies to directly adopt these algorithms for their crack evaluation. Oliveira and Correia (2013) designed their crack classification according to the crack types in the Portuguese Distress Catalog, but this protocol itself

was relatively simple and only defined longitudinal, transversal, and miscellaneous cracks.

Although the severity classification is another important task in the real-world crack survey, it has rarely been discussed in the existing literature. Zhou et al. (2005) used the energy in the wavelet domain to determine a distress severity value from 0-100, but didn't directly link it to any physical meaning. Georgopoulos et al. (1995) combined crack width, length, presence of joints, and polygon blocks to determine the severity according to the PAVER protocol (U.S. Army Corps of Engineers 1989). Oliveira and Correia (2013) used crack width only to determine severity according to the Portuguese Distress Catalog.

### **2.4.3 Physical Crack Characteristics for Classification**

Most existing literature investigates similar crack characteristics for classification purposes. Crack orientation is the most common one. Many studies (Bray et al. 2006; Cheng et al. 1999; Lee and Lee 2004; Saar and Talvik 2010; Salari and Bao 2010; Salari and Bao 2011) used a “1-D projection” approach to capture crack orientation: for a binary image containing crack and non-crack pixels, this approach projected the 2D image onto 1D vectors by summing up the crack pixels for each row, column, or diagonal; by investigating the variance or histogram of these 1D vectors, it identified the cracks along specific directions. Li et al. (2011) suggested using skeletonized crack sections through direction coding rather than simple crack pixels, since spatial distribution features held considerable significance for each type of crack in this representation. Another study by Adarkwa and Atttoh-Okine (2013) introduced tensor factorization for the crack direction extraction as well.

The number of crack pixels is another commonly used characteristics. A large number of crack pixels is likely to indicate the presence of alligator cracking. Some studies (Saar and Talvik 2010) used the number of crack pixels directly, while some others (Lee and Lee 2004; Salari and Bao 2010) used the number of crack cells. The use of image cells instead of pixels reduces the influence from isolated detection noises; on the other hand, the detailed information within each image tile is lost and the selection of tile size can be tricky.

As mentioned previously, the crack definitions in the real-world protocols involve a combination of multiple factors, and it is insufficient to simply rely on crack direction and the number of crack pixels to make a judgment. A few papers (Cheng and Miyojim 1998; Georgopoulos et al. 1995) have tried to interpret the topological structure of crack pattern, and provided some valuable crack features, including the presence of joint cracks, polygon blocks, and parallel cracks, etc. However, limited by the data quality and crack detection performance, the calculation of these features wasn't sufficiently accurate. Also, the proposed features were still fragmental, and there is a need for a systematic approach to representing the topological crack pattern and extracting crack features from the sensing data and detected crack maps.

#### **2.4.4 Common Methods for Feature Interpretation**

The crack characteristics extracted from the detected crack map need to be further transformed into different crack types and severities. Many studies (Cheng et al. 1999; Cheng and Miyojim 1998; Georgopoulos et al. 1995; Zhou et al. 2005) relied on the feature distinction and established corresponding decision rules (e.g. thresholding); they plotted the distributions of features for different crack types and severities, and picked the

optimal decision rules through trial and error. Some studies (Oliveira and Correia 2013; Salari and Bao 2010) only considered two features for classification (e.g. the variances of row sum and column sum), so they separated the 2-D space into several regions, each of which corresponded to one specific crack type. This approach may provide satisfactory results on a small dataset, but its performance at a larger scale is still questionable.

It is interesting to find that the neural network classifier has been widely applied for crack classification. Previous studies explored different features as the inputs for the neural networks. Bray et al. (2006) used the entire vector after 1-D projection as the inputs of the neural network. Lee and Lee (2004) revealed that using the proximity of each vector actually provides results that are as good as using the entire vector. Li et al. (2011) used the features of skeletonized crack sections rather than crack pixels to better preserve the spatial distribution of features. Overall, the neural network classifier is a good solution with sufficient, perfectly labeled training data; however, the outliers may impact the network performance in an uncontrolled way, and it is difficult to adjust a calibrated model with extra data.

Some studies transform the pavement image into a different domain instead of analyzing the image pixels directly. Zhou et al. (Zhou et al. 2005; Zhou et al. 2006) conducted wavelet transformation on each image, and they calculated a series of features on the spectral domain to classify the distress types and severities. They also explored Radon transformation and used the patterns of peaks after Radon transformation to indicate the properties of cracks on the original image. Based on the fact that pavement cracks are mostly linear objects, Ying and Salari (2010) conducted beamlet transformations, which are less sensitive to noises, and used the beamlets at different

scales for crack classification. Some recent studies combine multiple methods from previous studies. Nejad and Zakeri (2011) used a series of features after wavelet and Radon transformation as the input of a dynamic neural network, which enhanced the performance in terms of robustness against noise and computation speed.

Overall, by comparing the literature, different interpretation methods show very close classification performance when similar features are used. For example, in Lee's previous work (Lee and Lee 2004; Lee and Kim 2005), similar crack type index (CTI) features were used in both studies; one of them used primitive rules to interpret them, while the other one used neural networks to achieve the classification. Both studies showed very close classification accuracy on longitudinal, transverse, block, and alligator cracking. This reveals that the goodness of features, i.e. crack characteristics used for classification, is more important than the selection of interpretation methods.

#### **2.4.5 Performance Evaluation**

In terms of the performance evaluation of crack classification, most of the results available in the literature are only of a qualitative nature (Oliveira and Correia 2013). Also, due to the diversity of pavement distress protocols and the lack of a publicly available road pavement surface image database shared among research institutions, it is difficult to compare the achieved results with the published approaches. On the other hand, numerous large-scale studies (Albitres et al. 2007; Capurro et al. 2006; Fu et al. 2011; Tighe et al. 2008) have shown that current automatic crack classification and quantification survey results usually have poor correlation with manual survey results. This is explained by the incompatibility between existing survey manuals and the current outcomes from the new survey methods based on computer imaging technologies. While

existing survey manuals are based on the ability of human surveyors to subjectively recognize distresses by identifying crack patterns in various locations on the pavement surface, current automatic surveys are still not capable of fully mimicking this process and replacing human judgment (Fu et al. 2011). State DOTs still cannot obtain the maximum benefit from the new automatic survey methods.

#### **2.4.6 Summary**

The literature review reflects that the existing automatic crack classification methods cannot directly benefit agencies' pavement surface condition surveys. The following are some prominent areas of concern:

- The classification outcomes from most existing literature are highly simplified crack types, including longitudinal, transverse, block, and alligator cracking, etc. Comparatively, agencies usually have a much more detailed way of defining crack types and severity levels to serve the purposes of pavement performance monitoring, maintenance prioritization, and treatment method selection, etc. As a result, state DOTs cannot directly adopt existing crack classification methods to support their pavement condition assessment.
- The crack definitions among different protocols are quite diverse, yet state agencies need to cover multiple protocols at the same time. For example, GDOT conducts its pavement condition survey following the PACES protocol for its pavement management, and in the meantime, FHWA also requires it to provide crack data for HPMS and LTPP programs. This requires the desired automatic crack classification method to be adaptable to different protocols with minimum modification effort.



- Most existing literature investigates similar crack characteristics with the main focus on crack orientation and the number of crack pixels. However, these characteristics are insufficient to support the real-world crack definitions. Based on the previous review, the crack type and severity level definitions involve multiple factors, including crack location, length, width, orientation, intersections, and polygons, etc. There is a need to develop an automatic methodology to systematically and comprehensively extract these crack characteristics to mimic human perception in the field.
- The performance evaluation and validation in the existing literature are mostly qualitative. There is a need to validate the performance of automatic classification results following state DOTs' survey practices and compare with the corresponding manual survey data.

## **CHAPTER 3. PROPOSED ALGORITHM FOR CRACK DETECTION**

This chapter presents the proposed algorithm for automatic crack detection. The active contour based minimal path algorithms have demonstrated better performance in the pertinent literature, given their capability for detecting continuous crack curves and preserving the high-level topological features of the crack patterns, which is critical for the subsequent crack condition assessment. However, they require at least one prior input point for each crack curve, which introduces tedious and subjective manual work in practical use, especially for high-density cracks. In this study, a new crack detection algorithm to detect accurate and continuous crack curves in a fully automatic manner is proposed. It removes the prior-input constraint by automatically generating key points across the image through tensor voting and crack skeleton analysis, and then detects the crack curves between neighboring key points using a two-point-based minimal path procedure. This chapter is organized as follows. Section 3.1 presents the proposed algorithm, including a complete algorithm flowchart followed by a detailed explanation of each step. Section 3.2 demonstrates the proposed algorithm using selected images and illustrates how each step of the proposed algorithm works under different scenarios.

### **3.1 Proposed Algorithm for Automatic Crack Detection on Pavement Images**

#### **3.1.1 Algorithm Flowchart**

This section presents the flowchart of the proposed algorithm. The input is the raw pavement surface data; in this study, the pavement surface data is often represented in the format of 2D intensity and 3D range images. The output is a detected crack map,

which is a binary image representing the locations of all the crack pixels. Figure 3.1 shows the flowchart of the proposed algorithm. It consists of five major steps:

- 1) Image enhancement through non-crack feature removal and profile rectification, which reduces the impact of pavement surface noise on crack detection;
- 2) Crack potential map generation through adaptive thresholding and tensor voting, which enhances the curve structures on the image (which are very likely to be cracks) and further suppresses the isolated noises in the background;
- 3) Key point identification through iterative morphological thinning and skeleton analysis, which interprets the crack potential map and identifies the end points and branch points for all the possible crack structures on the image;
- 4) Crack curve detection using two-point-based minimal path procedure, which detects the precise crack curves between neighboring key points;

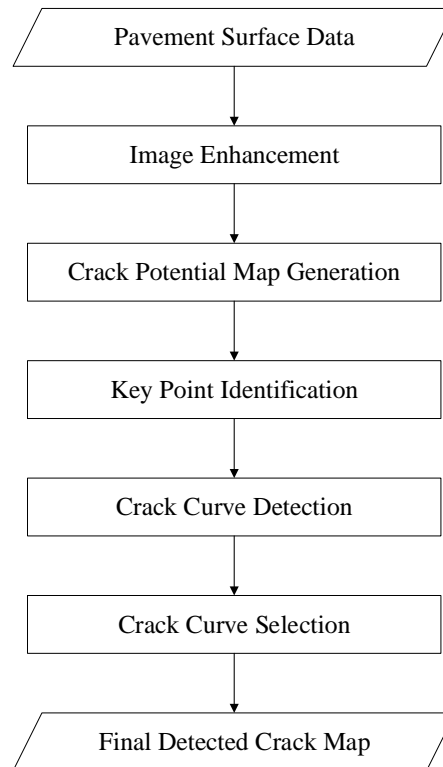


**Figure 3.1 Proposed algorithm for automatic crack detection**

- 5) Crack curve selection through statistical analysis, which investigates each detected crack curve and removes the false positive detections that are sometimes introduced by non-uniform pavement surface texture from the data or the skeleton analysis from the proposed algorithm.

The following subsections will present the details of these steps.

### **3.1.2 Image Enhancement through Non-Crack Feature Removal and Profile Rectification**

Crack detection using traditional 2D intensity images suffers from different lighting conditions, low contrast, and interference from other pavement surface objects, such as pavement markings and oil stains. How to remove these noises has become one of the major tasks for crack detection using 2D intensity images. This study focuses on utilizing 3D pavement surface data for crack detection. Comparatively, 3D surface data has an advantage when dealing with the above situations. However, since crack detection using 3D pavement surface data relies on the fact that cracks have a lower elevation compared to the surrounding area, any pavement surface features that involve elevation changes are potential noises for crack detection, which must also be removed / reduced to ensure an accurate and robust crack detection. The following are two major noise sources that will be handled through this step:

- *Profile outliers*

The outliers accompanying the raw 3D pavement surface laser range data are either black outliers or white outliers. Black outliers protrude below the surrounding data; white outliers protrude above the surrounding data. The black outliers are present when a valid range value was not successfully obtained during

the data collection process. This could be because either the physical pavement surface was out of the measurement range of the profiling sensor or the sensor failed to extract a valid range value from the observed laser image. The white outliers may be related to debris on the laser and/or camera windows. Both of these outliers cause sharp elevation changes on a 3D laser profile, and these changes are sometimes very similar to the cracks. Therefore, the outliers need to be removed before the crack detection to avoid potential false positives.

- *Cross-slope / rutting*

For traditional 2D intensity images, inhomogeneous backgrounds, which are usually caused by different lighting conditions, shadows, and surface appearance, are one of the major issues that influences crack detection performance. Similar problems still exist for 3D surface data, but they are now caused by the gradual elevation change of the pavement surface. As shown in Figure 3.3(a), the right side of the image clearly appears darker than the left side because the elevation of the pavement surface gradually drops from left to right. Cross-slope and rutting are usually the causes of such symptoms, which need to be removed to enhance the crack features.

A two-step Gaussian filter is presented here to remove the impacts from outliers and low-frequency surface features, such as cross-slope and rutting. The typical one-dimensional Gaussian filter with the standard deviation  $\sigma$  is:

$$g(x) = \frac{1}{\sqrt{2\pi}\sigma} e^{-\frac{x^2}{2\sigma^2}} \quad (3.1)$$

The function of the Gaussian filter depends on the value of  $\sigma$ . The first step is to remove the invalid points and outliers from the raw data. Therefore, a Gaussian filter with

a small  $\sigma$  (in this case  $\sigma=8$ ) is chosen to check if each point on the profile has an unusual sharp elevation change compared to its closest neighborhood, i.e.

$$Range'(x) = \begin{cases} Range(x) & \text{if } abs(Range(x) - FRange(x)) > thres \\ FRange(x) & \text{otherwise} \end{cases} \quad (3.2)$$

where  $Range(x)$  is the original profile at point  $x$ ,  $FRange(x)$  is the filtered profile at point  $x$ , and  $thres$  is a given threshold.

After the outlier removal, another Gaussian filter with a much larger  $\sigma$  (in this case  $\sigma=150$ ) is applied to smooth the entire profile and identify the cross-slope and rutting. Let  $FRange'(x)$  be the filtered profile based on  $Range'(x)$ , and then the rectified profile will be

$$RecRange(x) = FRange'(x) - Range'(x) \quad (3.3)$$

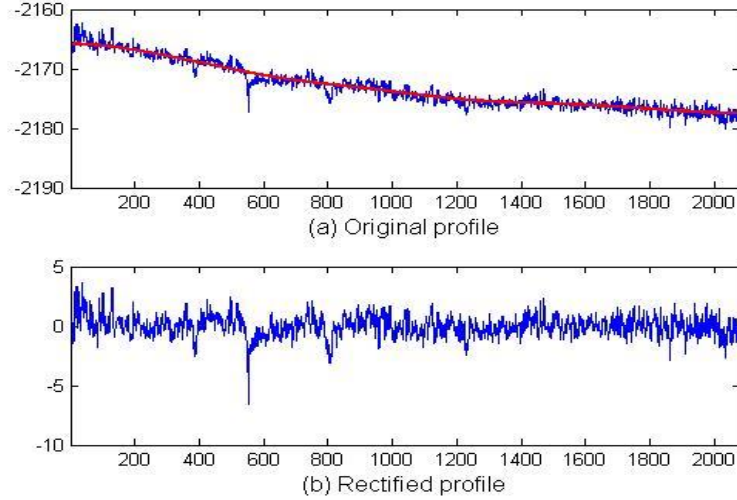


**Figure 3.2 Example of profile rectification on one transverse profile**

After this step, an image with reduced noises for crack detection is created by stacking the rectified profiles together (as shown in Figure 3.3(b)), which is referred to as the rectified image in the following context.

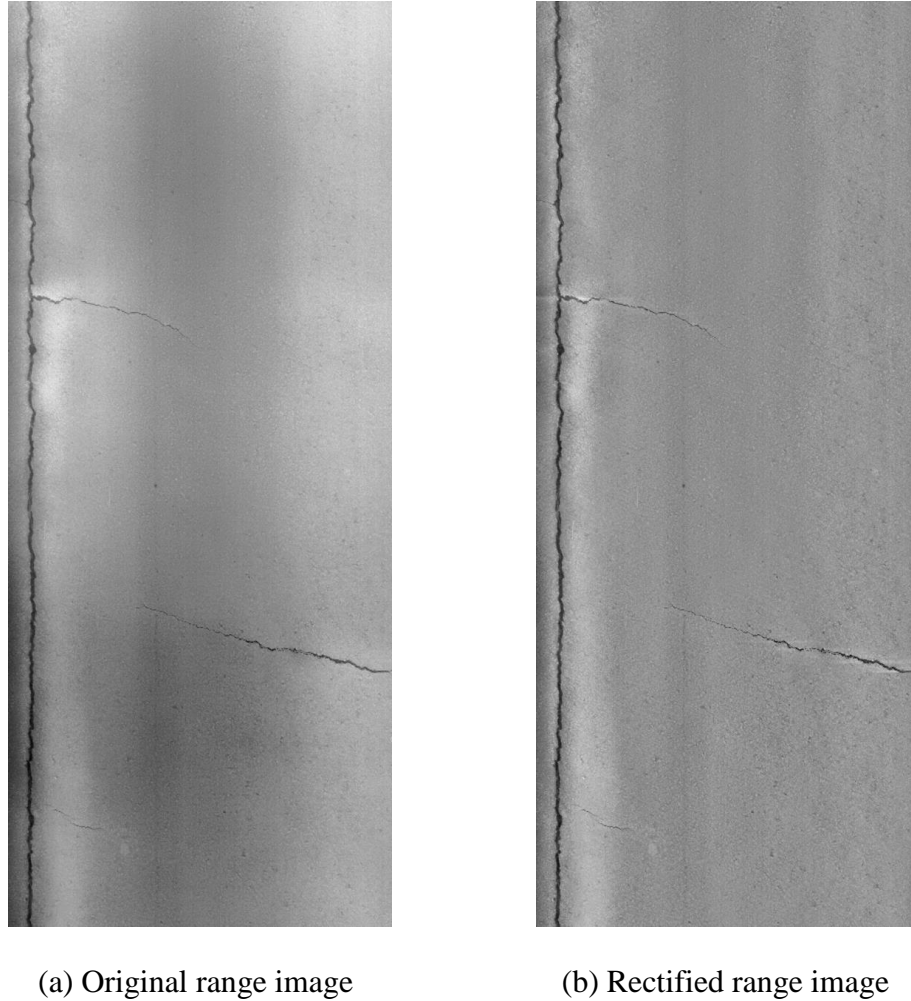


**Figure 3.3 Comparison between original range image and rectified range image**

### **3.1.3 Crack Potential Map Generation through Adaptive Thresholding and Tensor Voting**

Thresholding is then applied on the rectified image to get a rough idea of where the possible crack pixels are located. As we observe from the data, pavement surface roughness varies greatly among different images, which also influences the performance of crack detection. The variation of surface elevation can be as large as 10 mm on raveled pavement surfaces, about 5 mm on Open Graded Friction Course (OGFC) surface, and as small as 2 mm on newly paved dense graded surfaces and concrete surfaces. Even on the

same image, the variations of different regions may be quite different, especially with the existence of raveling. In this study, thresholding is adjusted adaptively according to the variation within the neighborhood on the entire rectified image. Figure 3.4(b) shows the results of this rough thresholding step.

As mentioned previously in the literature review, while in general cracks bear elevations that are lower than the surrounding pavement, the contrast of cracks may be seriously weakened by possible crack degradations, such as width and depth changes along the cracks and foreign debris inside the cracks. As a result, a local-based process, such as the thresholding, may have difficulty in detecting full crack curves; they usually detect a set of disjointed crack fragments with many false positives. As observed in Figure 3.4(b), most of the crack pattern has been preserved in the result, while a fair number of random noises over the image are also captured.

The tensor voting framework is then employed to enhance cracks in the pavement images. A detailed explanation of the tensor voting framework and its application on pavement images can be found in Appendix B. We use the crack pixels detected through thresholding as the initial tokens and want to incorporate perceptual cues of proximity and continuity to enhance the curves. However, these crack pixels have no orientation. Therefore, we first apply ball voting to estimate the crack-curve orientation at each crack pixel. More specifically, each detected crack pixel is initialized as a ball tensor with equal saliency and casts its votes to other crack pixels, i.e., non-crack pixels do not join this voting. After summing up the ball-voting fields from all the crack pixels, the principal direction at each crack pixel is found and set as the orientation of the stick token at this crack pixel. We then apply stick voting by casting the votes from each stick token to all



the pixels, including crack pixels and non-crack pixels. This dense stick voting will fill the gaps between the detected crack pixels to form longer crack curves (as shown in Figure 3.4(c)).

Through tensor voting, votes are cast from token to token and accumulated by tensor addition. The summed votes at each pixel can be represented by a covariance matrix, the analysis of which can be performed once the eigensystem of the accumulated second order  $2 \times 2$  tensor has been computed. As mentioned in Appendix B, the tensor can be decomposed into the stick and ball components:

$$T = \lambda_1 \hat{e}_1 \hat{e}_1^T + \lambda_2 \hat{e}_2 \hat{e}_2^T = (\lambda_1 - \lambda_2) \hat{e}_1 \hat{e}_1^T + \lambda_2 (\hat{e}_1 \hat{e}_1^T + \hat{e}_2 \hat{e}_2^T) \quad (3.4)$$

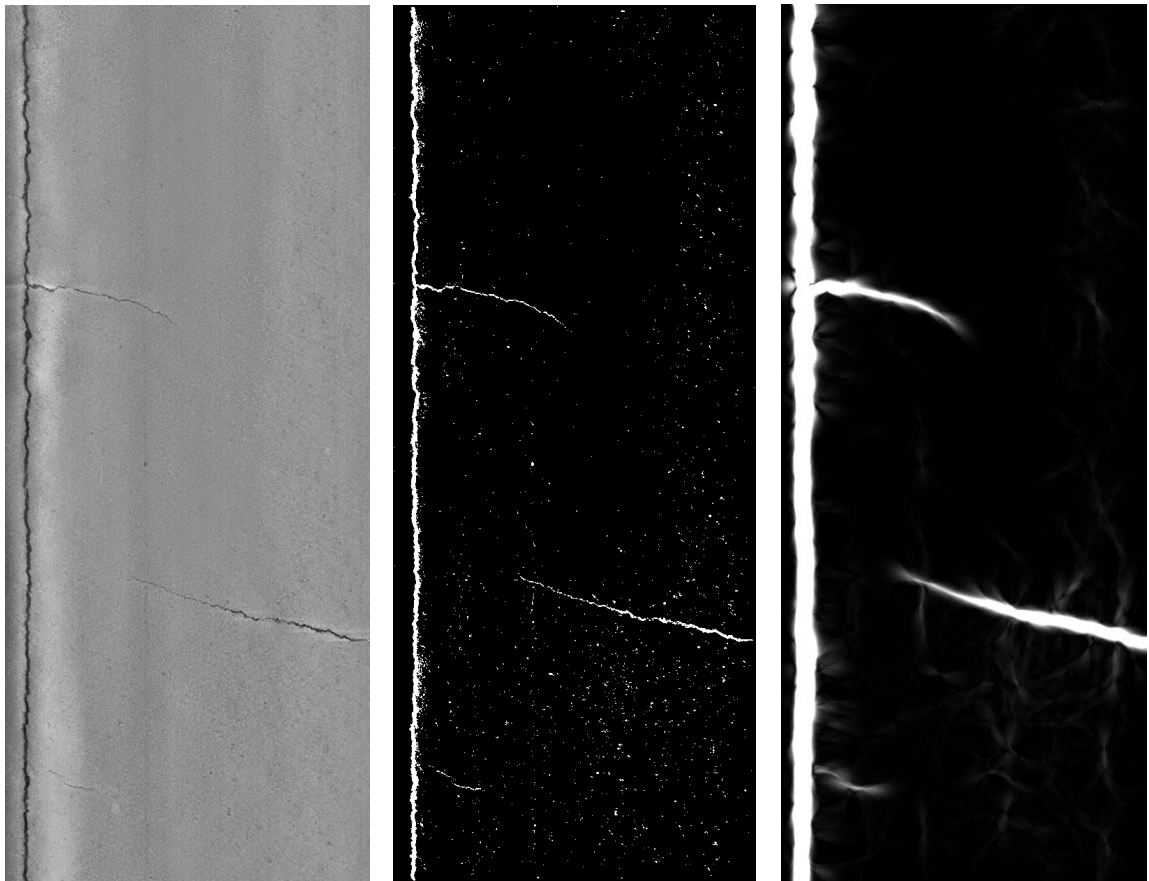
where  $\hat{e}_1 \hat{e}_1^T$  is a stick tensor, and  $\hat{e}_1 \hat{e}_1^T + \hat{e}_2 \hat{e}_2^T$  is a ball tensor. The following cases have to be considered:

- If  $\lambda_1 - \lambda_2 > \lambda_2$ , the saliency of the stick component is larger than that of the ball component and this indicates certainty of one normal orientation; therefore, the token most likely belongs on a curve whose estimated normal is  $\hat{e}_1$ .
- If  $\lambda_1 \approx \lambda_2 > 0$ , the dominant component is the ball, and there is no preference of orientation. This can occur either because all orientations are equally likely or because multiple orientations coexist at the location. This indicates either a token that belongs to a region, which is surrounded by neighbors from the same region at all directions, or a junction where two or more curves intersect and multiple curve orientations are present simultaneously. Junctions can be discriminated from region inliers since their saliency is a distinct peak of  $\lambda_2$ . The saliency of region inliers is more evenly distributed.

- Finally, outliers receive only inconsistent, contradictory votes, so both eigenvalues are small.

For the task of pavement crack detection, the areas of interest are both along the crack curves where a predominant orientation is found and at the junction where multiple curve orientations coexist. Therefore, it actually requires a sufficiently large  $\lambda_1$  value.

Figure 3.4(c) visualizes the  $\lambda_1$  value computed with the given input image.



(a) Rectified Range Image      (b) Thresholding Results      (c) Crack Potential Map

**Figure 3.4 Illustration of crack potential map generation**

### 3.1.4 Key Point Identification through Iterative Morphological Thinning and Skeleton Analysis

This section investigates where the cracks are likely to be on the crack potential map and further identifies the end points and branch points as the key points for all possible crack structures on the image. It consists of the following three steps:

#### **Binarization**

As mentioned previously, a sufficiently large  $\lambda_1$  is required to indicate the saliency of a continuous crack curve or a junction of multiple curves, i.e.

$$\lambda_1 \geq \Gamma \quad (3.5)$$

The parameter  $\Gamma$  is relevant to the scale of the image as well as the scale of voting. In this study, we set  $\Gamma = 200$  as the optimal parameter, which provides robust performance across various situations given the input range image resolution. Figure 3.5(a) shows an example of crack areas of interest after binarization on the crack potential map.

#### **Skeletonization**

One important advantage of employing the tensor voting procedure is that it automatically fills in the gaps between the crack fragments so that continuous and smooth crack patterns can be extracted. On the other hand, it does widen the crack area to an undesired extent. It can be observed that the crack areas of interest (as shown in Figure 3.5(a)) are much wider than the real cracks in the range image (as shown in Figure 3.4(a)). Therefore, a step of skeletonization is conducted to extract the underlying crack skeleton from these region-based areas of interest.

Skeletonization is a common process in image processing and pattern recognition that can be achieved through different techniques to compile with different requirements.

A topological skeletonization is applied here, which targets retaining the topology of the original object so that critical features, such as continuity and branching, are preserved for crack patterns. The morphological thinning process is employed to generate the skeleton, which not only preserves the topology, but also produces one pixel width skeleton result. Figure 3.5(b) shows the crack skeleton results generated through iterative morphological thinning operations from Figure 3.5(a).

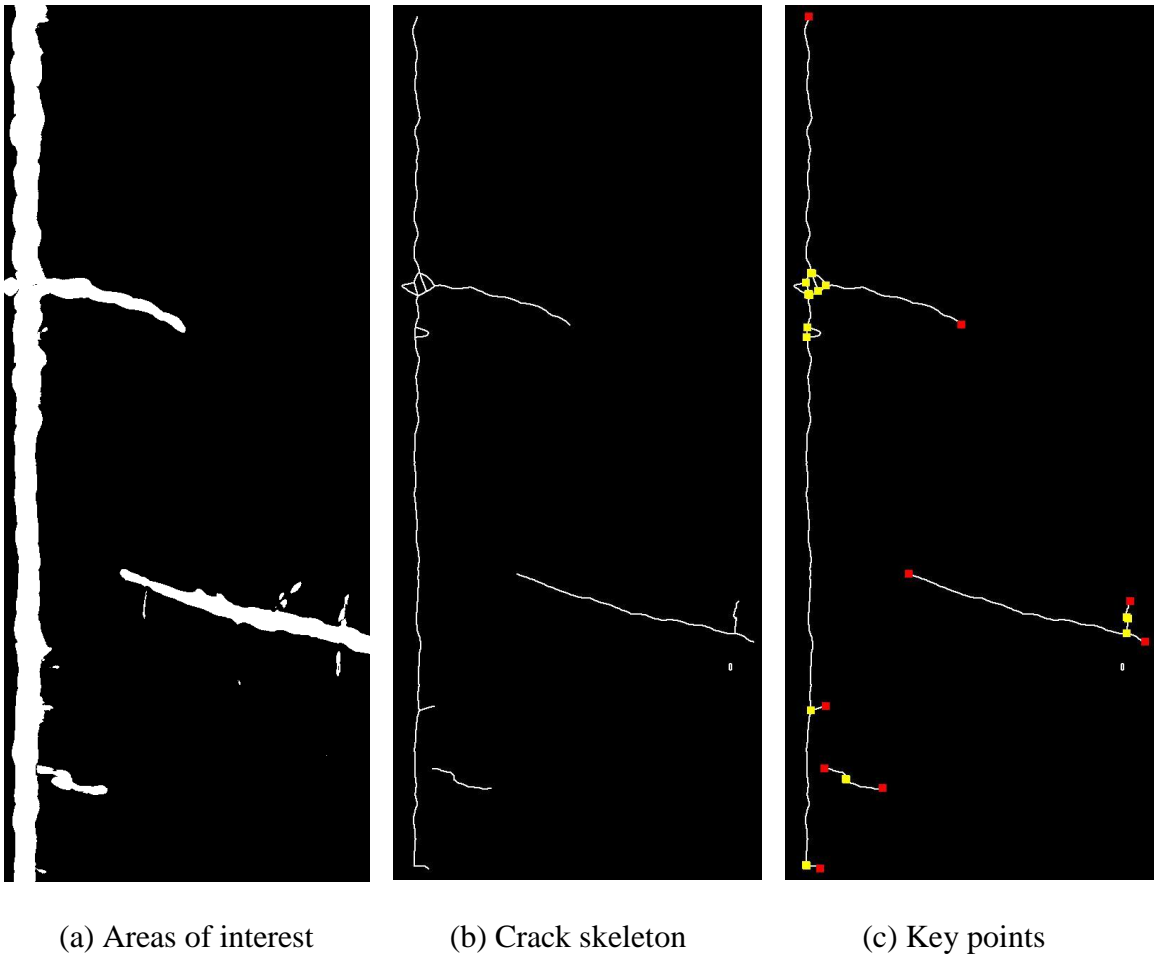


**Figure 3.5 Illustration of crack skeleton extraction**

#### **Key point extraction**

There are two types of key points that help represent the topology of the crack pattern. With the one-pixel width skeleton result, they are defined as follows:

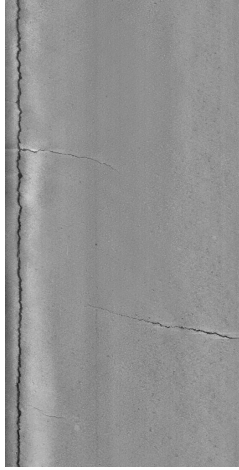
- End points: if they have less than two neighbors
- Branch points: if they have more than two neighbors

As shown in Figure 3.5(c), the end-point pixels are tagged with red dots, and the branch-point pixels are tagged with yellow dots. These pixels are the input for the subsequent crack curve detection with the minimal path procedure.

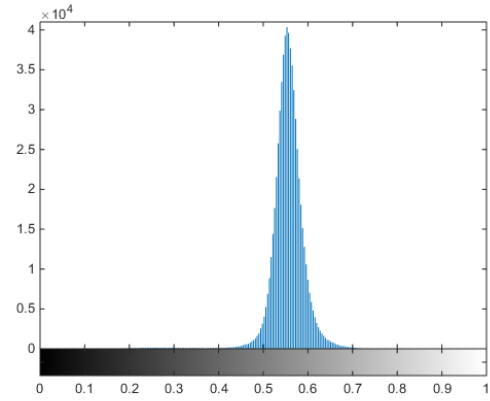
### **3.1.5 Crack Curve Detection Using Minimal Path**

The minimal path procedure is then employed to detect the continuous crack curves between the neighboring key points. The theory of minimal path procedure and its application on pavement crack detection are introduced in Appendix A.

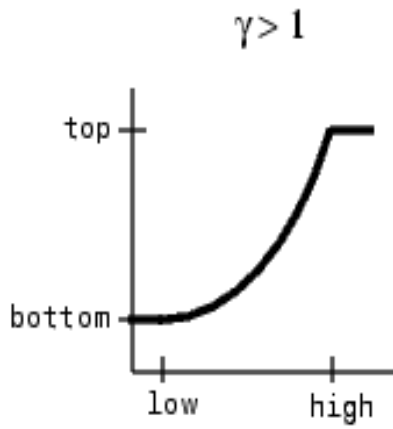
As the key points have been identified as the end points and branch points from the previous step, another important condition for the minimal path procedure to work properly is the selection of the potential function. In Appendix A, the simplest example of using the intensity value as the potential is explain. However, the low contrast nature of pavement images has been noticed through the study. As shown in Figure 3.6(a) and (b), the pixel values, even on a rectified range image, concentrate within a small range. This leads to poor differentiation between crack and non-crack pixels. Consequently, the shortest paths found between two key points will lean towards a Euclidean shortest path (straight lines) rather than a geodesic shortest path (actual crack curves) in some situations. To avoid that, a contrast enhancement process is applied to re-map the pixel values on the rectified range image to a wider range. A Gamma correction is applied to weight the mapping towards the lower (darker) output values because crack pixels, which have different depth and width values, take a wider range in the input, while the non-crack pixel values are relatively close after rectification.



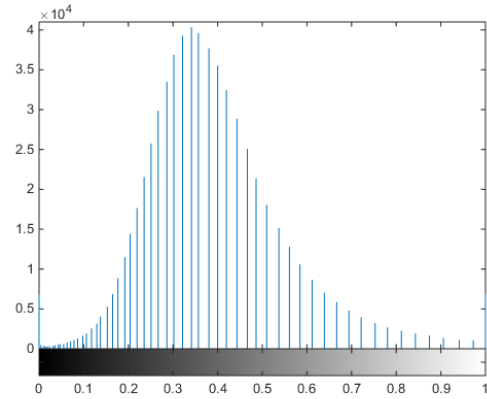
(a) Rectified range image



(b) Histogram before correction



(c) Concept of gamma correction



(d) Histogram after correction

**Figure 3.6 Low contrast nature of pavement images and gamma correction**

The pixel values after this enhancement process are then used in the potential function

$$\Phi(i, j) = (I(i, j))^\gamma + \varepsilon \quad (3.6)$$

where  $I(i, j)$  is the image pixel value at each point  $x = (i, j)$  and  $\varepsilon = 10^{-6}$  is a constant.

The purpose of adding a small constant is to avoid the back propagation that is trapped inside wide cracks with a pixel value of zero. The grid spacing for discretization step was

chosen to be 1. The crack curves between the neighboring key points are detected. Figure 3.7 demonstrates the crack curve detection results on the sample case.

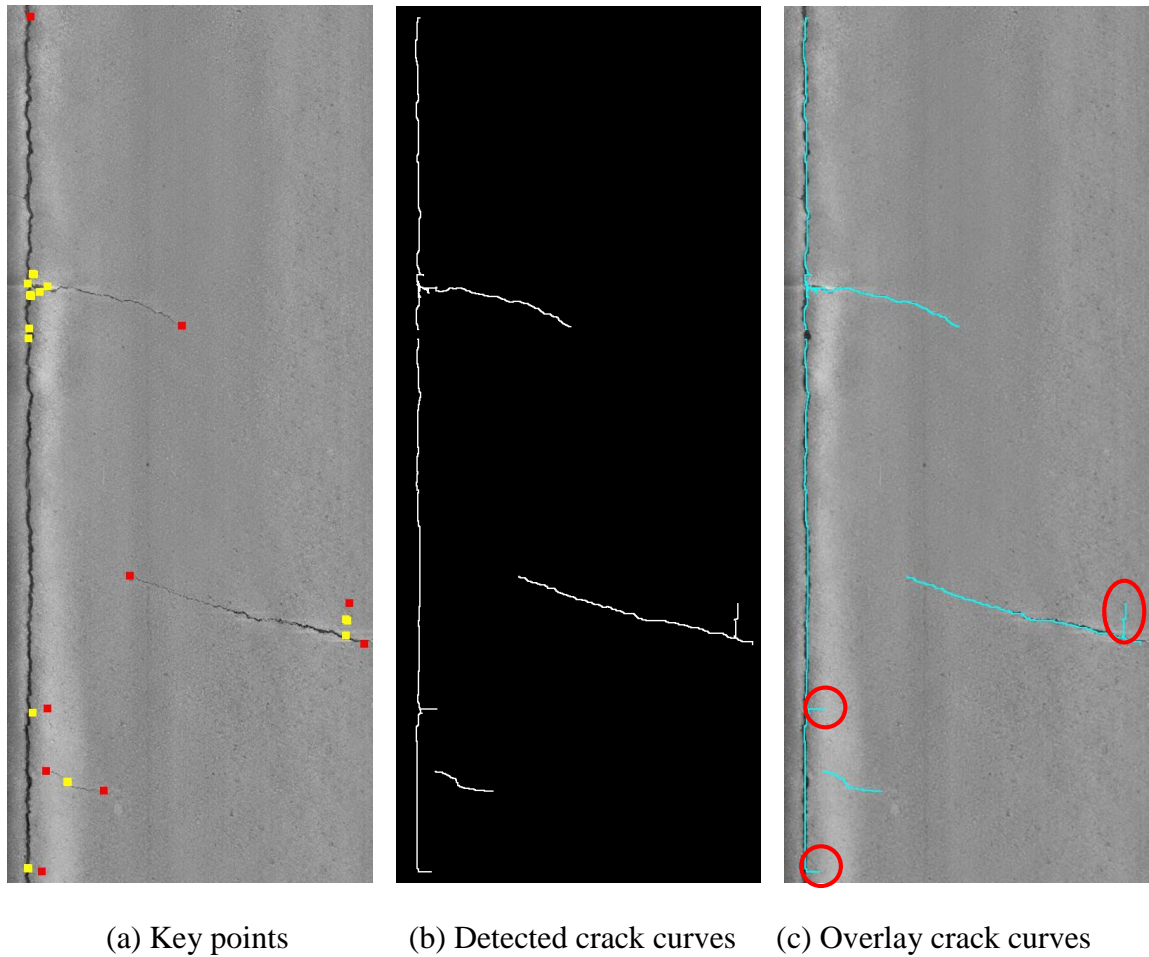


**Figure 3.7 Crack curve detection using minimal path procedure**

### 3.1.6 Curve Selection through Statistical Analysis

A subset of outliers is among the crack curves that have been detected in the previous steps. These false detections can be observed on Figure 3.7 as circled. They can be introduced through:

- Non-uniform pavement surface texture: although the initial thresholding value is adjusted according to the variation over the entire image, scenarios exist when a sub-portion of the image is particularly rougher than the rest. The noises in those

areas cluster together through the tensor voting procedure, which leads to undesired key points and, consequently, false positive crack curves.

- Skeletonization: as a morphological operation, skeletonization can easily create artifacts, such as “spikes” or “loops”, through the process (as shown in Figure 3.5(b)).

As a result, these artifacts further lead to key points outside the real crack pattern.

The purpose of this step is to remove these false detections by investigating the pixel values along each detected crack curve. A total of 564 detected crack curves are randomly selected from the previous stage from a set of test images. Each of these curves is manually labeled, among which 396 curves are correct detections and 168 curves are false positive detections. They are plotted in Figure 3.8 based on the mean and standard deviation of the pixel values along the curve. The blue dots represent the true detections, and the red dots represent the false detections; a clear differentiation is observed between them. The correctly detected crack curves concentrate in the region with a small mean value and a relatively linear trend; the false detections are distributed more randomly with a larger mean value. Based on the observation, a simple rule is set to drop the cracks with a mean pixel value greater than 0.2. By doing this, over 80% of the false positive detections are removed from the results at the cost of about 2% of the correct detections. Figure 3.9 shows the final crack map after crack curves selection on the sample image.



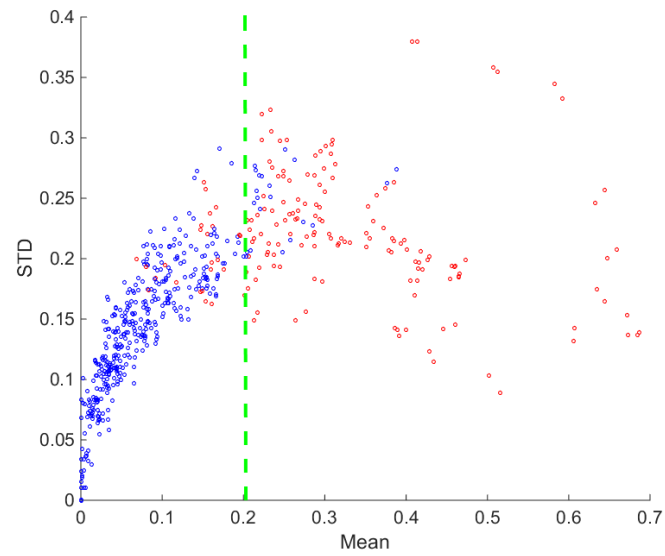
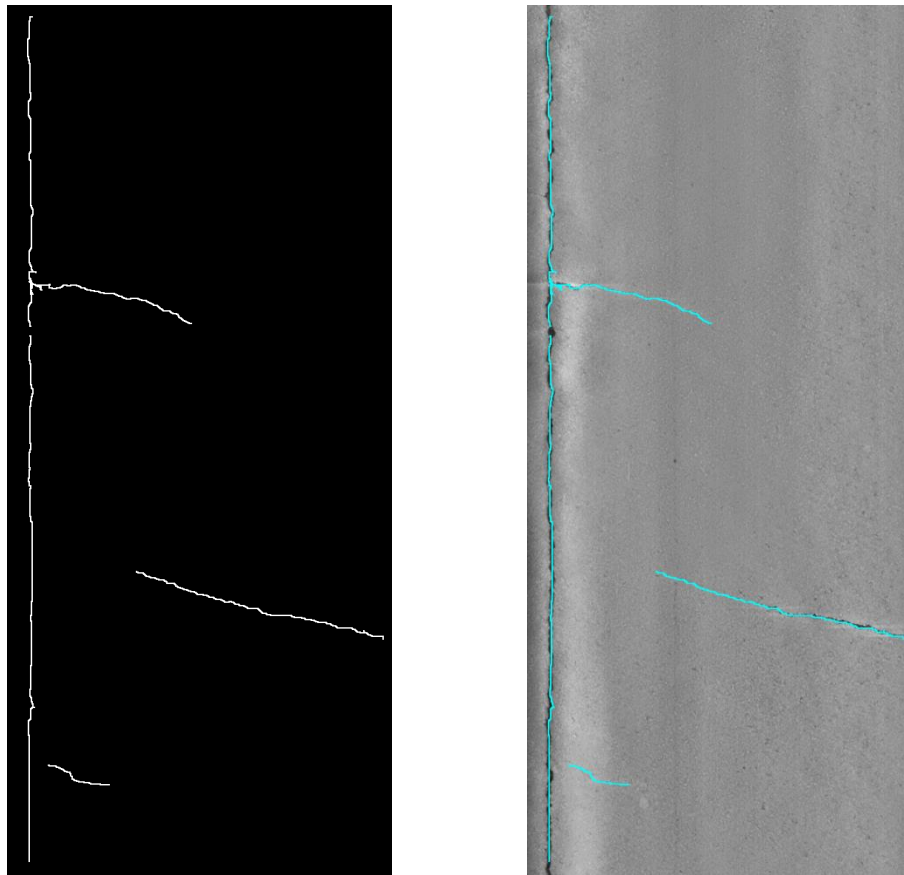


**Figure 3.8 Mean and STD of the pixel values along the detected crack curves**



(a) Final crack map after curve selection    (b) Final crack map on range image

**Figure 3.9 Illustration of crack curve selection to remove false positive detections**

### 3.2 Demonstration of the Proposed Algorithm

This section will further demonstrate the proposed algorithm using selected cases and illustrate how each step of the proposed algorithm works.

Figure 3.10 shows the case of a single transverse crack on the top of the image. Figure 3.10(a) shows the raw input image, and the subsequent figures show the intermediate and final results from each step of the proposed crack detection algorithm. A non-uniform background is observed in the image, which is corrected through the image enhancement step. The rectified image is shown in Figure 3.10(b). The adaptive thresholding and tensor voting are then applied on the rectified image to generate the crack potential map, and the results are shown in Figure 3.10(c). Despite the contrast between the crack and its neighborhood being very low on the rectified image, continuous crack patterns are clearly observed in the crack potential map. Then the key points are identified at the end and branch points through iterative morphological thinning and skeleton analysis (as shown in Figure 3.10(d)), and the crack curves between these key points are detected using the minimal path procedure (as shown in Figure 3.10(e)). A crack curve selection step is applied in the end to rule out possible false positive detections, and the final crack map is shown in Figure 3.10(f). It needs to be noted that there is a pavement scratch in the middle of the image, possibly caused by truck flat tires. It isn't considered pavement cracking, yet is still captured by the detection algorithm. It can be observed that the curve detected along the scratch is much smoother than normal cracks (i.e. the variance along its predominant orientation is much smaller than normal cracks), which can be used as a cue to further differentiate cracks and

scratches for the purpose of pavement condition survey. However, it is not within the scope of this study.

Figure 3.11 demonstrates the case in which the post-processing step helps provide a cleaner crack map. The pavement texture is non-homogeneous in the image: the bottom part is clearly rougher than the rest of the image. Under such a scenario, the thresholding step leaves a fair number of noise blobs in the image, which eventually lead to undesired key points (as shown in Figure 3.11(d)) and false crack curve detection (as marked in red circles in Figure 3.11(e)). The crack curve selection step removes the false detections, since their pixel values along the curve are too high, and the final crack map is shown in Figure 3.11(f).

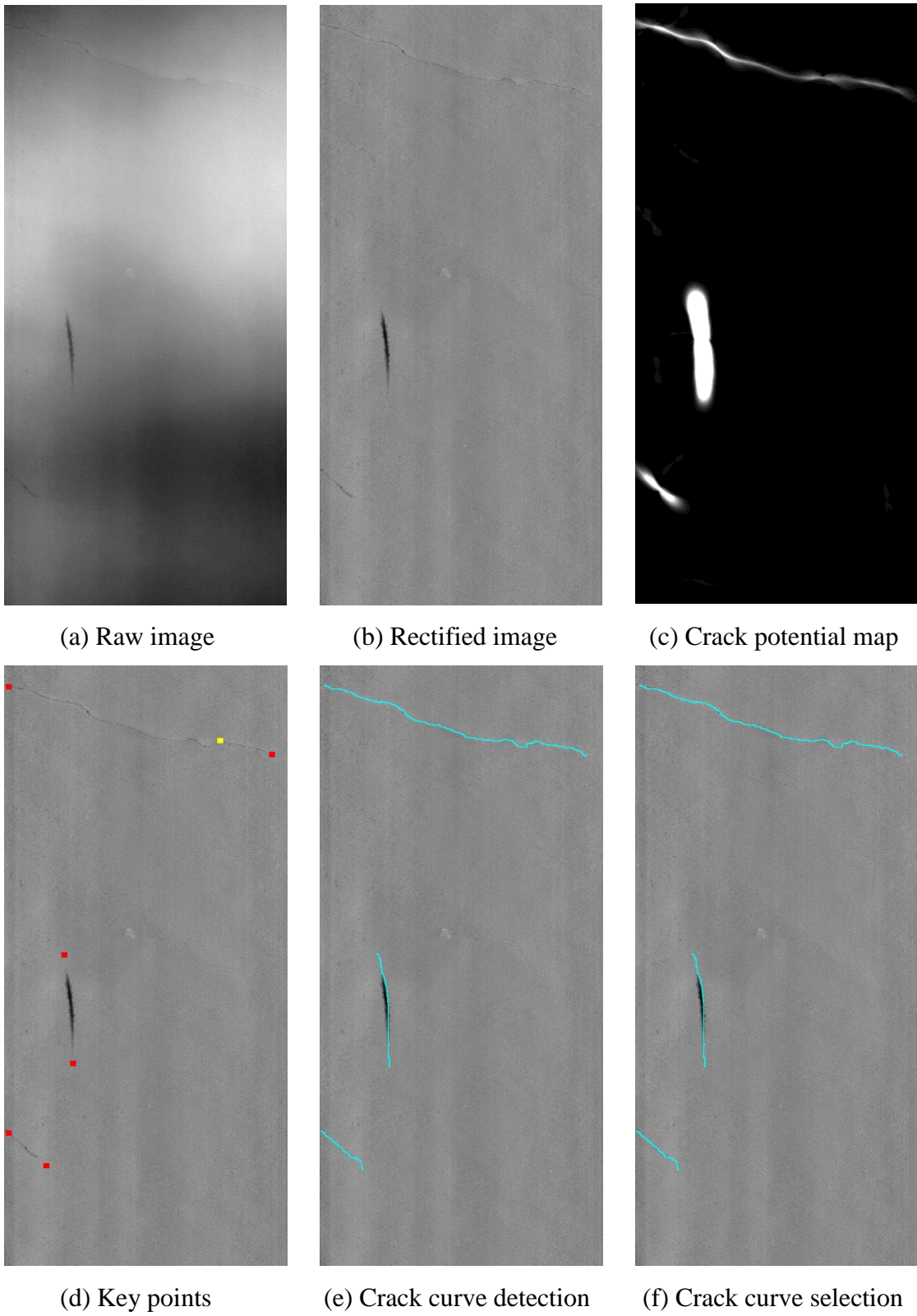
Figure 3.12 shows how the algorithm performs on the combination of cracks with different orientations. The proposed algorithm successfully captures the key points across the crack pattern and detects the crack curves in between. The final crack map is very close to the real crack pattern on the image through visual inspection.

Figure 3.13 shows a relatively challenging case in which the cracks are difficult to identify, even by human eyes. It can be seen that the proposed algorithm manages to capture the majority of the cracks on the image; however, it doesn't completely detect the connection between the crack curves and the hairline portion of the cracks.

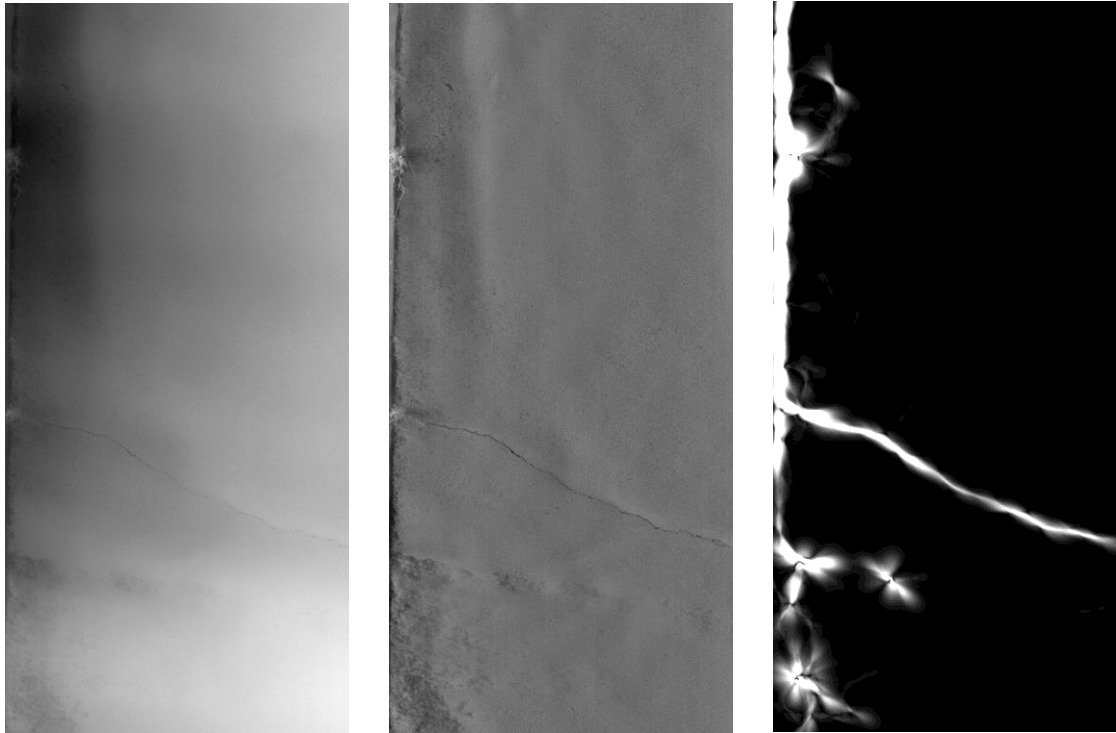
Figure 3.14 shows a case with alligator cracking, which is one of the most complex crack patterns on the real pavements. A large number of crack curves having various orientations intersect with each other and form small polygons. Such cases require a fair number of manual prior input points if using the original minimal path algorithm, which is tedious, subjective, and non-repeatable. On the other hand, the

proposed algorithm captures the crack pattern almost completely. Although there are limited missing cracks and false positive detections, they are not expected to influence the pavement condition assessment and maintenance decision-making.

Overall, the proposed algorithm performs robustly under a variety of scenarios. A comprehensive and quantitative evaluation will be presented in the next chapter.



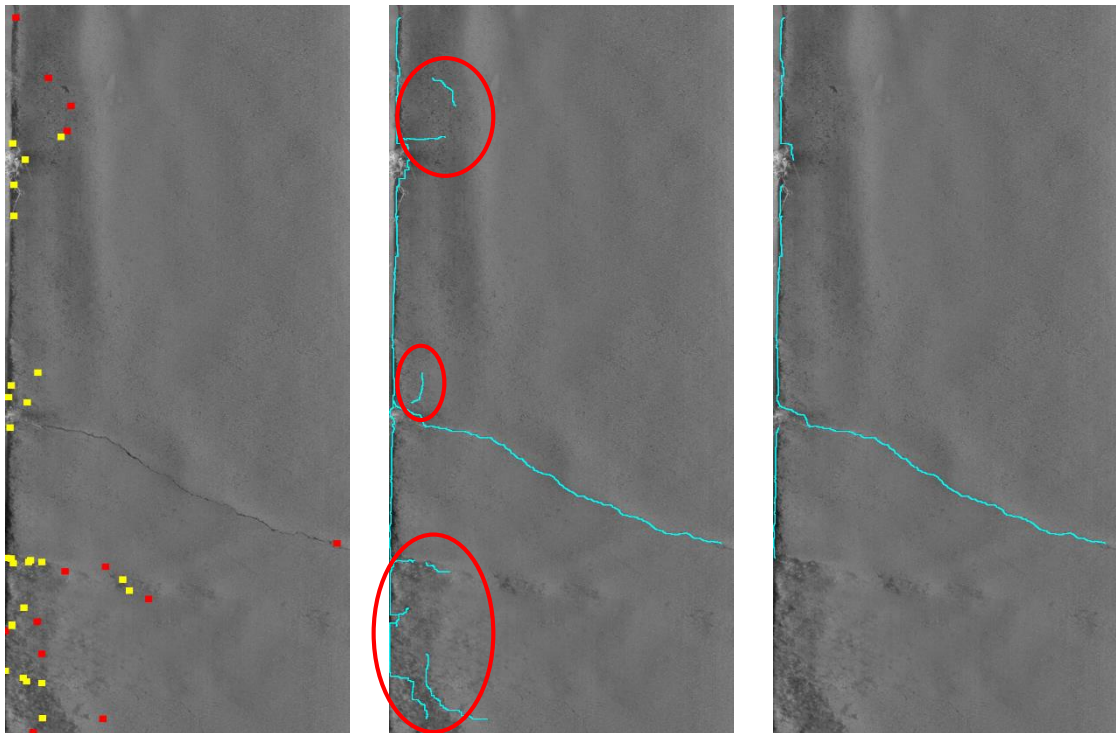
**Figure 3.10 Algorithm demonstration on Sample Image 1**



(a) Raw image

(b) Rectified image

(c) Crack potential map



(d) Key points

(e) Crack curve detection

(f) Crack curve selection

**Figure 3.11 Algorithm demonstration on Sample Image 2**

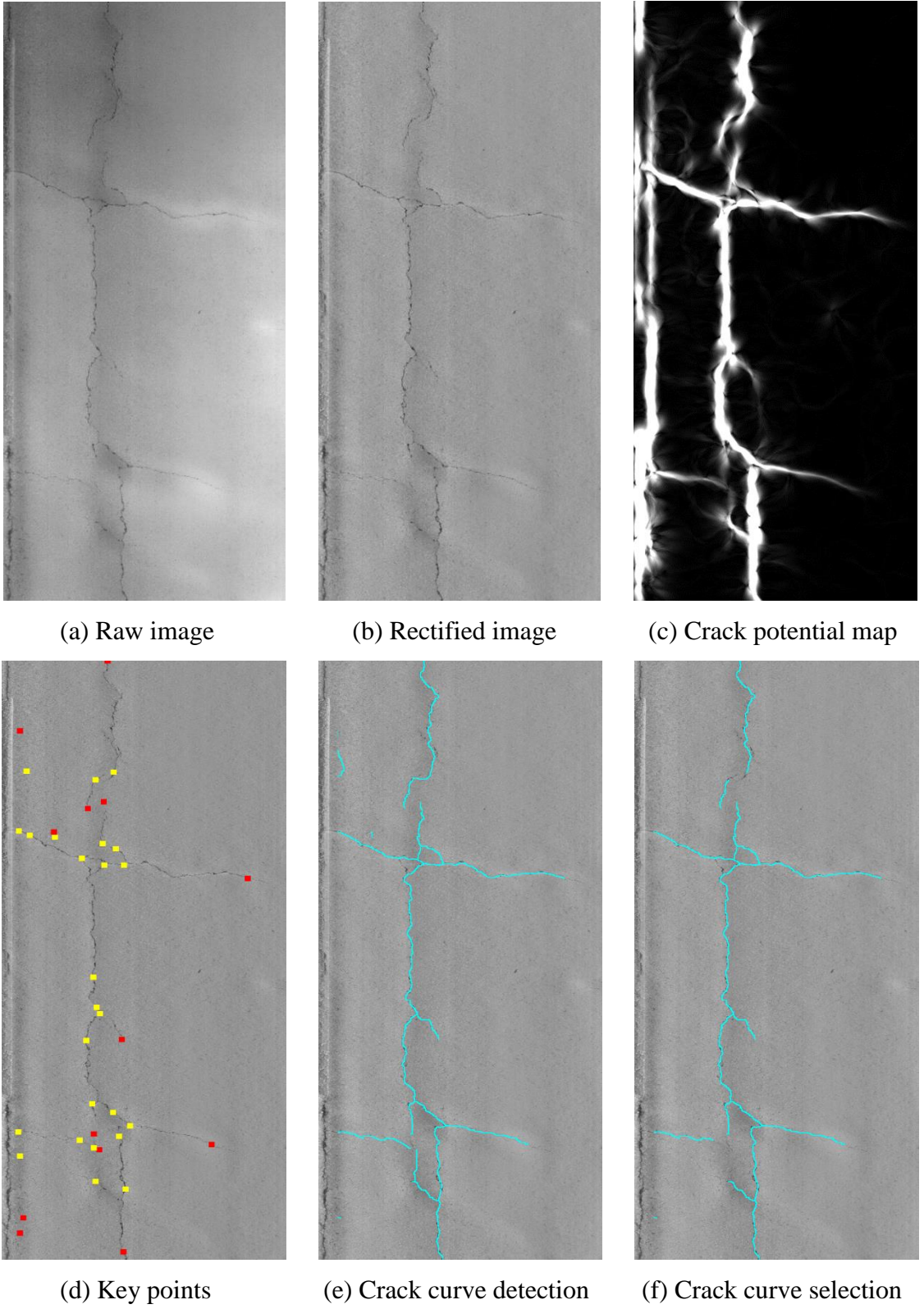


**Figure 3.12 Algorithm demonstration on Sample Image 3**



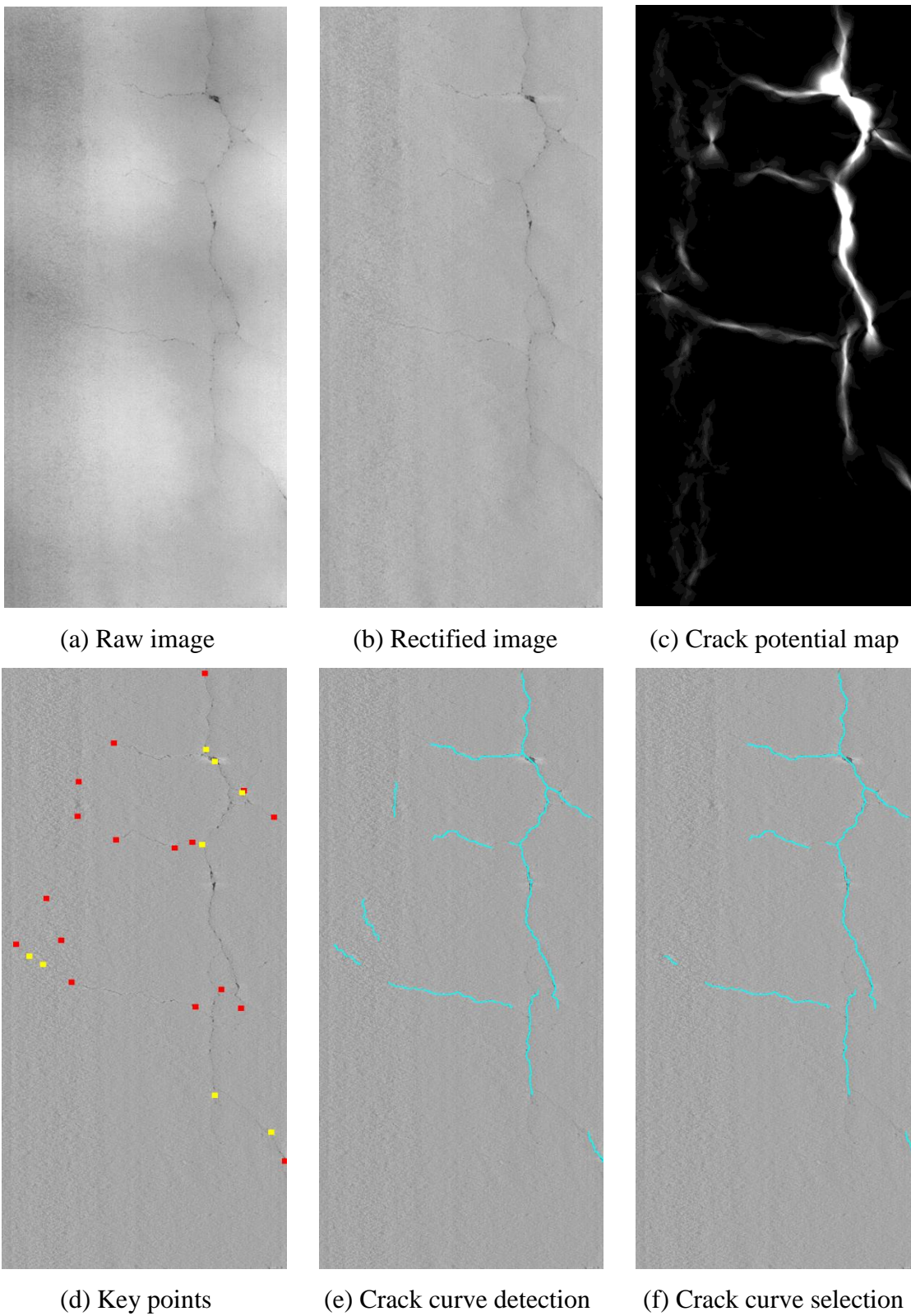


**Figure 3.13 Algorithm demonstration on Sample Image 4**



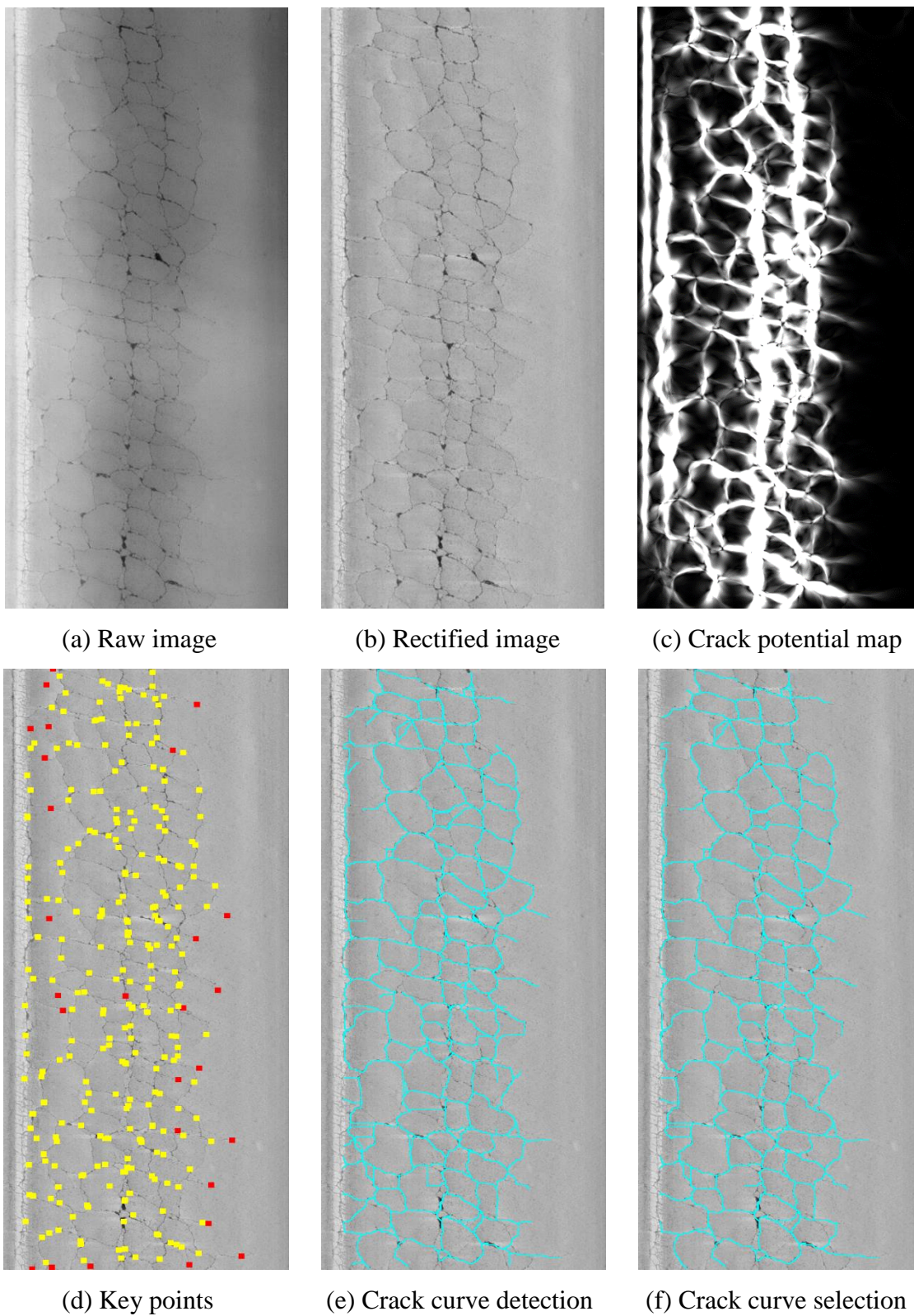


**Figure 3.14 Algorithm demonstration on Sample Image 5**

## **CHAPTER 4. PERFORMANCE EVALUATION OF THE PROPOSED ALGORITHM FOR CRACK DETECTION**

This chapter presents the performance evaluation of the proposed crack detection algorithm. It quantitatively evaluate the accuracy and repeatability of the proposed algorithm through comprehensive tests. The chapter is organized as follows: Section 4.1 demonstrates the algorithm performance on several synthetic pavement images, which contains common crack structures with artificially added noises. Section 4.2 evaluates the accuracy of the proposed algorithm on a diverse, real pavement image dataset. Three existing crack detection algorithms have also been incorporated through the experimental tests in order to demonstrate the improvements and superiority of the proposed algorithm. The buffered Hausdorff distance scoring method is employed to provide a quantitative comparison between the manual digitized ground truth and the crack maps detected by different algorithms. Section 4.3 evaluates the robustness and repeatability of the proposed algorithm. Two test sites are selected on real pavements, and multiple runs of pavement surface data are collected on the same sites. The detected crack maps are compared across these different runs.

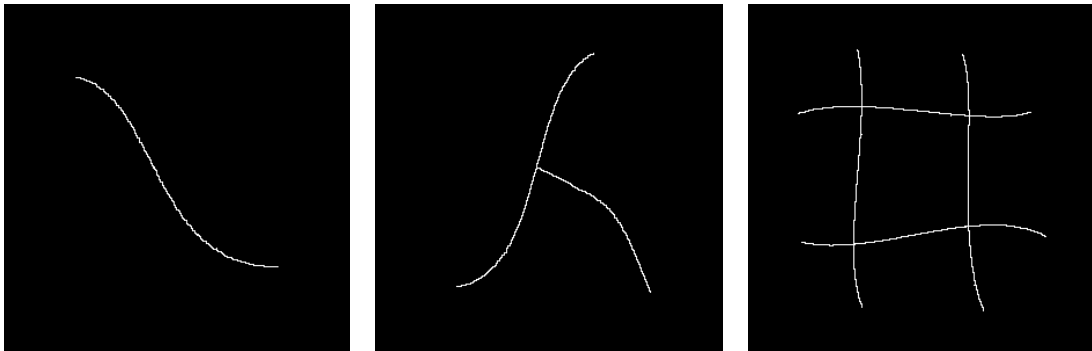
### **4.1 Demonstration on Synthetic Images**

Synthetic images are created to simulate how the proposed algorithm performs on the most fundamental crack structures in real pavements. The background intensity of the synthetic images is set to be 0.6, between 0 and 1, which has been observed to be the normal value for real pavement images after rectification. Three different crack structures are manually drawn on the background, including a single crack curve, a crack

intersection, and a crack polygon. More complex crack patterns in real pavements are usually a combination of these fundamental structures. The crack curves are drawn with one-pixel thickness and an intensity of 0.3. After that, a Gaussian noise with a mean of 0 and a standard deviation of 0.02 is added to each synthetic image to better simulate the roughness texture of real pavements and increase the challenge of crack detection. The strength of the noise is selected so that it will blur the distinction between backgrounds and cracks. The input synthetic images are shown in Figure 4.1(a). It can be observed that with the artificially added noises, some spots along the crack curves are already blurred into the background.



(a) Synthetic crack patterns with Gaussian noises (1-pixel-wide cracks)



(b) Detected crack maps using the proposed algorithm

**Figure 4.1 Performance demonstration on synthetic images**

The proposed crack detection algorithm is applied on these images, and the detected crack maps are shown in Figure 4.1(b). The algorithm performs quite well under

all three synthetic scenarios. The crack structures are detected almost completely with no false positive detections, and the existence of intersections and polygons in the crack structure doesn't influence the algorithm's performance. A closer inspection on the results reveals that there is sometimes a short portion (up to 5 pixel long on the given synthetic images) around the crack curve termini that are missed. The reasons are twofold: 1) in the proposed algorithm, the key points are generated through morphological operations on binary images and may not capture the exact endpoints of the crack curves, but they will be located closely; 2) the background noises tamper the crack curves near the ends. Overall, these artifacts are quite insignificant and are not expected to influence the subsequent crack condition assessment. In the following sections, we will further evaluate the proposed algorithm using real pavement images.

## 4.2 Accuracy Evaluation on Real Pavement Images

### 4.2.1 Buffered Hausdorff Distance Scoring Method

To effectively assess the accuracy of the proposed algorithm, a measuring method is required to quantify the difference between the ground truth and the algorithm-detected crack map. In this study, the buffered Hausdorff distance scoring method is adopted, which has demonstrated outstanding performance compared to four other measures under the task of evaluating the accuracy of crack detection algorithms (Kaul et al. 2009).

Suppose that  $G$  and  $S$  are the corresponding sets of crack pixels in the ground truth image and the detected crack map. The following distance is defined to measure the difference from  $G$  to  $S$  :

$$h(G, S) = \frac{1}{m} \sum_{a \in G} \min_{b \in S} \|a - b\| \quad (4.1)$$

where  $m$  is the number of crack pixels in  $G$ , and  $L$  is a buffer. This distance is designed as follows:

- First, for each crack pixel in  $G$ , a distance is calculated from it to  $S$ . This distance is defined as the smallest among its distances to all the pixels in  $S$ .
- Second, once a crack pixel in  $G$  falls substantially away from the closest pixel in  $S$ , it no longer makes sense to heavily penalize this distance. Wrong detections beyond a certain distance should be penalized equally. Therefore, a buffer  $L$  is introduced as the maximum penalization distance.
- Finally, we average the distances from each pixel in  $G$  to  $S$  as the distance from  $G$  to  $S$ .

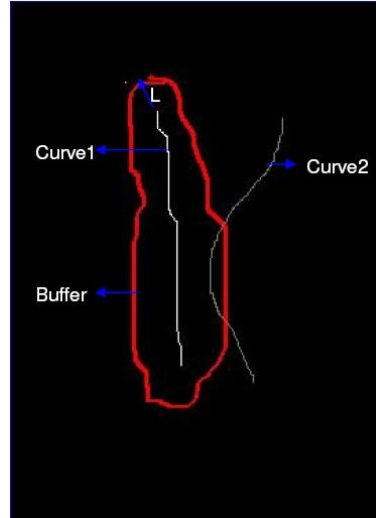


**Figure 4.2 Illustration of buffered Hausdorff distance (Kaul et al. 2009)**

In order to create a symmetric measure, the buffered Hausdorff distance is defined as follows:

$$BH(G, S) = \max(h(G, S), h(S, G)) \quad (4.2)$$

which is the larger of the distance from  $G$  to  $S$  and the distance from  $S$  to  $G$ . This ensures that the measure takes both false positive and negative detections into account. Based on the definition, if the crack pixels in  $G$  perfectly overlap with the ones in  $S$ , the buffered Hausdorff distance will be 0; on the other hand, if all the crack pixels in  $G$  are substantially far away from the ones in  $S$ , the buffered Hausdorff distance will be  $L$ . The buffered Hausdorff distance is further scaled into a score from 0 to 100:

$$Score = \left(1 - \frac{BH(G, S)}{L}\right) \times 100 \quad (4.3)$$

where a score of 100 indicates a perfect crack detection, and a score of 0 indicates the worst possible detection outcome. In this series of experimental tests, the buffer  $L$  is set to be 20, as suggested by Kaul et al. (2009), based on the resolution of the test images.

#### 4.2.2 Existing Crack Detection Algorithms for Benchmarking

In addition to the proposed algorithm, three existing crack detection algorithms are also used for performance comparison. These algorithms are as follows: 1) minimal path with one arbitrary input point (Kaul et al. 2012), which is a recent variant of the minimal path procedure in order to demonstrate the improvement of the proposed algorithm; 2) dynamic optimization algorithm (Alekseychuk 2006), which was introduced to pavement crack detection by Tsai et al. (2010). It is selected for comparison because it outperformed other existing algorithms in terms of detection accuracy and is considered as the best benchmark; and 3) LCMS commercial software (Laurent et al. 2008), which is a commonly used commercial package to analyze pavement surface distresses. These algorithms are briefly introduced as follows.

#### 4.2.2.1 Minimal Path

The proposed algorithm is built upon the active contour based minimal path procedure. Therefore, the minimal path procedure is used here to demonstrate the improvements of the proposed algorithm. As mentioned in the previous chapter, the active contour based minimal path procedure manages to provide accurate crack detection, yet requires user-input endpoints. Kaul et al. (2012) further improved the algorithm, which only required one arbitrary input point along the desired crack curve. We employed this variant of the minimal path procedure throughout the tests. Since this is still a semi-automatic process of crack detection, it is expected to generate accurate crack map outcomes. To achieve a fair comparison, we keep track of not only the detected crack maps, but also the user-input points through the tests and then compare them with the proposed algorithm, which is completely automatic and free of user inputs.

#### 4.2.2.2 Dynamic Optimization

Traditional crack detection algorithms, especially the local-based algorithms mentioned in the literature review, cannot be applied to low signal-to-noise ratio images that occur commonly in pavement image datasets; the detected crack maps contain discontinuous crack curves and fair number of isolated noises. An alternative approach is to formulate the crack detection problem as a global optimization task. The dynamic optimization algorithm proposed by Alekseychuk (2006) employs such an approach. It defines an objective function based on two primary parameters: the minimum signal-to-noise ratio of indications of interest (which controls algorithm sensitivity) and the a-priori probability of indication presence (which influences detection of indications with gaps). Then, under all possible shapes and positions of the crack indications, the one that

maximizes such an objective function are selected. This algorithm, which has previously been developed for medical images, was introduced to pavement crack detection by Tsai et al. (2010). It outperformed five other crack detection algorithms, including statistical thresholding, Canny edge detection, a multi-scale wavelet method, a crack seed identification method, and an iterative clipping method. Later, Jiang and Tsai (2013) further enhanced the algorithm and applied it to the 3D pavement data. Since the performance of this algorithm is parameter sensitive, the two key parameters are adjusted through trial and error for each image in this test in order to provide optimal crack detection results.

#### 4.2.2.3 LCMS Commercial Software

INO/Pavemetrics (Laurent et al. 2008) has developed a commercial system using the line laser imaging technique to collect 3D pavement surface data. Along with the hardware system, analyzer software has also been developed, which provides the functionality to automatically detect cracks from the data. This commercial software has been actively updated, and has been commonly used by many state DOTs and vendors. The most recent update (version 4.1.1) is used for comparison in this study; it was released in March 2015.

### **4.2.3 Performance Evaluation on Different Pavement Surface Textures**

In this section, the proposed algorithm is evaluated on pavement images with different surface textures. Three typical categories of pavement surface textures are selected: asphalt surface with dense graded mix, asphalt surface with open graded friction courses, and concrete surface. Ten real pavement images are selected in each category. The ground truth is manually digitized based on the original images. Four crack detection



algorithms, including the proposed algorithm, minimal path, dynamic optimization, and LCMS commercial software are used to generate the crack maps independently. The buffered Hausdorff distance scoring method is used to provide a quantitative evaluation on different algorithms. The results are summarized in Table 4.1.

**Table 4.1 Accuracy scores on different pavement surface textures**

Type	No.	Proposed Algorithm	Minimal Path (*)	Dynamic Optimization	LCMS Software (ver. 4.1.1)
Asphalt Surface: Dense Graded	1	100.0	100.0 (0)	100.0	100.0
	2	98.3	94.6 (3)	82.1	80.8
	3	100.0	100.0 (0)	100.0	100.0
	4	91.5	91.9 (5)	45.2	59.6
	5	96.4	89.6 (10)	79.8	78.0
	6	79.4	55.4 (64)	66.5	80.0
	7	87.0	61.2 (55)	66.1	87.0
	8	89.7	87.5 (5)	82.2	86.0
	9	92.5	91.0 (11)	65.9	77.3
	10	94.8	94.1 (2)	84.8	84.4
	AVG	93.0	86.5 (15.5)	77.3	83.3
Asphalt Surface: OGFC	11	0.0	100.0 (0)	100.0	0.0
	12	94.7	96.5 (4)	69.5	50.4
	13	91.2	96.3 (2)	88.2	88.7
	14	100.0	100.0 (0)	0.0	0.0
	15	97.1	90.3 (3)	64.5	58.6
	16	91.3	94.6 (2)	49.2	89.6
	17	99.0	95.0 (1)	83.8	88.3
	18	96.8	91.2 (4)	88.0	77.7
	19	100.0	100.0 (0)	0.0	100.0
	20	96.9	90.9 (5)	61.6	79.3
	AVG	86.7	95.5 (2.1)	60.5	63.3
Concrete Surface	21	100.0	100.0 (0)	0.0	0.0
	22	94.7	94.0 (2)	79.7	37.2
	23	95.4	92.8 (2)	82.4	43.7
	24	88.3	91.0 (1)	19.6	30.4
	25	98.0	94.2 (3)	67.7	47.6
	26	94.8	91.7 (3)	40.9	26.3
	27	98.7	86.5 (3)	46.6	28.2
	28	100.0	100.0 (0)	0.0	100.0
	29	77.8	92.3 (3)	7.4	40.2
	30	92.0	89.8 (5)	29.9	44.9
	AVG	94.0	93.2 (2.2)	37.4	39.9
Overall	AVG	91.2	91.7 (6.6)	58.4	62.2

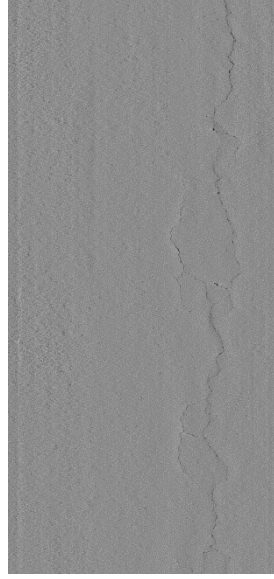
(\*) The number of the user-input points for minimal path are marked in the parenthesis.

#### 4.2.3.1 Asphalt Surface: Dense Graded

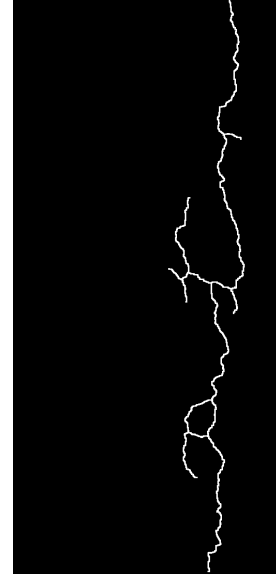
The asphalt surface with dense graded mix can usually be found on local highways. Since the HMA mixture is well-graded, the pavement surface with good condition is relatively smooth, which creates a better environment for crack detection task. On the other hand, the crack patterns on the local roads are quite diverse and complex, which brings challenge for the algorithms to capture the crack patterns completely.

Figure 4.3 shows an example of how the crack detection algorithm performs on this category. Figure 4.3(a) shows the rectified range image, and Figure 4.3(b) shows the manually digitized ground truth. Figure 4.3(c) – (f) are the detected crack maps generated by four different algorithms in the following order: the proposed algorithm, minimal path, dynamic optimization, and LCMS software. It can be observed that none of detected crack maps are exactly the same as the ground truth, but the proposed algorithm provides the closest result. For the minimal path algorithm, even with user-input points, it still fails to capture the transverse parts of the crack pattern. The dynamic optimization algorithm has a similar problem in this case. The LCMS software does manage to detect the general crack pattern on the image; however, the detected crack curves are mixed up and randomly connected together at some locations.

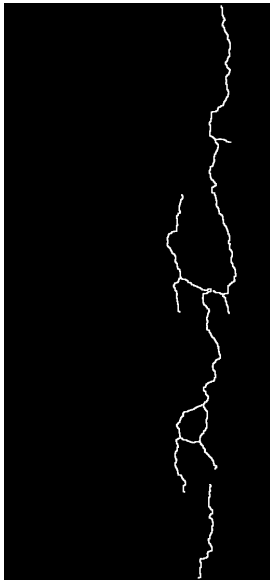
Based on Table 4.1, the proposed algorithm performs better than the other three algorithms with an average score of 93.0 in this category. The dynamic optimization algorithm suffers from both false positive and false negative detections, while the LCMS software fails to preserve the details of the crack patterns.



(a)



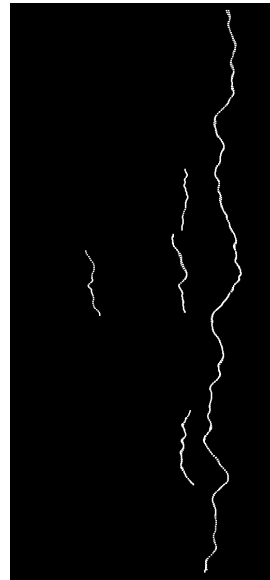
(b)



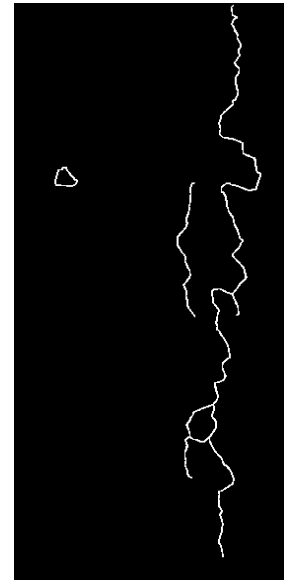
(c) Score = 96.4



(d) Score = 89.6



(e) Score = 79.8



(f) Score = 78.0

**Figure 4.3 Performance on asphalt dense graded surface (Image No. 5) (a) range image (b) ground truth crack map (c) proposed algorithm (d) minimal path (user-input points as red dots) (e) dynamic optimization (f) LCMS software (ver. 4.1.1)**

#### 4.2.3.2 Asphalt Surface: OGFC

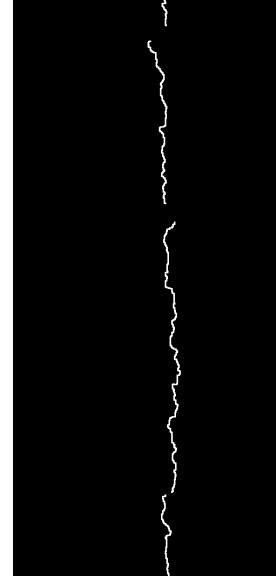
Open graded friction courses (OGFCs) are a type of pavement that have been built across the United States since the 1950's. They are mostly used on interstate highways. These asphalt mixes contain only a small portion of fine aggregate, creating a pavement with a relatively large percentage of air voids. Consequently, the pavement surface becomes much rougher, and the contrast between cracks and normal pavement backgrounds shrinks.

Figure 4.4 shows a case with OGFC surface, where the proposed algorithm demonstrates an outstanding performance. This is mainly because that through the tensor voting framework, the isolated noises in the background are suppressed, and the potential crack curves are enhanced. The minimal path algorithm provides a close result with user-input key points. The major issue for the dynamic optimization algorithm is that it captures a long false positive crack curve on the left, which directly impacts the score. The LCMS software appears to be less robust under the existence of noise; the detected crack curve meanders from the real cracks into the background.

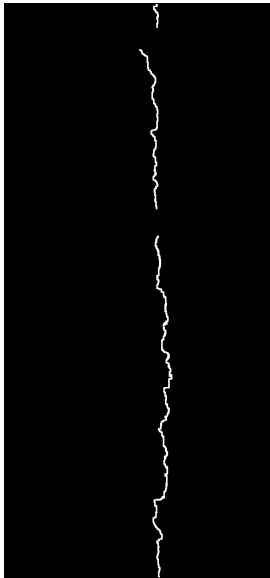
The results in Table 4.1 show that the minimal path algorithm does a better job in this category. A score of 0 is observed on Image No. 11 with the proposed algorithm. As shown in Figure 4.5, this is because it detects false crack curves on an image with no cracks. On the other hand, with manual inputs, the minimal path algorithm avoids the false positive detections. Besides this single image, the proposed algorithm shows consistent performance in the other cases.



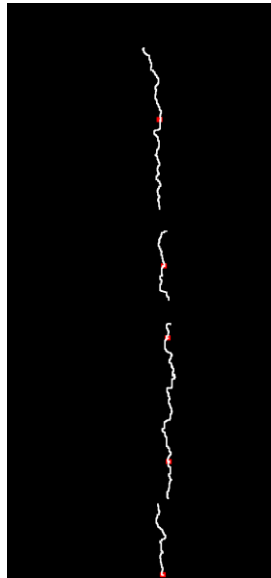
(a)



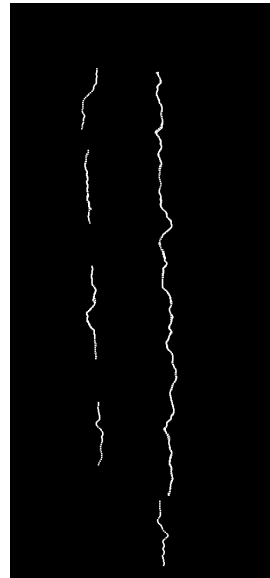
(b)



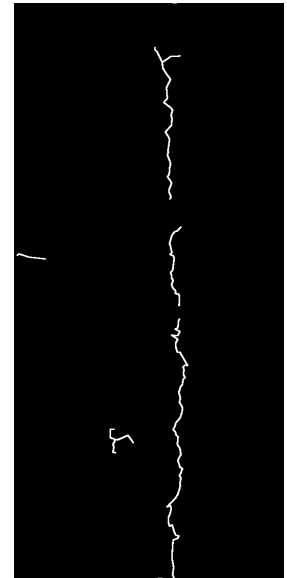
(c) Score = 96.9



(d) Score = 90.9

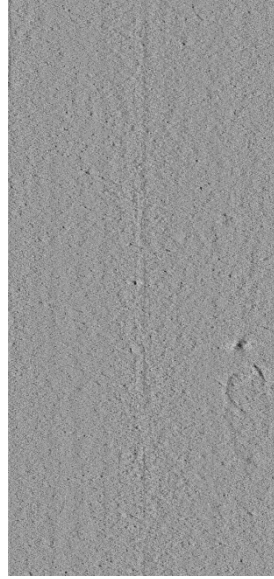


(e) Score = 61.6



(f) Score = 79.3

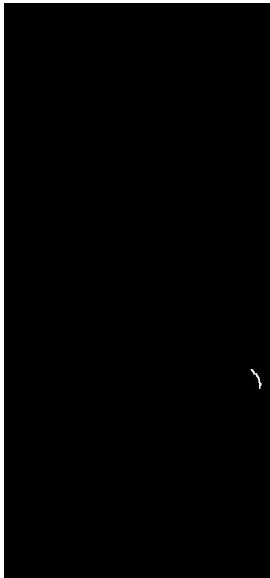
**Figure 4.4 Performance on asphalt OGFC surface (Image No. 20) (a) range image (b) ground truth crack map (c) proposed algorithm (d) minimal path (user-input points as red dots) (e) dynamic optimization (f) LCMS software (ver. 4.1.1)**



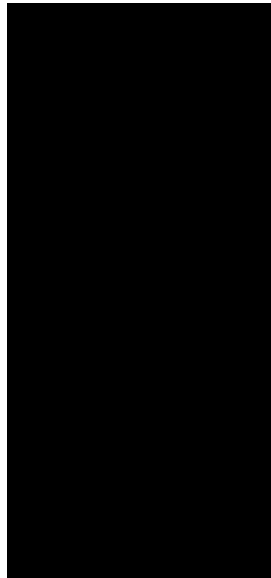
(a)



(b)



(c) Score = 0.0



(d) Score = 100.0



(e) Score = 100.0



(f) Score = 0.0

**Figure 4.5 Performance on asphalt OGFC surface (Image No. 11) (a) range image (b) ground truth crack map (c) proposed algorithm (d) minimal path (user-input points as red dots) (e) dynamic optimization (f) LCMS software (ver. 4.1.1)**

#### 4.2.3.3 Concrete Surface

Concrete surface is often built on interstate highways, bridges, and specific locations on local highways, such as intersections. Unlike asphalt surface, which is usually a mixture of aggregates, it is topped with complete concrete layers. Therefore, the surface is smoother with fewer isolated noises for crack detection. Concrete surface is often grooved with longitudinal or transverse texture to increase friction. The crack detection algorithms need to be robust to these surface textures.

Figure 4.6 shows an example of crack detection on concrete pavement surface. It needs to be noted that since construction joints and cracks share some very similar characteristics on the images, none of these crack detection algorithms has the capability to differentiate them. Thus, to achieve a fair comparison, the construction joints are counted as part of the ground truth (e.g. the horizontal line shown in Figure 4.6(b)). The crack map detected by the proposed algorithm is almost identical compared to the ground truth. For a minimal path algorithm, it fails to detect the bottom part of the longitudinal crack, which appears to be very thin and discontinuous on the image. False positive detections are the major issue for dynamic optimization and LCMS software. The dynamic optimization captures the light scratch in the middle of the image, while the false positives of LCMS software are randomly distributed across the image. The proposed algorithm uses the local variance to determine the initial tokens that go into the tensor voting framework. Therefore, it is less sensitive to some light scratches, as the one in the middle of the image.

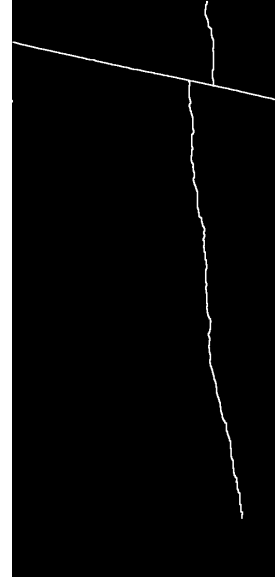
In this category, the performance of LCMS software degrades significantly, given the excess existence of false positive detections. The dynamic optimization performs



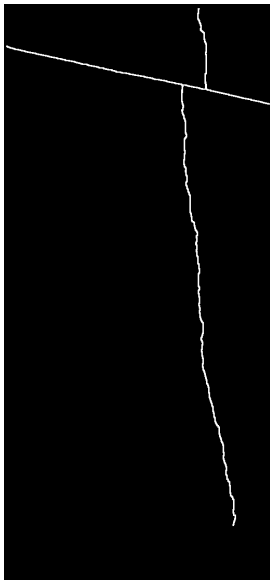
slightly better, but it also suffers from both false positive and false negative errors. The proposed algorithm and the minimal path algorithm present similar performance.



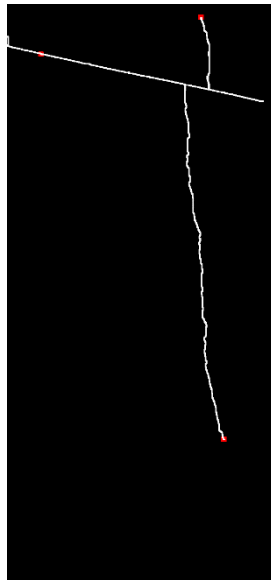
(a)



(b)



(c) Score = 98.7



(d) Score = 86.5



(e) Score = 46.6



(f) Score = 28.2

**Figure 4.6 Performance on concrete surface (Image No. 27) (a) range image (b) ground truth crack map (c) proposed algorithm (d) minimal path (user-input points as red dots) (e) dynamic optimization (f) LCMS software (ver. 4.1.1)**

In summary, the proposed algorithm has demonstrated superior performance with all three pavement surface textures with an overall average score of 91.2. The crack detection results with asphalt dense-graded surfaces and concrete surfaces are consistently better than the other three algorithms, while improvements can be made with asphalt surfaces with rougher texture. It needs to be noted that the minimal path algorithm's performance is close to the proposed algorithm, but about 7 user-input points are, on average, required on each image.

#### **4.2.4 Performance Evaluation on Different Crack Patterns**

In this section, the proposed algorithm is evaluated on pavement images with different crack patterns. Five categories of crack patterns are selected, mainly based on crack types, including no cracking, longitudinal cracking, transverse cracking, the combination of longitudinal and transverse cracking, and alligator cracking. For the second and third categories, cracks with various widths are selected to compose a diverse test set. Five real pavement images are selected in each category. These selected images are all with asphalt dense graded surfaces. Similarly, the ground truth is manually digitized based on the original images. Four crack detection algorithms are applied to generate the crack maps independently. The buffered Hausdorff distance scoring method is then used to evaluate the algorithm quantitatively. The experimental results are summarized in Table 4.2.

In the first category, the proposed algorithm doesn't generate any false positive detections on the pavement images with no cracking. Comparatively, the issue on dynamic optimization and LCMS software still exists. It needs to be noted that the current evaluation process is not able to reveal how much false positive detection has

been generated when the input image contains no crack at all. It is possible that only a short curve is falsely detected, yet the scoring method still shows zero.

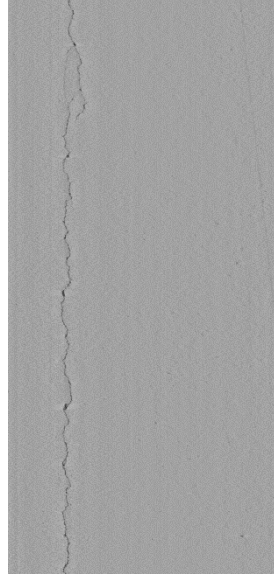
All the algorithms perform relatively well on the second category (longitudinal cracking), which contains longitudinal cracking. The proposed algorithm and the minimal path algorithm lead the performance, followed by the LCMS software. As shown in Figure 4.7, the dynamic optimization is oversensitive to any potential linear features on the image, constantly capturing false positive crack curves. On the other hand, the proposed algorithm appears to be more robust.

The third category is pavement images with transverse cracking. For the pavement data acquisition system used in this study, the scanning interval along driving direction is five times the one along transverse direction. Consequently, the transverse cracks are usually more challenging to differentiate on the images. Figure 4.8 shows such an example in which the transverse cracking on the middle of the image mostly blurs into the background, and it is difficult to differentiate even by human eyes. None of the four crack detection algorithms capture the entire crack curve. The three algorithms, except dynamic optimization, detect the majority of the crack curve but into multiple segments. The proposed algorithm and the minimal path algorithm manage to achieve it without introducing extra false detections. For dynamic optimization, a horizontal line is falsely detected in the middle of the image; for the LCMS software, some random false detections are observed on the bottom-left corner of the image. Overall, the proposed algorithm and the minimal path algorithm outperform the other two automatic algorithms in detecting transverse cracks, which are mostly vague and discontinuous on the images.

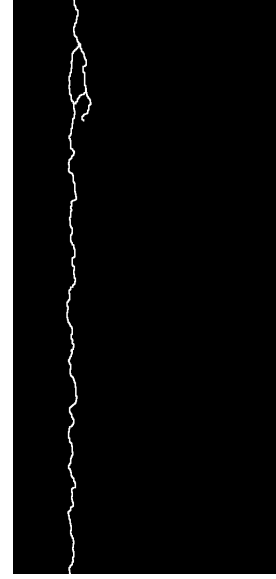
**Table 4.2 Accuracy scores on different crack patterns**

Crack Type	No.	Proposed Algorithm	Minimal Path (*)	Dynamic Optimization	LCMS Software (ver. 4.1.1)
No Cracking	31	100.0	100.0 (0)	100.0	100.0
	32	100.0	100.0 (0)	100.0	0.0
	33	100.0	100.0 (0)	100.0	100.0
	34	100.0	100.0 (0)	0.0	100.0
	35	100.0	100.0 (0)	0.0	100.0
	<b>AVG</b>	<b>100.0</b>	<b>100.0 (0)</b>	<b>60.0</b>	<b>80.0</b>
Longitudinal Cracking	36	96.4	89.6 (10)	79.8	78.0
	37	88.5	92.2 (5)	76.2	84.9
	38	95.6	94.1 (3)	84.2	81.7
	39	88.1	88.0 (2)	63.0	85.1
	40	94.8	94.1 (2)	84.8	84.4
	<b>AVG</b>	<b>92.7</b>	<b>91.6 (4.4)</b>	<b>77.6</b>	<b>82.8</b>
Transverse Cracking	41	90.8	76.9 (4)	62.7	58.6
	42	98.3	94.6 (3)	82.1	80.8
	43	91.5	91.9 (5)	45.2	59.6
	44	96.2	98.8 (1)	91.3	20.1
	45	90.3	94.7 (4)	64.9	87.2
	<b>AVG</b>	<b>93.4</b>	<b>91.4 (3.4)</b>	<b>69.2</b>	<b>61.3</b>
Combination of Longitudinal and Transverse Cracking	46	97.0	94.0 (4)	87.1	84.4
	47	89.7	88.2 (4)	66.4	92.3
	48	89.7	87.5 (5)	82.2	86.0
	49	92.5	91.0 (11)	65.9	77.3
	50	94.0	91.2 (10)	79.6	67.5
	<b>AVG</b>	<b>92.6</b>	<b>90.4 (6.8)</b>	<b>76.2</b>	<b>81.5</b>
Alligator Cracking	51	84.1	61.1 (57)	68.9	79.5
	52	79.4	55.4 (64)	66.5	80.0
	53	85.2	59.1 (58)	66.7	83.5
	54	86.0	57.0 (52)	69.5	85.3
	55	87.0	61.2 (55)	66.1	87.0
	<b>AVG</b>	<b>84.3</b>	<b>58.8 (57.2)</b>	<b>67.5</b>	<b>83.1</b>
<b>Overall</b>	<b>AVG</b>	<b>92.6</b>	<b>86.4 (14.4)</b>	<b>70.1</b>	<b>77.7</b>

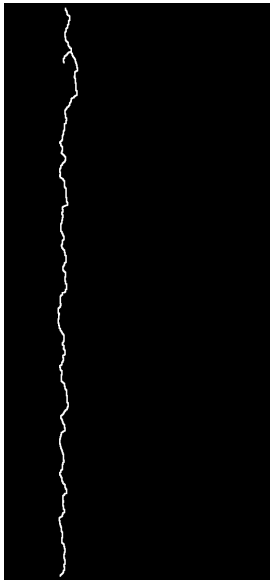
(\*) The number of the user-input points for minimal path is marked in the parenthesis.



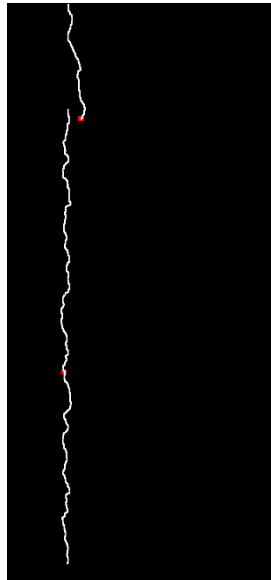
(a)



(b)



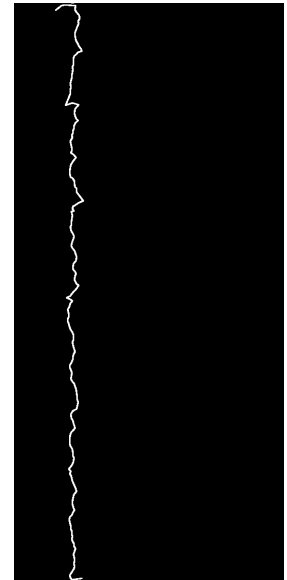
(c) Score = 88.1



(d) Score = 88.0



(e) Score = 63.0

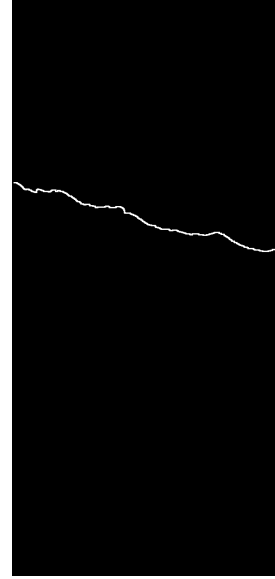


(f) Score = 85.1

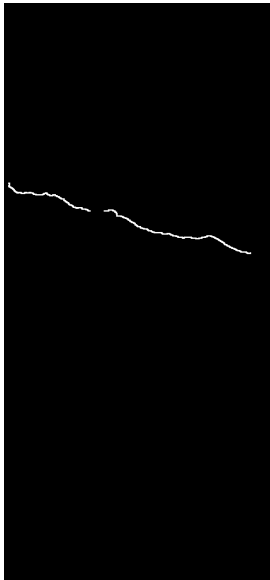
**Figure 4.7 Performance on longitudinal cracking (Image No. 39) (a) range image (b) ground truth crack map (c) proposed algorithm (d) minimal path (user-input points as red dots) (e) dynamic optimization (f) LCMS software (ver. 4.1.1)**



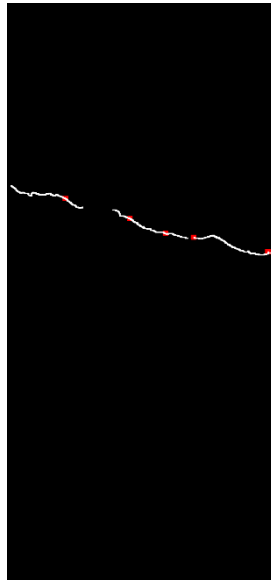
(a)



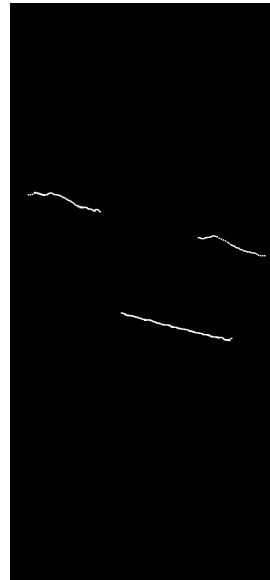
(b)



(c) Score = 91.5



(d) Score = 91.9



(e) Score = 45.2



(f) Score = 59.6

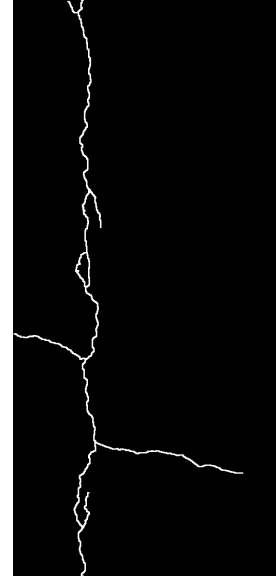
**Figure 4.8 Performance on transverse cracking (Image No. 43) (a) range image (b) ground truth crack map (c) proposed algorithm (d) minimal path (user-input points as red dots) (e) dynamic optimization (f) LCMS software (ver. 4.1.1)**

Similar to longitudinal cracking, all four algorithms perform relatively well on the fourth category, which contains the combination of longitudinal and transverse cracking. Figure 4.9 shows an example in this category. All four algorithms manage to detect the general crack pattern on the image. The crack map generated by the LCMS software appears bizarre near the crack terminus, where the crack curves randomly and meanders into the background. As shown on the ground truth, there are some small branching structures along the major crack curves. However, none of the algorithms detect these fine structures completely. The proposed algorithm captures some of them but misses the others, while the dynamic optimization algorithm fails to preserve any of these small branches.

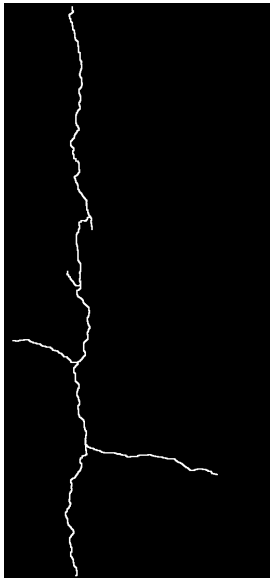
Alligator cracking is another challenging category in which the crack patterns consist of many short curves on various orientations and an excessive number of crack intersections and polygons. In addition, the crack widths inside the alligator pattern are not uniform, and the crack curves can be quite vague in many cases. It is interesting to see that the minimal path algorithm basically doesn't work on alligator cracking. As shown in Figure 4.10, user-input points have been assigned all across the image; however, the complex crack pattern triggers the termination criteria almost immediately, leaving short and fragmented curves with each input point. The dynamic optimization algorithm performs slightly better and successfully captures the larger polygons across the alligator pattern, but it misses the smaller ones inside. The proposed algorithm misses some short crack curves, and the LCMS software randomly adds false positive curves into the detected crack map. Overall, the crack detection performance in this category is not as good as in the previous four categories, but still relatively acceptable.



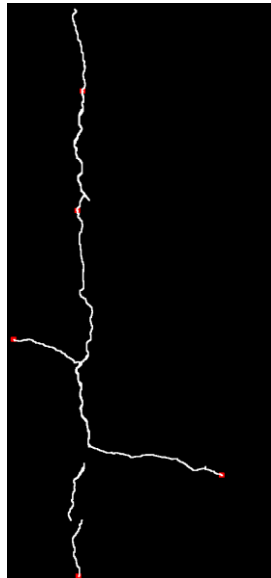
(a)



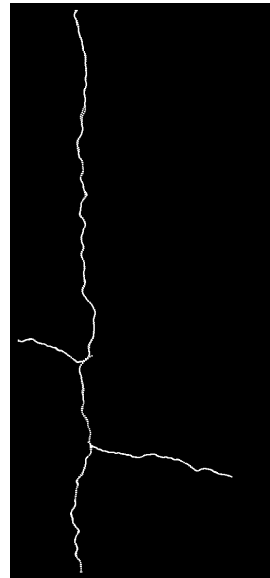
(b)



(c) Score = 89.7



(d) Score = 87.5



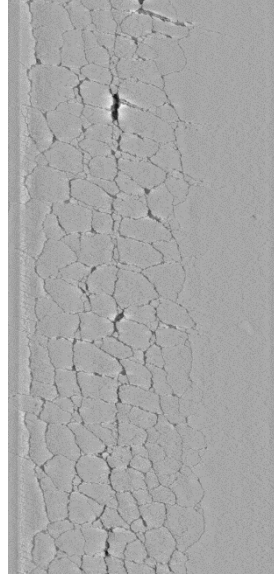
(e) Score = 82.2



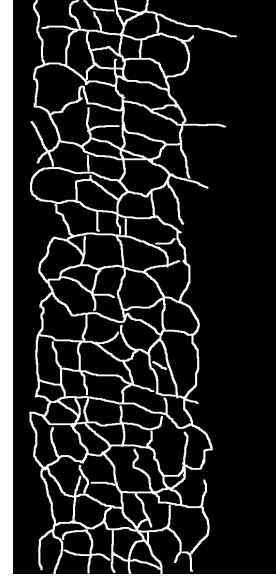
(f) Score = 86.0

**Figure 4.9 Performance on the combination of longitudinal and transverse cracking (Image No. 48) (a) range image (b) ground truth crack map (c) proposed algorithm (d) minimal path (user-input points as red dots) (e) dynamic optimization (f) LCMS software (ver. 4.1.1)**

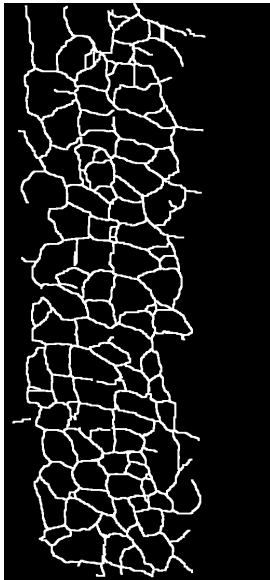




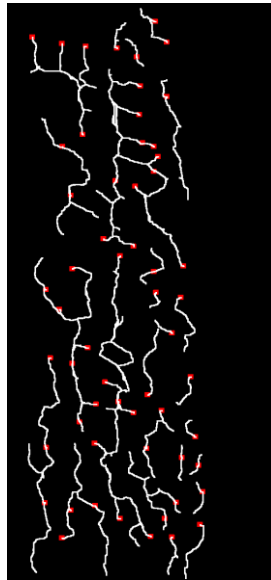
(a)



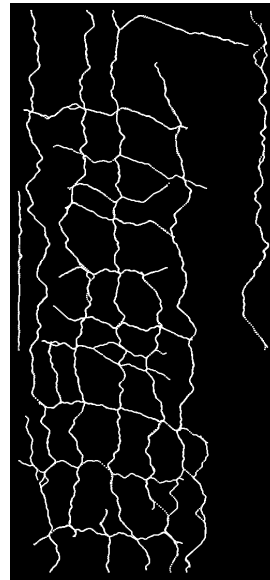
(b)



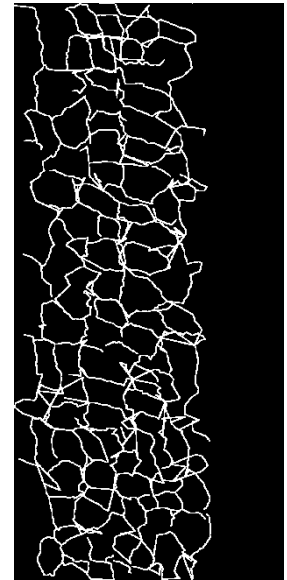
(c) Score = 85.2



(d) Score = 59.1



(e) Score = 66.7



(f) Score = 83.5

**Figure 4.10 Performance on alligator cracking (Image No. 53) (a) range image (b) ground truth crack map (c) proposed algorithm (d) minimal path (user-input points as red dots) (e) dynamic optimization (f) LCMS software (ver. 4.1.1)**

In short, the proposed algorithm has demonstrated robust performance with different crack patterns, having an overall average score of 92.6. Specifically, it shows

better capability to capture vague and discontinuous cracks that are difficult to identify (even by human eyes) from the pavement images. The accuracy with alligator cracking is slightly lower than with the other categories, but the results are still acceptable; based on the detected crack map, one can still determine alligator crack patterns for subsequent pavement condition assessment.

In addition to accuracy evaluation, we also compare the computation time between the three automatic detection algorithms. The results are shown in Table 4.3. These results are generated on the same desktop computer with Intel Xeon E3 3.30GHz and 32.0GB RAM. The dynamic optimization and LCMS software are released libraries in C/C++, while the proposed algorithm is currently implemented in MATLAB.

- First, the LCMS software significantly outperforms the other two algorithms. The crack detection is finished in about 1 second, even on the most complex alligator patterns. The proposed algorithm follows with an average computation time of 59.5 seconds on the selected images. The dynamic optimization is the slowest of the three algorithms, having an average processing time of almost 2 minutes.
- Second, it can be observed that the computation time for all three algorithms is related to the complexity of the crack pattern. For the proposed algorithm, the complex crack pattern (such as alligator cracking) significantly increases the number of crack-like pixels after the rough thresholding at the beginning. These pixels are the input tokens for the tensor voting framework. This increases the computation through the tensor voting, correspondingly, and, thus, increases the computation time.

**Table 4.3 Computation time on different crack patterns (unit: second)**

Crack Type	No.	Proposed Algorithm	Dynamic Optimization	LCMS Software (ver. 4.1.1)
No Cracking	31	22.4	31.8	0.5
	32	13.9	57.9	0.5
	33	13.2	22.9	0.6
	34	35.4	84.0	0.5
	35	32.6	66.7	0.5
	<b>AVG</b>	<b>23.5</b>	<b>52.7</b>	<b>0.5</b>
Longitudinal Cracking	36	23.8	111.5	0.5
	37	39.4	65.6	0.5
	38	38.3	57.2	0.5
	39	37.9	63.6	0.5
	40	30.3	39.4	0.5
	<b>AVG</b>	<b>34.0</b>	<b>67.5</b>	<b>0.5</b>
Transverse Cracking	41	11.1	170.0	0.5
	42	13.1	66.9	0.4
	43	12.4	93.0	0.5
	44	17.5	66.7	0.5
	45	15.1	92.9	0.5
	<b>AVG</b>	<b>13.8</b>	<b>98.0</b>	<b>0.5</b>
Combination of Longitudinal and Transverse Cracking	46	53.5	123.5	0.6
	47	36.7	39.6	0.5
	48	38.3	74.7	0.5
	49	23.7	116.4	0.6
	50	37.9	99.5	0.7
	<b>AVG</b>	<b>38.0</b>	<b>90.7</b>	<b>0.6</b>
Alligator Cracking	51	174.2	181.0	0.9
	52	142.7	262.4	0.9
	53	186.5	311.1	1.9
	54	214.2	301.3	1.1
	55	222.4	298.4	1.1
	<b>AVG</b>	<b>188.0</b>	<b>270.8</b>	<b>1.2</b>
<b>Overall</b>	<b>AVG</b>	<b>59.5</b>	<b>116.0</b>	<b>0.7</b>

(\*) The number of the user-input points for minimal path is marked in the parenthesis.

- To further improve the computation speed of the proposed algorithm, incorporating parallel processing through the tensor voting framework and the minimal path based crack curve findings is suggested. From the perspective of computation time, the major bottleneck of the current algorithm is the tensor voting framework. In this process, each token will independently cast votes to its neighborhood. Therefore, these votes can be calculated in a parallel manner and then added together. After the key points are identified, the crack curve detection between every pair of key points are again an independent process, the efficiency of which can also be improved if conducted in parallel. As this study focuses on improving the accuracy of the crack detection algorithm, the implementation of these strategies is beyond the scope. It is recommended to conduct future research for practical implementation.

### **4.3 Repeatability Test**

The limitations of traditional manual crack surveys have not only low productivity and safety concerns, but also repeatability and reproducibility concerns. Human judgment can be subjective; on the same pavement section, different raters may provide different opinions on the pavement condition. For automatic crack detection algorithms, the detected crack maps need to be both accurate and repeatable. Since the previous section has validated the accuracy of the proposed algorithm, this section will demonstrate its repeatability.

The repeatability test in this study does not refer to applying the crack detection algorithm on the same pavement images several times. We are more interested in how the algorithm performs on the pavement images collected from multiple runs on the same

site. The detected crack maps are expected to be different between multiple runs, because of the following:

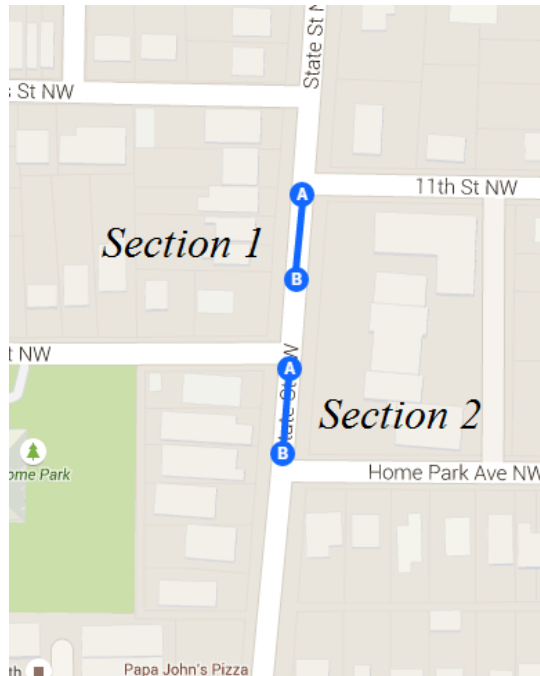
- The collected pavement images are naturally different. The vehicle movement speed, sensor condition, and environment factors all have more or less influence on the collected images, although such influence is expected to be limited with the emerging sensing techniques. For example, the vehicle heading orientation may have a direct impact on the similarity between detected crack maps. The vehicle may lean slightly towards left or right during the data collection process. Consequently, a perfectly oriented longitudinal crack in one crack map may appear at a different angle in another crack map.
- The image-splitting process may impact the proposed crack detection algorithm. The pavements are continuous on the road. However, for the convenience of data storage and analysis, the continuous pavements are split into multiple consecutive images through the data collection. One single crack is very likely to be located at different regions on the pavement images. Considering that the proposed algorithm emphasizes the continuity of the crack curves, this may potentially influence the crack detection outcomes.

In order to evaluate how different the detected crack maps between multiple runs are, the experimental tests are conducted as follows:

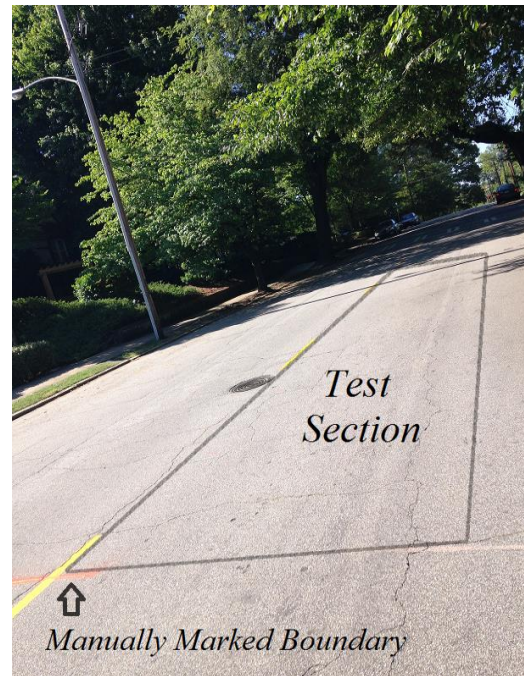
- Two 100-ft. sections are manually marked on State Street in Atlanta, Georgia. The terminus of the sections are labeled on the pavement for consistent comparison between multiple runs. Figure 4.11 shows the selected test sections.

The combination of longitudinal and transverse cracking is the major crack pattern in the selected sections.

- Five runs of pavement data are collected on each site. The data used in this study were collected between 1 – 2 pm on February 2, 2015. The environment was relatively consistent during the data collection.
- The proposed algorithm is applied on all the collected pavement images.
- The detected crack maps are manually cropped to make sure that the comparison is consistent based on the exact same areas between multiple runs. The marked section termini are the boundaries of the survey area along driving direction. The right edge of the left lane marker is the left boundary of the survey area; the survey area extend 2.8 meters from this boundary to the right.
- The cropped crack maps are merged together and compared.



(a) Locations of test sections



(b) Illustration of a test section

**Figure 4.11 Selected sections for repeatability test**

To begin with, the crack length statistics are compared, which is the most fundamental crack property that can be extracted from the crack map. Each 100-ft. section is further separated into five 20-ft. sections; within each section, the total crack length is calculated from different runs. The results on the first section are shown in Figure 4.12. We employ the statistical indicator “relative standard deviation” to describe the difference between multiple runs. It is defined as follows:

$$RSD = \left| \frac{SD}{Mean} \right| \times 100\% \quad (4.4)$$

which is standard deviation of the total crack length with respect to the average of the total crack length. The RSD value for each section is labeled above the bars in Figure 4.12. On the first site, the overall RSD of the total crack length is 0.86%.

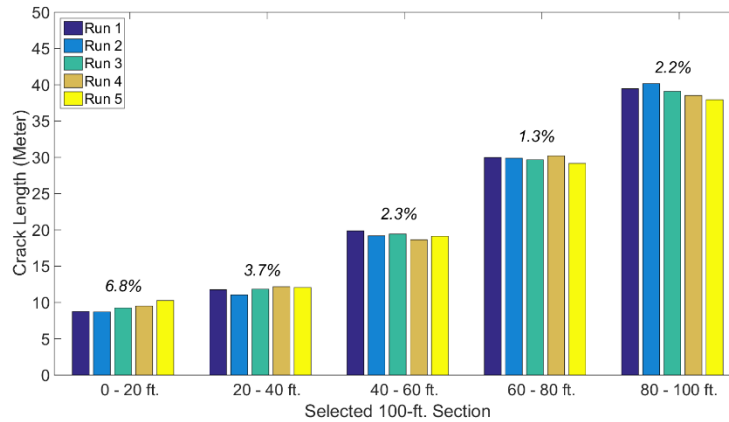


**Figure 4.12 Crack length statistics in five different runs collected on Section 1**

Similarly, the crack length statistics on the second section are shown in Figure 4.13. A larger variance is observed in this section. Specifically, there is a relatively large difference on the part of 40-60 ft. between Run 4 and Run 5, as highlighted. Figure 4.14 compares the detected crack maps on this specific spot. It can be observed that the crack maps are generally similar to each other; however, the detection of the transverse cracks

(inside the red box) is not satisfactory. This is because the transverse crack happens to be at the conjunction between two consecutive images in Run 4; consequently, the crack continuity is broken, and the crack feature is not significant in either image; thus, the challenge for detection is increased. The overall RSD of total crack length on this site is 2.20%. Based on the experimental results, we can see that the difference between the detected crack maps in multiple runs does exist, but is rather insignificant from the perspective of crack length statistics.

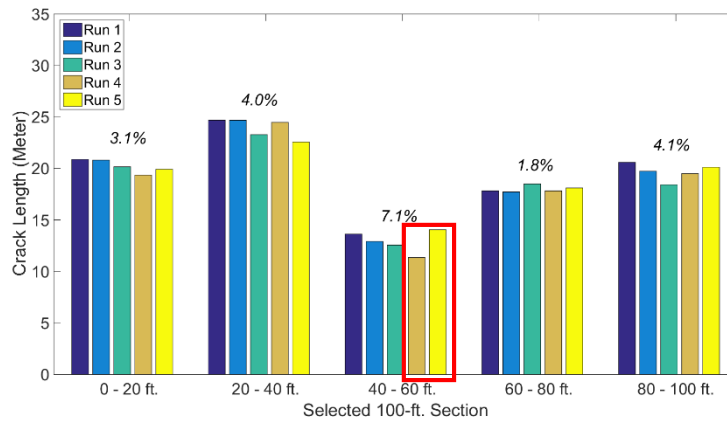
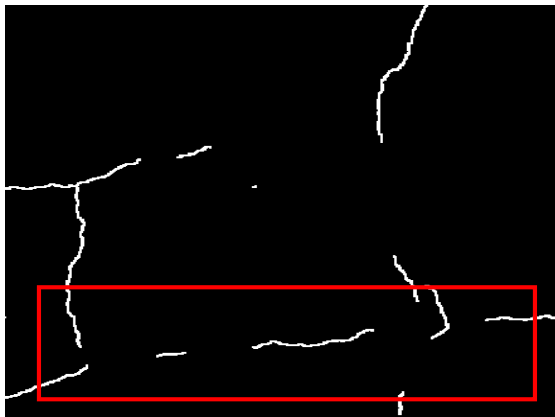


**Figure 4.13 Crack length statistics in five different runs collected on Section 2**



(a) Run 4



(b) Run 5

**Figure 4.14 Crack map comparison on the highlighted location on the second section between Run 4 and Run 5**



Considering that crack length statistics may not be able to represent the entire detect crack map, it is preferable to quantify the similarity between the crack maps directly. The buffered Hausdorff distance scoring method, which has been used to evaluate the accuracy of the crack detection algorithm, can be applied here. Instead of comparing the detected crack maps with manually digitized ground truth, they are now compared with the detected crack maps in a different run; the buffered Hausdorff distance score becomes a similarity score. Figure 4.15 presents such a similarity matrix on the first section. The largest difference between Run 3 and Run 5 gives a similarity score of about 90, which indicates that both detected crack maps are still geometrically close to each other.

Overall, based on the test results, we can conclude that the proposed algorithm is capable of generating robust and repeatable crack maps, which will be critical to objective and reproducible automated pavement crack surveys.

	Run 1	Run 2	Run 3	Run 4	Run 5
Run 1	100.0	94.9	91.1	92.2	90.7
Run 2	94.9	100.0	91.4	92.6	91.5
Run 3	91.1	91.4	100.0	91.3	89.8
Run 4	92.2	92.6	91.3	100.0	91.0
Run 5	90.7	91.5	89.8	91.0	100.0

**Figure 4.15 Similarity scores between the detected crack maps in five different runs**

## **CHAPTER 5. PROPOSED FRAMEWORK FOR PAVEMENT CRACK DIAGNOSIS**

Traditional studies on pavement condition and deterioration use aggregated data. For example, a traditional crack survey mostly records the total length or the affected area of cracks but doesn't track of when, where, and how the cracks happen. However, this information is important for determining pavement surface condition, supporting maintenance decision-making, and improving pavement design. Improperly aggregated data loses critical granularity and creates a situation in which there is lack of proper understanding about the crack condition and crack deterioration behavior.

With the advances in sensing technology, it has become possible to preserve the spatial and temporal characteristics of pavement cracks in detail. In the previous chapters, we proposed and validated an algorithm to generate crack maps from sensor data. In this chapter, we will further investigate how these detected crack maps can be transformed into engineeringly meaningful decision support information. This chapter is organized as follows. Section 5.1 presents the proposed generalized crack diagnosis framework. Section 5.2 presents the first stage of the proposed framework, which is to extract rich crack properties from the detected crack maps with a multi-scale crack representation based on a crack fundamental element model. Section 5.3 and 5.4 demonstrate the second stage of the framework, which is to interpret these crack properties into real-world crack types and severity levels. Section 5.3 presents the implementation with AASHTO PP 67 standard. Section 5.4 presents the implementation with GDOT's PACES distress

protocol. Besides crack classification and quantification, Section 5.5 presents an extended study to monitor crack deterioration behaviors from a temporal domain.

### **5.1 Overview of the Pavement Crack Diagnosis Framework**

Crack diagnosis is defined as studying and utilizing crack condition and crack behavior at a detailed level to support next-generation pavement management. It consists of three conceptual stages:

- The first stage is to represent and quantify crack condition and behavior.

Although the emerging sensing technology can preserve cracks at great detail, the raw data and detected crack maps are still less informative for agencies' pavement management systems. So, the major questions to answer at this stage are what crack properties should be considered to represent the crack condition and behavior without losing the critical granularity, and how these properties can be extracted. For the sake of clarification, in this study, the term “crack characteristic” refers to the physical crack characteristics that we can observe on real pavements, and the term “crack property” refers to the information that has been modeled mathematically through the proposed methods and used for decision support.

- The second stage is to convert the crack condition and behavior into engineering-meaningful information and utilize them for decision support. From the spatial perspective, we can assess the crack type and severity based on topological crack patterns and use the information to prioritize maintenance projects and determine proper treatments. From the temporal perspective, the crack deterioration and

propagation can be observed and used to forecast future conditions and determine the optimal timing for maintenance.

- The final stage aims to establish a knowledge base, which integrates the information from previous stages and engineering knowledge. We can study the inhomogeneity of crack spatial distribution and temporal propagation behavior, and we can establish the link with external factors, such as construction quality, materials, climate change, extreme events, and specific maintenance operations, etc. It can be used to improve infrastructure sustainability by providing the optimal maintenance and rehabilitation strategies in the most cost-effective way, and it can also be used to retrofit infrastructure design and enhance infrastructure resilience to foreseeable events.

The objectives of this study focus on the first and second stages (as shown in Figure 5.1). Section 5.2 proposes a multi-scale crack representation model using crack fundamental element (CFE), which provides a systematic and comprehensive approach of extracting engineeringly meaningful crack properties from the detected crack maps. Then, automatic crack type and severity level classification algorithms for real-world distress protocols are developed to interpret these crack properties, which directly complement the DOT's current crack survey practice. Two crack survey protocols from federal and state level are implemented: Section 5.3 discusses the implementation of the AASHTO provisional standard PP 67, and Section 5.4 discusses the implementation of the GDOT PACES protocol. Section 5.5 presents a pilot study to evaluate the feasibility of using the emerging sensor data and the proposed crack detection algorithm and CFE model to study crack deterioration behavior from the temporal domain.

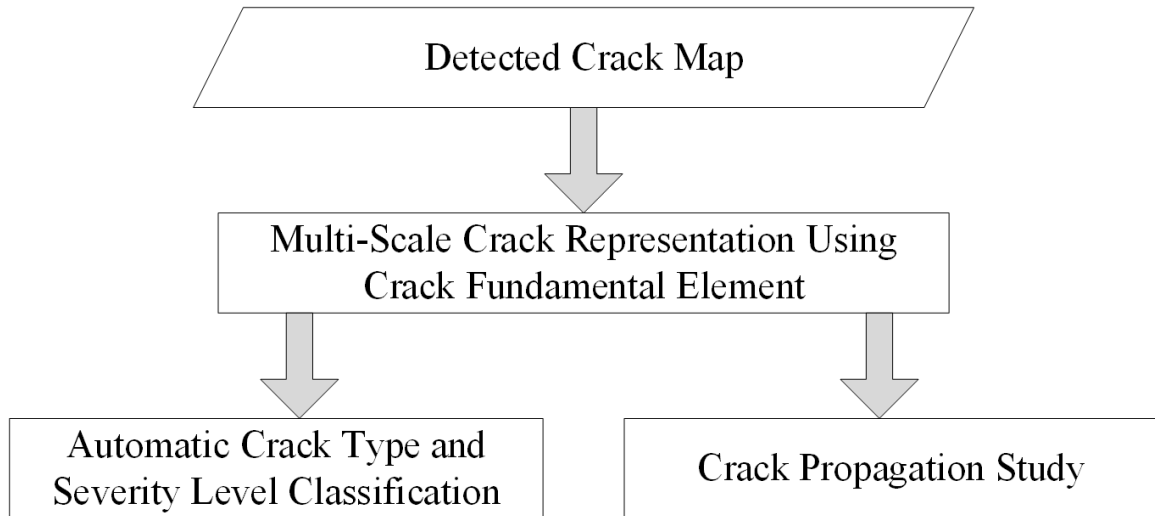


**Figure 5.1 Objectives of pavement crack diagnosis in this study**

## **5.2 Multi-scale Crack Representation Using Crack Fundamental Element**

### **5.2.1 Crack Fundamental Element**

The purpose of developing a crack fundamental element model is to generalize the real-world crack characteristics into computerized crack properties mathematically and topologically, which can be used to develop crack diagnosis applications, such as crack type and severity level classification. A crack fundamental element is defined in this study by clustering a group of cracks using a bounding box based on their spatial proximity to better present their topological properties. A Crack Fundamental Element is the basic component of the proposed model, and the crack pattern is characterized by clustering and analysis of CFEs at different scales.

To classify cracks, inspecting the detected crack map pixel by pixel is not necessary. In this model, we start from a group of crack pixels that form an roughly linear segment, and define it as the CFE at the initial scale, as shown in Figure 5.2. These initial CFEs are gradually clustered together into higher scales, where each CFE contains a

group of crack curves instead of pixels. At each scale, an ellipse is created as a “bounding box”. CFE geometrical properties are equivalent to the properties of this ellipse, which are used to support the subsequent CFE clustering and crack analysis, including

- Length

Length (L) is defined as the length of the major axis of the ellipse that has the same normalized second central moments as the group of crack curves that are clustered together in a CFE:

$$L = 2 \times \sqrt{2 \left( (\mu_{xx} + \mu_{yy}) + \Delta \right)} \quad (5.1)$$

where  $\mu_{xx} = \frac{\sum_{i=1}^N x_i^2}{N}$ ,  $\mu_{yy} = \frac{\sum_{i=1}^N y_i^2}{N}$ , and  $\mu_{xy} = \frac{\sum_{i=1}^N x_i y_i}{N}$ , which are the second

moments of the crack curves in that CFE,  $N$  is the number of initial CFEs and

$$\Delta = \sqrt{(\mu_{xx} - \mu_{yy})^2 + 4 \times \mu_{xy}^2}.$$

- Width

Width (W), similarly, is defined as the length of the minor axis of the ellipse that has the same normalized second central moments as the group of crack curves that are clustered together in a CFE:

$$W = 2 \times \sqrt{2 \left( (\mu_{xx} + \mu_{yy}) - \Delta \right)} \quad (5.2)$$

- Center

Center (C) is defined as the centroid of crack curves in the CFE:

$$C = (\mu_x, \mu_y) = \left( \frac{\sum_{i=1}^N x_i}{N}, \frac{\sum_{i=1}^N y_i}{N} \right) \quad (5.3)$$

- Orientation

Orientation (O) is a measure of the CFE direction relative to the horizontal axis of the data sample:

$$O = \begin{cases} \frac{180}{\pi} \times \tan^{-1} \left( \frac{\mu_{xx} + \mu_{yy} + \Delta}{2\mu_{xy}} \right), & \text{if } \mu_{xx} < \mu_{yy} \\ \frac{180}{\pi} \times \tan^{-1} \left( \frac{2\mu_{xy}}{\mu_{xx} + \mu_{yy} + \Delta} \right), & \text{if } \mu_{xx} \geq \mu_{yy} \end{cases} \quad (5.4)$$

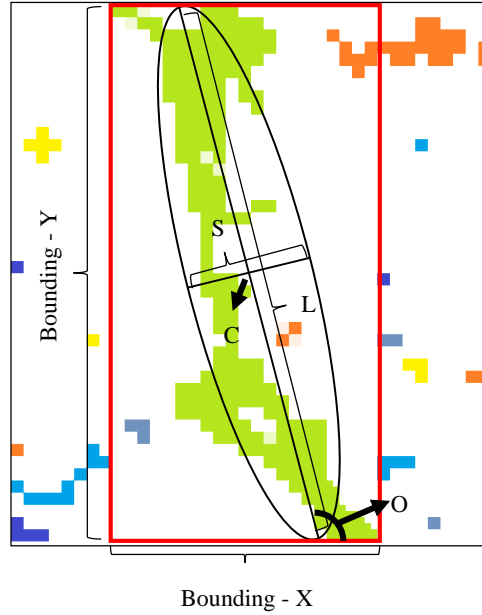


**Figure 5.2 Illustrations of a crack fundamental elements at initial scale (Tsai et al. 2014)**

## 5.2.2 Multi-Scale Topological Crack Representation

This section presents a multi-scale crack representation concept to systematically and comprehensively extract engineeringly meaningful crack properties from the detected

crack maps. Figure 5.3 shows the logic of multi-scale crack property extraction using the CFE concept. It first decomposes the detected crack map into initial CFEs, and then it gradually clusters them into higher scales until it covers all the detected cracks in the region. At different scales, different crack properties are modeled and can be extracted.

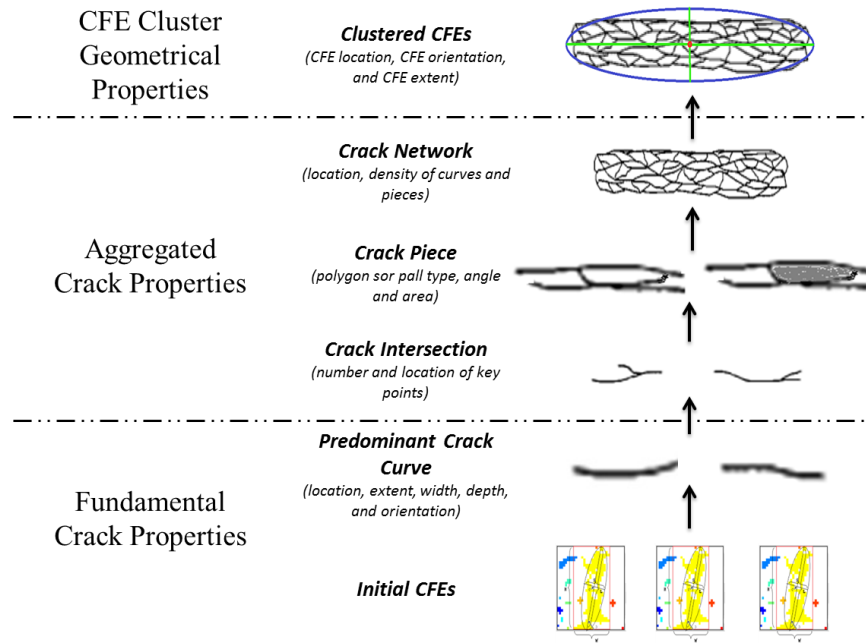


**Figure 5.3 Multi-scale crack properties from CFE model (Tsai et al. 2014)**

This multi-scale CFE model provides rich crack properties at three different scales:

- Fundamental crack properties focus on each crack segment and describe the fundamental and physical properties of cracks (such as crack location, length, width, orientation, etc.).
  - Initial CFE results are the approximate straight lines decomposed from the original crack map. Each of these small segments can be treated with a fixed orientation and similar width.
  - Crack curves are generated by connecting neighboring initial CFEs. At this level, crack location, orientation, extent, width, and depth are useful



properties. The location of a crack curve is directly associated with crack types. The orientation of a crack curve helps differentiate longitudinal cracking and transverse cracking etc. The extent and width reflect the severity level of cracking to some extent.

- Aggregated crack properties focus more on crack patterns inside the clustered CFE and represent how cracks interact with each other.
  - Crack intersections locate the crossing points of the predominant crack curves. Obviously, the number of crack intersections indicates the complexity of the crack pattern and the severity of the crack condition.
  - Many crack curves intersect with each other and form an enclosed piece-like area, which is referred to as a crack piece. The polygon type of the crack piece (normal surface polygon or pop-out) needs to be identified in order to classify high severity level cracks. The extent (including the angle) of the polygonal crack pieces is an important attribute that differentiates crack pieces of different severity levels of block and alligator cracking.
  - Crack network is a combination of crack curves, intersections, and pieces. The density of these elements inside a network and the extent of the network are directly associated with crack type and severity. The location of the crack network determines potential isolated treatment.
- CFE cluster geometrical properties treat each CFE as a whole and describe its overall properties.

As shown in Figure 5.3, from the bottom, the model represents more of the physical characteristics of pavement cracks; from the top, it tends to mimic the pavement

engineers' manual evaluation procedure in the field (from macro to micro level observation). When experienced pavement engineers conduct a crack survey, they do not usually measure the crack width and depth first; instead, they first identify a group of cracks that should be clustered together; then, they look at the crack pattern inside the cluster, and, finally, they measure the physical and fundamental crack properties if necessary. By clearly defining three scales of crack properties, this representation can better incorporate both physical crack characteristics and the logic of human judgment.

Crack properties at each of these scales characterize the pavement surface cracks in a comprehensive manner, which provides a rich basis to support the subsequent crack diagnosis. The proposed multi-scale CFE model features in the following two aspects:

- **Consistency:** The crack properties are directly extracted from the detected crack map; thus, they are completely independent from the diverse distress protocols or survey practices from federal and state agencies. This consistency is critical as a standardized pavement condition measure to fulfill the need of MAP-21.
- **Compatibility:** It is still compatible with these protocols, which means that the crack properties can be flexibly transformed into the crack definitions across different agencies. This helps maintain the legacy of a state DOT's historical data and pavement management practice.

The following sections present how the proposed multi-scale CFE model can be used for crack classification with federal and state distress protocols.

### **5.3 Crack Classification on AASHTO Provisional Standard PP 67**

In 2010, the American Association of State Highway and Transportation Officials (AASHTO) developed the provisional standard PP 67-10 for crack classification and

quantification. It outlines the procedures for quantifying cracking distress in asphalt pavement surfaces using automated methods. According to the definitions, crack classification and quantification can be implemented in a straightforward manner using the proposed CFE model. The implementation consists of three major steps.

The first step is to separate the lane space into measurement zones. Figure 5.4 presents an illustration of the five measurement zones on a typical 12-ft. road lane. The inside and outside wheelpaths are defined as longitudinal strips of pavement 0.75m wide and centered at 0.875 m from the centerline of the lane on both sides. Five measurement zones are created by two wheelpaths and three areas between the wheelpaths and lane edges. It needs to be noted that Zone 5 is extended slightly towards the outside lane edge to cover possible edge cracking. In the automated implementation, the lane edges can be easily identified by the locations of the pavement marking.

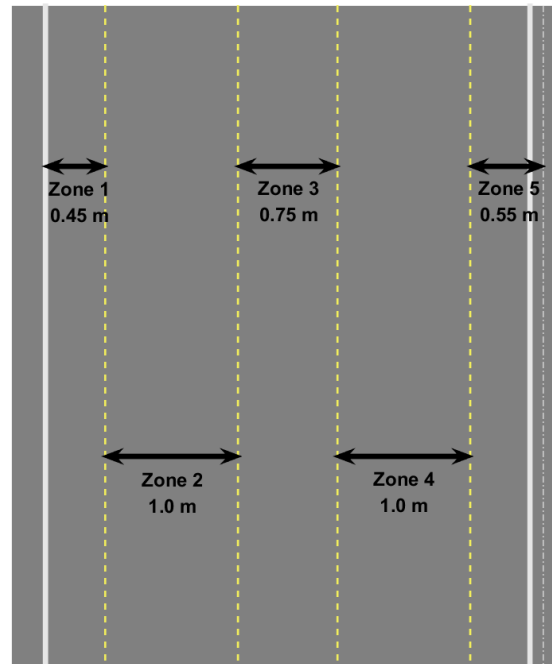
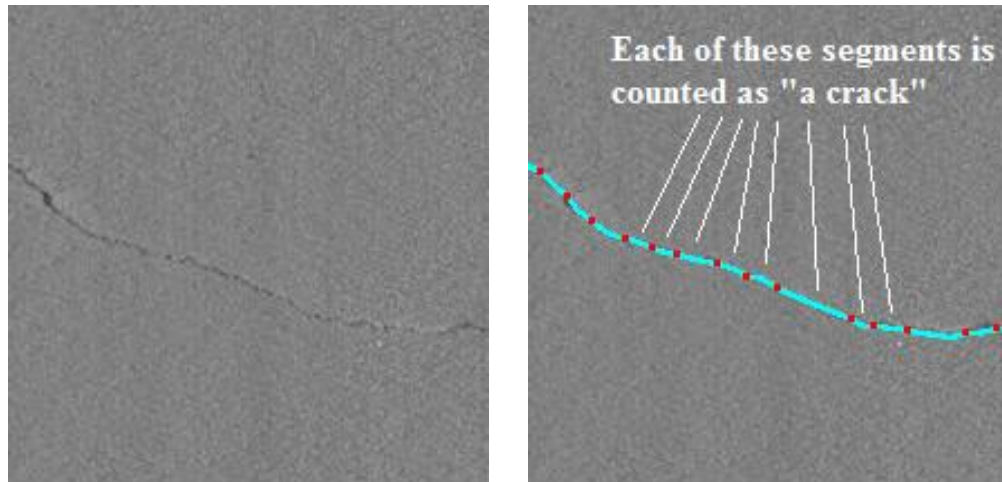


**Figure 5.4 Illustration of five measurement zones on a typical 12-ft. road lane**

The second step is to classify the detected cracks into different types. In human perception, a crack is usually a continuous long curve on the pavement surface; however, in the AASHTO definition, a crack is bounded by two crack terminuses (as shown in Figure 5.5), which are the points of one of the following scenarios: beginning or ending of a continuous crack curve, a change of crack orientation, a change of crack width, or a junction with another crack. In short, the detected crack map is considered as a combination of many short, straight segments, each of which is considered as one crack with similar orientation and width. This setup is very similar to the proposed CFE model, where the initial CFEs are a group of crack pixels that form an approximately linear segment. Three types of cracks are further defined in this protocol:

- Longitudinal crack: a crack with an orientation between +10 and -10 degrees of the lane centerline;
- Transverse crack: a crack with an orientation between 80 and 100 degrees to the lane centerline; and
- Pattern crack: ideally a crack that is part of a network of cracks that form an identifiable grouping of shapes. In current practice, it includes all cracks that are not defined as transverse or longitudinal.

It can be observed that these crack type definitions are strictly orientation-based. The orientations of each initial CFE is provided as part of the fundamental crack properties in the multi-scale crack representation of the detected crack map. A simple orientation filter is applied on the initial CFEs to classify the cracks into all three types.



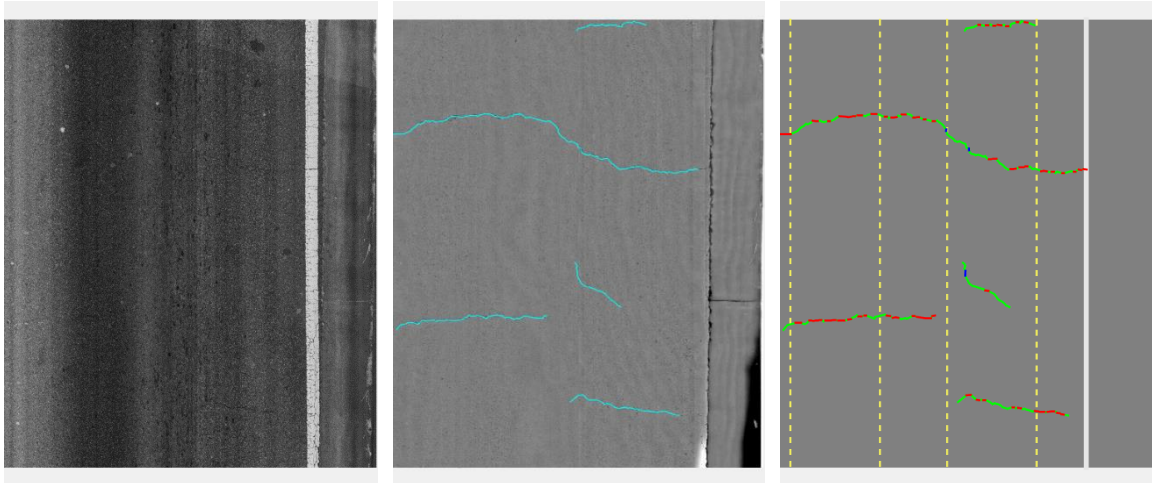
(a) Pavement image

(b) Illustration of crack definition

### Figure 5.5 Definition of “a crack” in AASHTO PP 67

The last step is to report the extent and severity for each crack category. Each of the five measurement zones is reported separately for longitudinal and pattern cracks, while the measurement zones are not applicable to transverse cracks. Therefore, there are a total of 11 crack categories. In each category, the extent is defined as the sum of the lengths of all the cracks of that type, and the severity is defined as the corresponding average crack width. A total of 22 values will be reported that characterize the cracking contained in the survey section.

Figure 5.6 and Figure 5.7 show a couple examples of automatic crack classification based on the AASHTO PP67 protocol. In each figure, the image on the left is the intensity image, where the lane marking is detected for the lane zoning step; the image in the middle is the detected crack map, which is the outcome of the previous automatic crack detection; the image on the right is the crack classification results. The boundaries of the five measurement zones are drawn on the image, and the three types of cracks are plotted with different colors. Table 5.1 and Table 5.2 present the crack extent and severity values for two selected examples respectively.



(a) Intensity image      (b) Detected crack map      (c) Classification results

**Figure 5.6 Crack classification based on AASHTO PP67 – Example 1**

**Longitudinal Cracks** — **Transverse Crack** — **Pattern Crack** —

**Table 5.1 Data reporting for the example in Figure 5.6**

	Longitudinal		Pattern		Transverse	
	Extent (m)	Severity (mm)	Extent (m)	Severity (mm)	Extent (m)	Severity (mm)
Zone 1	0	0	0.12	7.1	2.45	3.9
Zone 2	0	0	1.36	4.5		
Zone 3	0.02	2.7	1.00	4.1		
Zone 4	0.08	5.8	3.14	4.1		
Zone 5	0	0	0.54	4.3		

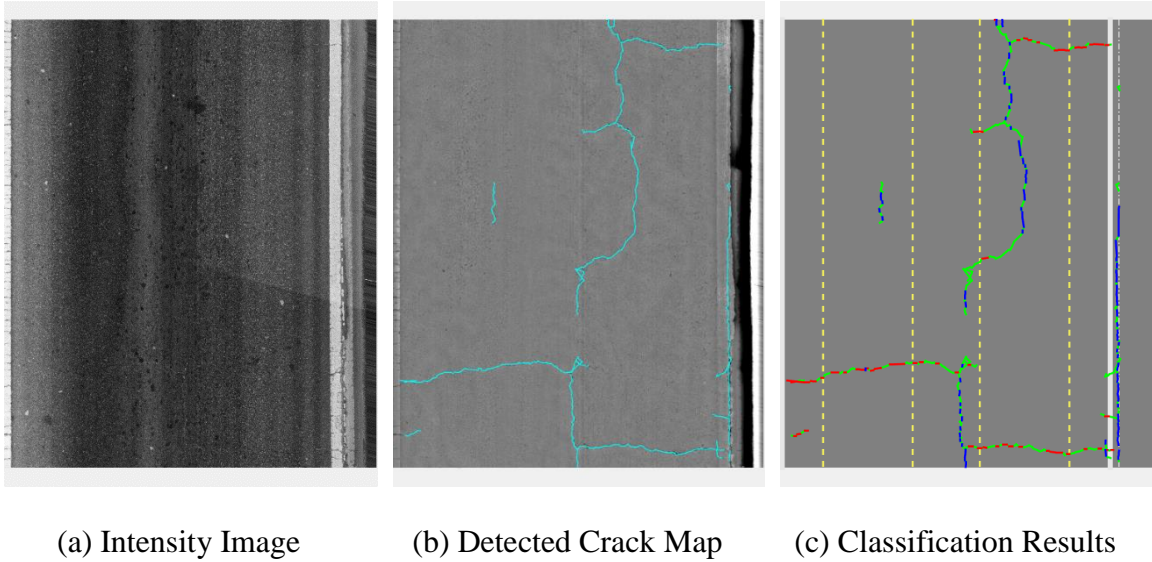


**Figure 5.7 Crack classification based on AASHTO PP67 – Example 2**

**Longitudinal Cracks** — **Transverse Crack** — **Pattern Crack** —

**Table 5.2 Data reporting for the example in Figure 5.7**

	Longitudinal		Pattern		Transverse	
	Extent (m)	Severity (mm)	Extent (m)	Severity (mm)	Extent (m)	Severity (mm)
Zone 1	0	0	0.29	3.0	2.3	3.7
Zone 2	0.17	3.5	0.99	3.6		
Zone 3	0.58	4.5	2.82	4.2		
Zone 4	1.10	4.2	3.90	4.6		
Zone 5	1.94	11.2	2.37	8.6		

Overall, the proposed CFE model is fully compatible with the AASHTO provisional standard PP 67. Actually, we only use the fundamental crack properties, which are the most basic properties from the proposed model, to implement this protocol because 1) the definition of a “crack” in the AASHTO PP 67, which is a straight line

segment between two crack terminuses, is very close to our definition of a CFE at the initial scale, so the properties of these initial elements from the CFE model can be directly used; and 2) the crack types in the AASHTO PP 67 are strictly based on crack orientation. The AASHTO standard is designed for automated implementation, so it avoids the complex crack definitions that are difficult to model automatically at current stage. However, defining the crack types in such a broad manner leads to potential ambiguity. Based on the experimental results, it is observed that a large portion of the detected crack map is consistently classified as pattern crack, and the definition of pattern crack starts to lose its engineering meaning in pavement condition assessment. Many state DOTs usually further specify the pattern crack into more detailed crack definitions. The next section presents another example in which multi-scale crack properties from the CFE model are used to implement a more sophisticated crack classification task.

#### **5.4 Crack Classification on GDOT PACES Protocol**

The GDOT PACES protocol, which has been briefly reviewed in the Chapter 2, is an example that demonstrates how multi-scale crack properties from the CFE model can be used to implement a more sophisticated crack classification. The Pavement Condition Evaluation System (PACES) protocol defines four crack-related distresses on asphalt pavements, including load cracking, block/transverse (B/T) cracking, reflection cracking, and edge distress, each of which are further specified into three or four severity levels. Unlike AASHTO standard PP 67, in which the severity is solely based on crack width, the severity level definitions here involve changing crack patterns. Figure 5.8 shows several examples of different crack types and severity levels on actual pavements. We can see that according to AASHTO PP 67, these cracks are very likely to be classified as



pattern crack with no further differentiation; however, in GDOT's survey practice, it is required to not only classify the crack types, but also differentiate the severity levels. In this study, we focus on load cracking and block/transverse (B/T) cracking, which are the two predominant asphalt pavement distresses in Georgia<sup>1</sup>.



(a) B/T cracking Severity Level 1



(b) B/T cracking Severity Level 3



(c) Load cracking Severity Level 3



(d) Load cracking Severity Level 4

**Figure 5.8 Examples of PACES crack distresses on actual pavements**

---

<sup>1</sup> In GDOT survey practice, pavement rating is calculated by converting distresses into deduct values based on the distress type, severity level, and extent. Load cracking and B/T cracking contributed to over 80% of the total deduct values in the statewide survey in Fiscal Year 2013.

### 5.4.1 Algorithm Flowchart

Utilizing the crack properties from CFE model, this section presents the proposed algorithm to automatically classify and quantify load cracking and B/T cracking, including their severity levels. The flowchart of the proposed algorithm is shown in Figure 5.9.

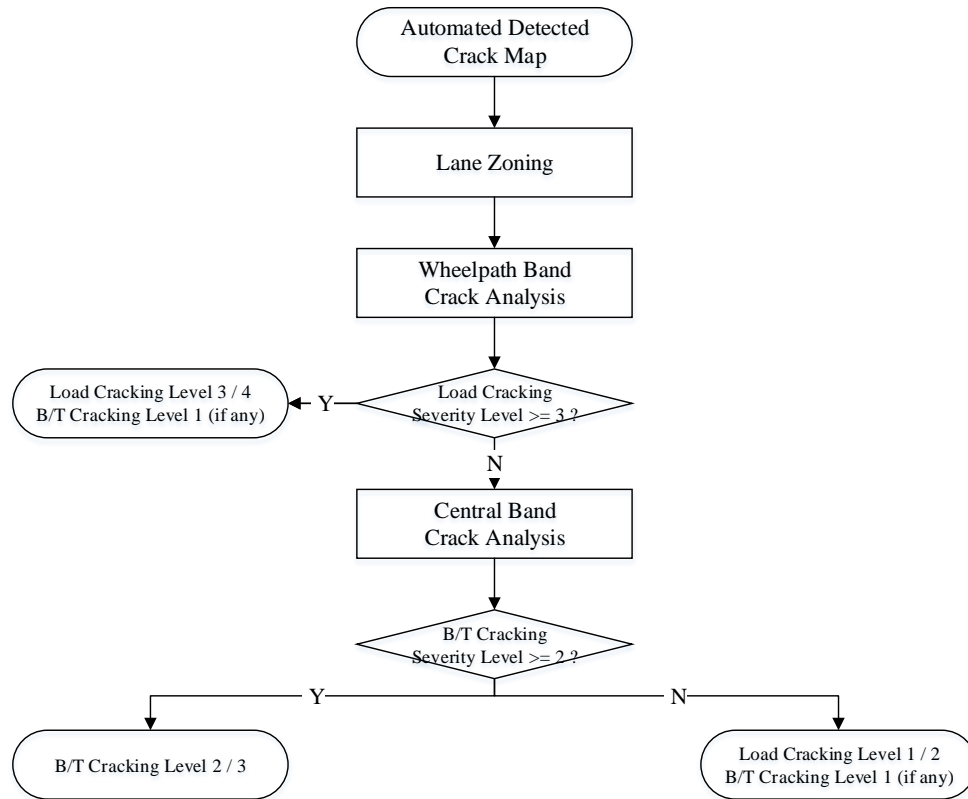


**Figure 5.9 Flowchart of automatic crack type and severity level classification for load cracking and B/T cracking (Tsai et al. 2014)**

Similar to the implementation of the AASHTO protocol, the lane zoning step is first applied, which divides the pavement surface into five different bands based on the lane edges and wheelpaths. The entire lane is split into one central band, two wheelpath bands, and two edge bands. Based on the experience from GDOT pavement engineers, the wheelpaths are set to be two 3-ft. bands located symmetrically on the lane, and their

location and extent are adjustable for interstate and local highways. The wheelpath bands and central band are the regions of interest in this study for load cracking and B/T cracking, while the edge bands can further be explored to evaluate other edge distresses. Then, given the detected crack map, the cracks are separated into wheelpath cracks and non-wheelpath cracks.

At the steps of wheelpath band and central band analysis, a list of crack properties is calculated following the multi-scale CFE model to represent the topological pattern of the crack map. Table 5.3 shows the crack properties used in this study; all these crack properties are intuitively related to different crack types and severity levels.

**Table 5.3 Crack properties extracted from wheelpath and central bands**

<b>Fundamental Crack Properties</b>	Length of longitudinal cracks
	Length of total cracks
	Ratio of longitudinal to total crack length
	Number of initial CFEs
	Number of continuous crack lines
	Average crack width
<b>Aggregated Crack Properties</b>	Maximum crack width
	Number of crack intersection points
	Area of surface loss
	Crack distribution based on orientations
<b>CFE Cluster Geometrical Properties</b>	Length of clustered CFEs
	Width of clustered CFEs

These properties are then interpreted into crack types and severity levels through a data-driven approach. A pavement image dataset is prepared in which each image is manually labeled as load cracking, B/T cracking, and the corresponding severity levels.

The proposed crack properties are then calculated on each image. A machine-learning classifier is used to establish the link between the input features, which are the calculated crack properties and the output labels, which are the different crack type and severity level. The parameters in the classifier are calibrated with the prepared dataset and will be used for future classification task. An ordered logistic regression, which is a commonly used machine-learning technique, is employed in this study. It is a form of discrete outcome regression that relate dependent variables in an ordered discrete scale to independent variables (which can be discrete or continuous). It has also been used successfully in the modeling of pavement serviceability ratings and raveling classifications (Ong et al., 2008; Shafizadeh & Mannering, 2006). An ordered logistic regression starts by defining an unobserved variable  $y^*$ , which is typically a linear function for each observation, such as

$$y^* = x^T \beta + \varepsilon \quad (5.5)$$

where  $x$  is the vector of independent variables, and  $\beta$  is the vector of regression coefficients to be estimated, and  $\varepsilon$  is a random disturbance. In this case, vector  $x$  contains one or more crack properties, as proposed previously. Since  $y^*$  is an unobserved variable,  $y^*$  is further transformed into observed categories of responses  $y$ , which, in this case, are the corresponding crack types and severity levels:

$$y = \begin{cases} 0 & \text{if } y^* \geq \mu_1, \\ 1 & \text{if } \mu_2 < y^* \leq \mu_1, \\ 2 & \text{if } \mu_3 < y^* \leq \mu_2, \\ 3 & \text{if } \mu_4 < y^* \leq \mu_3, \\ \dots & \end{cases} \quad (5.6)$$

Then, the ordered logistic method will use the observations on  $y$ , which are a form of censored data on  $y^*$ , to fit the parameter vector  $\beta$  and  $\mu$ . The ordered logistic regression is only used as an example here, and it can be replaced with more sophisticated machine learning classifiers if needed.

## 5.4.2 Experimental Tests

In order to evaluate the performance of the proposed algorithm, experimental tests are conducted using the real data collected from State Route 236 / Lavista Road in Atlanta, Georgia. The selected project starts from Milepost 0 (Atlanta city limit) to about Milepost 6.8 (I-285 Bridge), with an excessive amount of load cracking and B/T cracking. The ground truths are established manually with the help from GDOT pavement engineers. Two sets of experimental tests are conducted: image-based validation and site-based validation. The experimental results are presented in the following subsections.

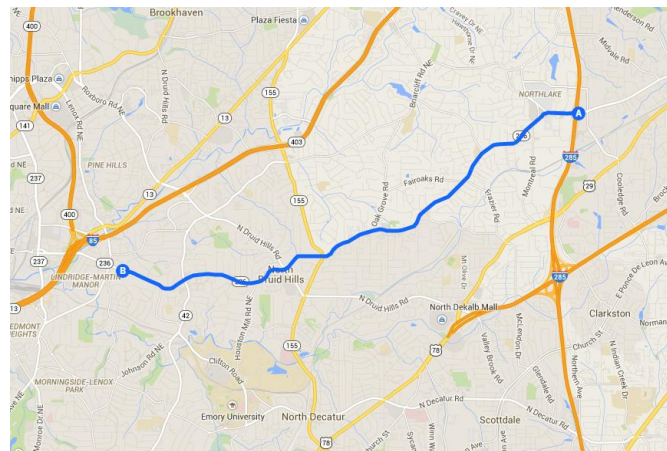


**Figure 5.10 Selected project for crack classification evaluation on GA State Route 236**

#### 5.4.2.1 Image-based Validation

In the image-based validation, each pavement image is visually reviewed, and the presence and severity level of load cracking and B/T cracking are manually labeled. The data from each crack type and severity level are randomly separated into two sets: of the data, 70% are used for model training and calibration, while the other 30% are used for testing. The training and testing for load cracking and B/T cracking classification are conducted separately.

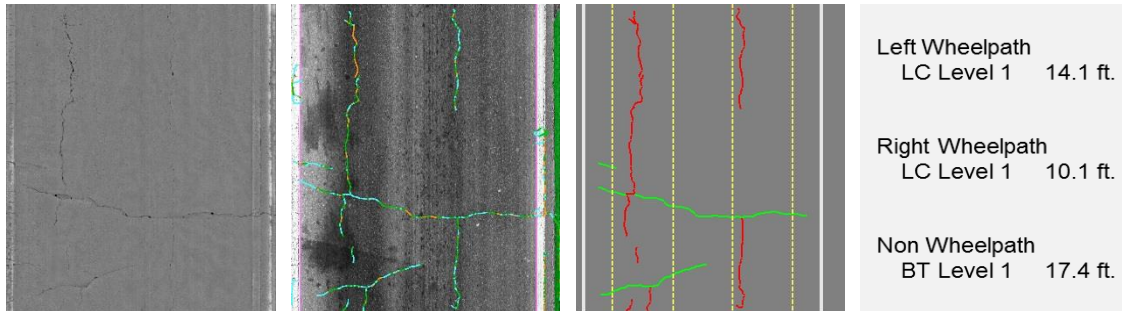
For load cracking evaluation, the training set contains a total of 1635 images, which include 619 images of no load cracking, 798 images of Severity Level 1, 108 images of Severity Level 2, and 99 images of Severity Levels 3 and 4. The algorithm is then evaluated on an independent test set with 701 images, and the performance is shown in Table 5.4.

**Table 5.4 Performance of load cracking classification**

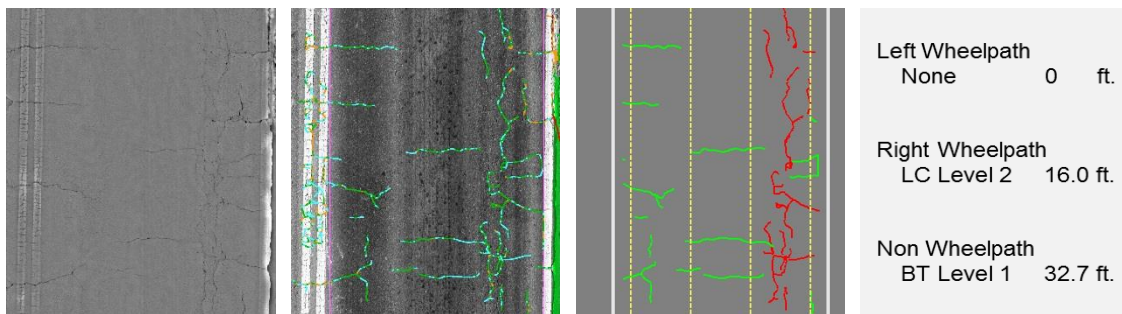
		<i>Classified Severity Level</i>					Total	Recall (%)
		None	Level 1	Level 2	Level 3	Level 4		
<i>Actual Severity Level</i>	None	247	15	0	0	0	262	94.3
	Level 1	10	317	20	0	0	347	91.4
	Level 2	0	6	42	2	0	50	84.0
	Level 3	0	0	2	35	0	37	94.6
	Level 4	0	0	0	0	5	5	100.0
	Total	257	338	64	37	5	701	
Precision (%)		96.1	93.8	65.6	94.6	100.0		92.2

As shown in Table 5.4, the algorithm has overall high classification accuracy at about 92.2%. From the perspective of recall, a relatively larger portion of Severity Level 2 are not correctly classified compared to other severity levels. Load cracking Severity Level 2 is a transition stage in the crack pattern development, where polygons start to

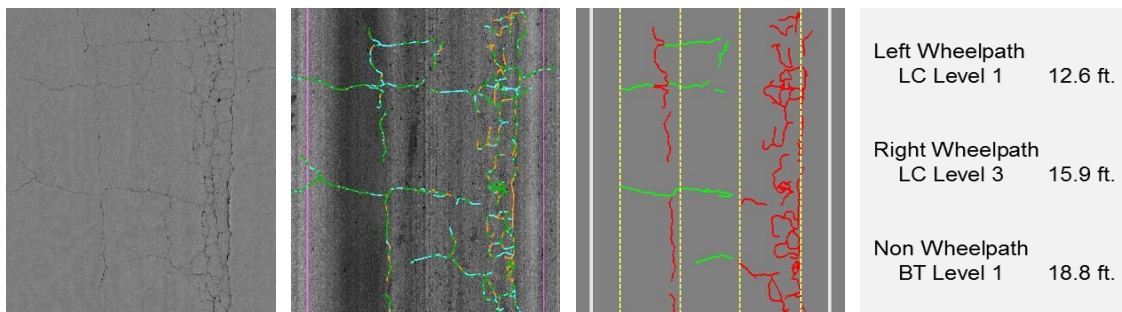
form but haven't yet spread on the entire wheelpath; it is sometimes difficult even for human surveyors to make a judgment. From the perspective of precision, the classification for Severity Level 2 is quite low, which is mainly due to the clear difference between the sample sizes. Some representative cases for load cracking and their automatic evaluation outcomes are shown in Figure 5.11.



(a) Severity Level 1

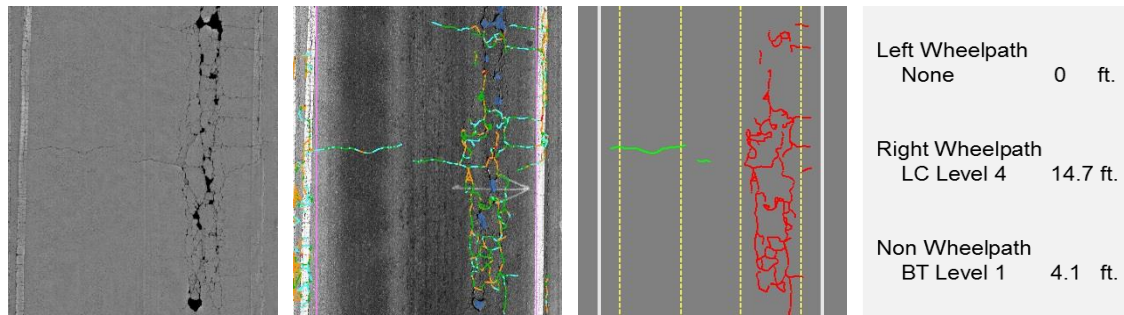


(b) Severity Level 2



(c) Severity Level 3





(d) Severity Level 4

**Figure 5.11 Representative load cracking evaluation outcomes, from left to right: range image, crack map on intensity image, load cracking — and B/T cracking —, and evaluation outcomes.**

For B/T cracking evaluation, the training set consists of a total of 855 images, which include 68 images of no B/T cracking, 703 images of Severity Level 1, and 84 images of Severity Level 2 and 3. The algorithm is then evaluated on an independent test set with 368 images, and the performance is shown in Table 5.5.

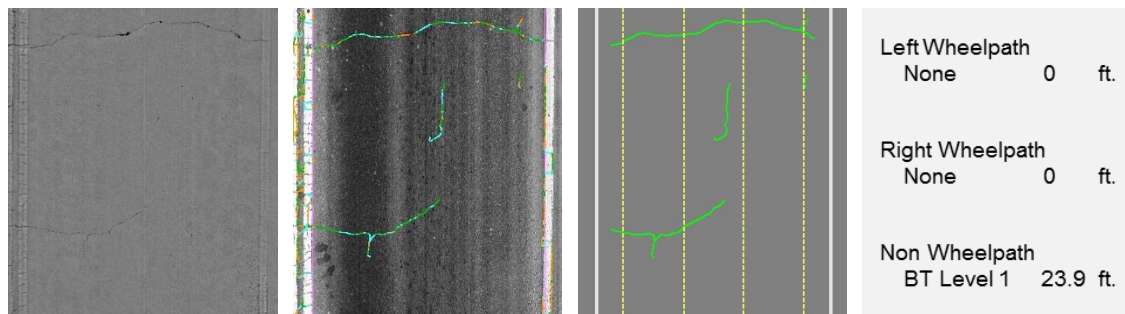
**Table 5.5 Performance of B/T cracking classification**

		<i>Classified Severity Level</i>				Total	Recall (%)
		None	Level 1	Level 2	Level 3		
<i>Actual Severity Level</i>	None	27	2	0	0	29	93.1
	Level 1	1	298	4	0	303	98.3
	Level 2	0	0	31	3	34	91.2
	Level 3	0	0	0	5	5	100.0
	Total	28	300	40	8	368	
Precision (%)		96.4	99.3	90.0	62.5		98.1

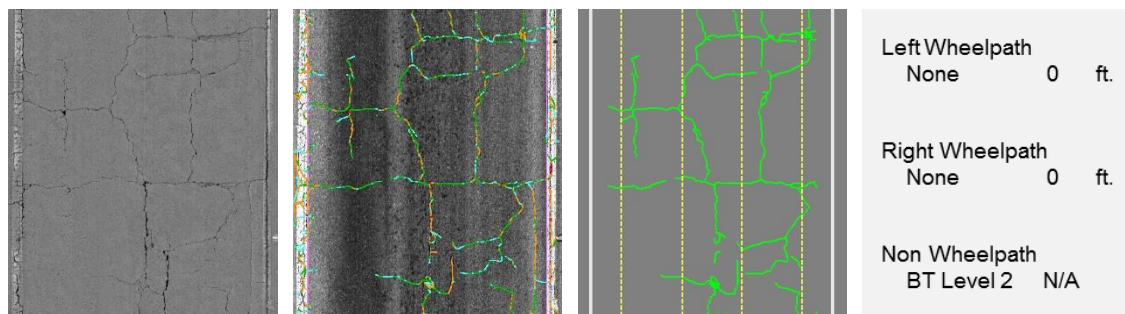
As shown in Table 5.5, the algorithm has an overall high classification accuracy at about 98.1%. The results are also promising from the perspectives of both precision and recall. One possible reason is that the three target classes have quite distinctive differences on the crack properties. Currently, the crack density on the image is the



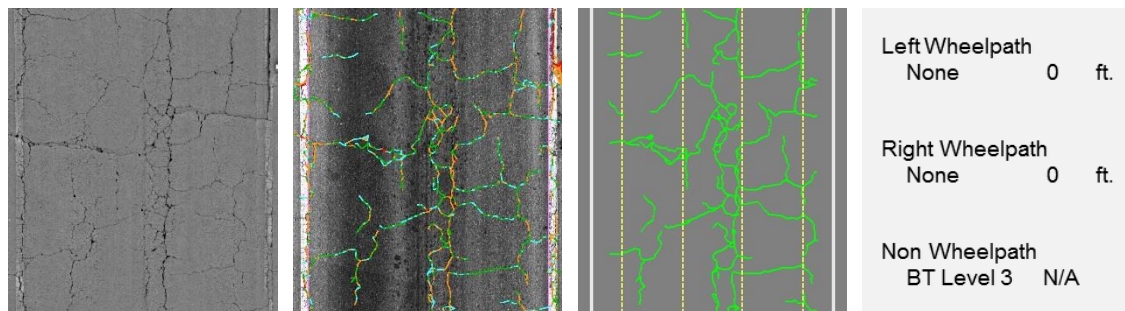
predominant factor to further differentiate B/T cracking Severity Levels 2 and 3; more data samples are still needed to provide a more robust solution. Some representative cases for B/T cracking and their automatic classification and quantification outcomes are shown in Figure 5.12.





(a) Severity Level 1



(b) Severity Level 2



(c) Severity Level 3

**Figure 5.12 Representative B/T cracking evaluation outcomes, from left to right: range image, crack map on intensity image, load cracking  and B/T cracking , and evaluation outcomes**

#### 5.4.2.2 Site Comparison

Site comparison are conducted to evaluate the accuracy of crack quantification along with crack classification with comparison to manual survey. Three 100-ft. pavement sections from SR 236 and one extra section from SR 275 are selected. The manual survey is established as follows: GDOT pavement engineers visually identify the crack types and severity levels in the field, and the crack extents are precisely measured using a measuring wheel. On the other hand, crack types, severity levels, and extents are provided through the proposed automatic algorithm. The extents for each type and severity level and the corresponding deduct values (which GDOT uses to rate the pavement surface condition) are calculated and compared between manual survey and automatic results.

The experimental results are shown in Table 5.6. The columns on the left are field crack measurement results and their corresponding deducts, and the columns on the right are the results from automatic evaluation. Based on the results, the crack extents measured by field survey and automatic evaluation are generally close. The reason of the higher discrepancy on load cracking Severity Level 1 is that some fine cracks are not even visible from the collected range data and cannot be captured through the crack detection. It is also observed that the 2 percent of load cracking at Severity Level 2, which is equivalent to 2 ft. in a 100-ft. section, has been overlooked by the automatic method. This is because that the proposed method conducts an image-based classification, and the extent of the load cracking at Severity Level 2 is too small to impact the classification on one specific image. Following GDOT's practice, the overall deduct is calculated by adding the highest deducts from both crack types. The overall

deducts given by automatic results are also close to those in the field measurement; for the four selected sites, the average absolute difference on the overall deduct between automatic crack evaluation and field measurement is 3.25, which is within the error tolerance ( $\pm 5$  deduct points) in GDOT's current survey practice.

**Table 5.6. Site comparison on SR 236 and SR 275**

(a) SR 236 Site #1

	Field Measurement		Automatic Evaluation	
	Extent(%)	Deduct	Extent(%)	Deduct
<b>Load Lvl 1</b>	56	15	48	15
<b>B/T Lvl 1</b>	100	18	100	18
<b>Overall</b>		33		33

(b) SR 236 Site #2

	Field Measurement		Automatic Evaluation	
	Extent(%)	Deduct	Extent(%)	Deduct
<b>Load Lvl 1</b>	30	10	25	9
<b>Load Lvl 2</b>	7	9	7	9
<b>Load Lvl 4</b>	11	29	7	22
<b>B/T Lvl 1</b>	99	18	100	18
<b>Overall</b>		47		40

(c) SR 236 Site #3

	Field Measurement		Automatic Evaluation	
	Extent(%)	Deduct	Extent(%)	Deduct
<b>Load Lvl 1</b>	41	13	27	9
<b>Load Lvl 2</b>	2	2	0	0
<b>B/T Lvl 1</b>	100	18	100	18
<b>Overall</b>		31		27

(d) SR 275 Site

	Field Measurement		Automatic Evaluation	
	Extent(%)	Deduct	Extent(%)	Deduct
<b>Load Lvl 1</b>	71	15	47	15
<b>Load Lvl 3</b>	9	19	8	17
<b>B/T Lvl 1</b>	78	18	80	18
<b>Overall</b>		37		35

#### 5.4.3 Full-Coverage Pavement Crack Survey

The subjectivity of the traditional manual survey is introduced not only by the inconsistency of human judgments, but also by the potential bias of the sampling process. In GDOT's current survey practice, the crack survey is conducted on a sampled 100-ft. section out of each 1-mile segment; that is, for each mile within the highway network, the rater selects the most "representative" 100-ft. section, surveys the crack condition of that 100-ft. section from the shoulder, and then records it as the overall condition of the entire mile. The selection of section location clearly determines the effectiveness of the survey.

With the proposed methods, it becomes possible to conduct a pavement crack survey with a full coverage. We select a one-mile segment between Milepoints 4 and 5 on the selected project on SR236, and automatic crack detection, classification, and quantification are conducted on the entire mile. To link with GDOT's survey practice, the results are still aggregated into 100-ft. sections; however, in this case, the survey results for all 52 sections within the mile are generated rather than one single section as in manual survey. Figure 5.13 shows the crack condition distribution across the entire mile. Each bar represents one 100-ft. section and the height of the bar represents the deduct values caused by cracking from one 100-ft. section, which consists of two stacking parts: the blue part is the deduct values caused by B/T cracking, and the yellow part is the

deduct values caused by load cracking. The result is clearly more informative from the perspective of pavement maintenance and management. It shows that the B/T cracking condition is relatively consistent; a further look on the classification results reveals that B/T cracking Severity Level 1 is observed on almost all the sections with a 100% extent, which corresponds to a deduct value of 18. Considering the potential causes of B/T cracking, this further reveals that pavement aging may be the major reason that leads to such crack pattern. Comparatively, the distribution of load cracking is clearly non-uniform, within the high-severity load cracking concentrating in the middle of the mile. This indicates possible structural failure around that area, and the specific spot may require isolated treatments. Furthermore, the full-coverage survey result provides an opportunity to consistently and scientifically select the “representative” section and further aggregate the data into higher scales. Different statistical indicators can be calculated from the population; for example, as shown in Figure 5.13, we can take the median value of crack deducts from all the 52 sections as the overall crack condition for the entire mile.

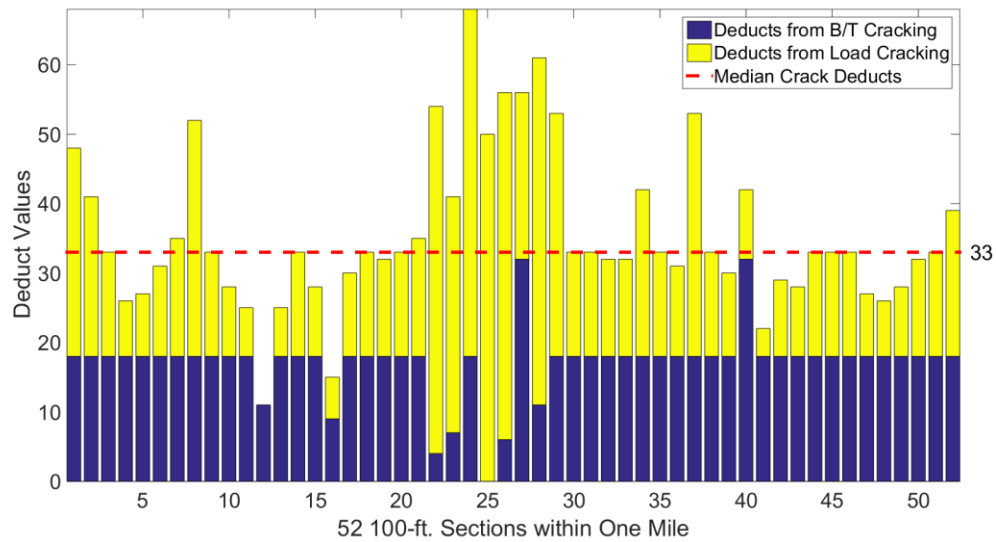


**Figure 5.13 Crack survey results for all 52 100-ft. sections within one-mile segment following GDOT survey practice**

In summary, the proposed multi-scale CFE model has demonstrated its full compatibility with existing federal and state distress protocols. With the proposed model, automatic crack classification and quantification methods can be developed, which can directly benefit agencies' pavement surface condition surveys. It also creates the opportunity to conduct a full-coverage pavement crack survey, which avoids the subjectivity of manual surveys, and also provides more informative crack spatial information for pavement maintenance and management. On the other hand, the proposed model achieves a significant level of standardization, since the crack properties are directly extracted from the detected crack map and are completely independent from the diverse distress protocols or survey practices. Compared to the AASHTO PP 67 standard, the proposed model provides richer crack properties at higher scales, which are necessary for the sophisticated crack definitions in many protocols. It will contribute to the production of consistent pavement condition estimates to fulfill the need of MAP-21.

## 5.5 Crack Deterioration Analysis: A Pilot Study in Real-world Environment

This section will present a pilot study of utilizing the emerging sensing data and the proposed crack detection algorithm and crack diagnosis framework to quantify and analyze crack deterioration behaviors from temporal domain. Figure 5.14 shows the selected project for this pilot study on GA State Route 26 / U.S. 80 between Milepost 5.5 and Milepost 11.5. According to the GDOT's traffic count data, the selected project has an AADT of 24,020, and a truck percentage of 11.94% in 2013. It was resurfaced in 2004 but has deteriorated rapidly due to the heavy truck traffic near the Port of Savannah. Pavement surface data have been collected on multiple timestamps from 2011 to 2013.

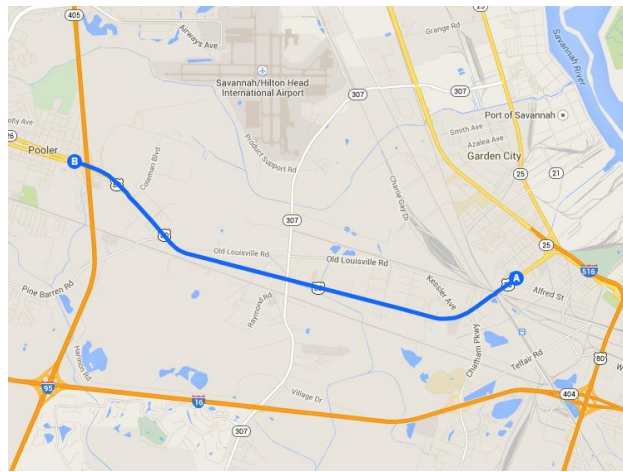


**Figure 5.14 Selected project for crack deterioration analysis on GA State Route 26**

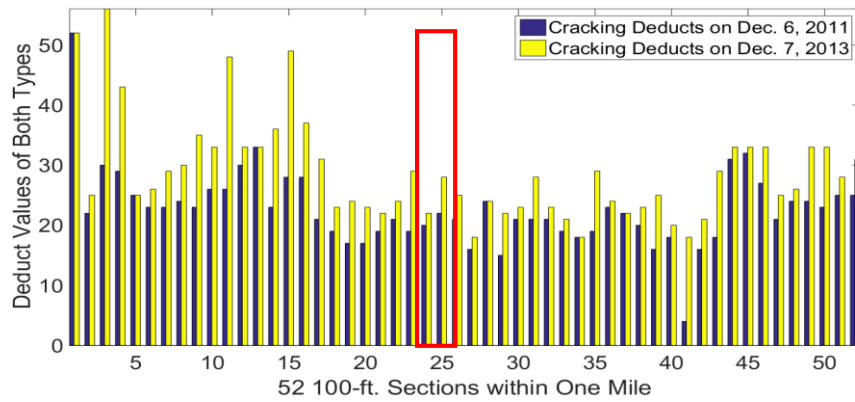
The one-mile segment between Milepoints 8 and 7 is selected here as an example for demonstration purpose. According to the COPACES database, which records the annual manual survey results conducted by GDOT pavement engineers, the overall composite condition rating of this specific segment drops from 60 to 53 over the same period of time. However, such a composite rating is clearly insufficient to reveal where and how the pavement deterioration happens in detail. With the previously proposed crack classification method, we can now compare the changes between two timestamps

side by side on different crack types, including their severity levels. Figure 5.15 shows the comparison between crack deduct values between Dec. 6, 2011 and Dec. 7, 2013 across all 52 100-ft. sections on the selected one-mile segment. Each 100-ft. section is represented by two consecutive bars, where the blue one on the left is the result for Dec. 6, 2011, and the yellow one on the right is the result for Dec. 7, 2013. According to Figure 5.15(a), the crack condition in some sections deteriorated significantly, while it remained almost unchanged in some other sections. Furthermore, in most 100-ft. sections, no significant deterioration was observed on the load cracking as shown in Figure 5.15(b), while the deduct values of B/T cracking changed quite a bit as shown in Figure 5.15(c).

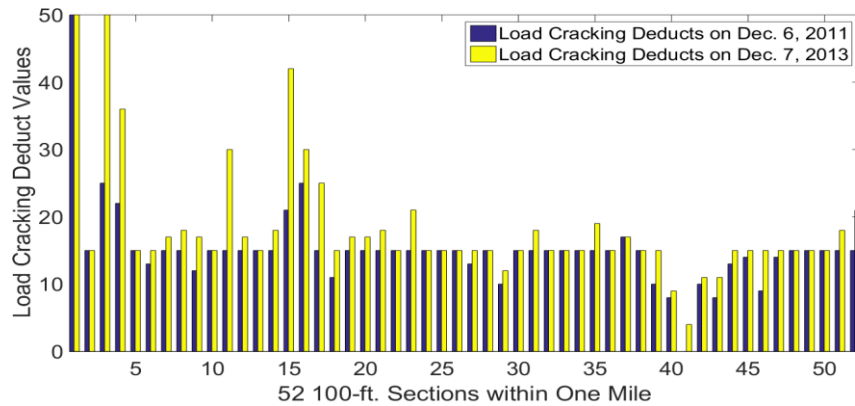
Crack types and severity levels are only one approach of interpreting the crack patterns. Actually, since the detected crack maps are generated at multiple timestamps, the changes of more fundamental crack properties extracted from the multi-scale CFE model can be investigated. A 200-ft. section near Milepoint 7.5 in the negative direction is selected (as highlighted in Figure 5.15), and the following crack properties are calculated between different timestamps:

- Crack length
- Number of crack intersection
- Number of crack polygons

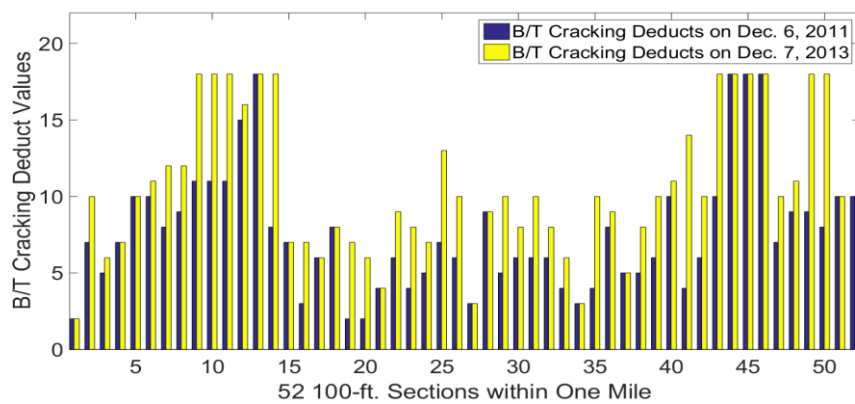




(a) Comparison on both crack types combined



(b) Comparison on load cracking



(c) Comparison on B/T cracking

**Figure 5.15 Crack condition comparison on the one-mile segment between Dec. 6, 2011 and Dec. 7, 2013**

### **Crack length**

Crack length is one of the most basic properties to describe the crack pattern. Many state DOTs use crack length to report the extents for different crack types. In this study, we measure the arc lengths of the detected crack curves within the selected sections. Figure 5.16 shows the change in total crack length, which is the sum of the lengths of all detected crack curves. It can be observed that the crack deterioration led to a 30-percent increase in crack length over the two-year period.

Moreover, the analysis in crack length can be linked with other crack properties, such as crack orientations. Figure 5.17 shows the comparison between crack growth along longitudinal (within 30 degrees of the driving direction) and other directions. It shows that the crack growth along other directions are more significant than the one along the longitudinal direction, which indicates that long and continuous longitudinal cracks already existed in both wheelpaths, and the crack deterioration was more of branching out from these cracks rather than further extending them. This is also consistent with the more significant deterioration with B/T cracking (as shown in Figure 5.15).

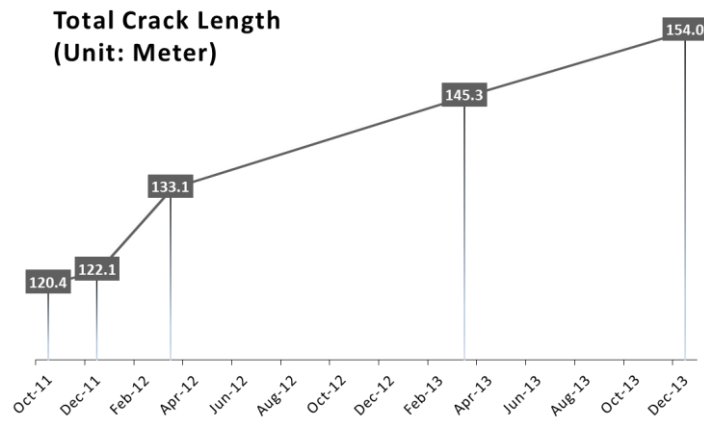


**Figure 5.16 Change in total crack length across five different timestamps on the selected 200-ft. section near Milepoint 7.5**

The precise locations where these deterioration behavior happened can be identified by comparing the detected crack maps. Figure 5.18 and Figure 5.19 present two examples of crack growth along longitudinal and transverse directions correspondingly.

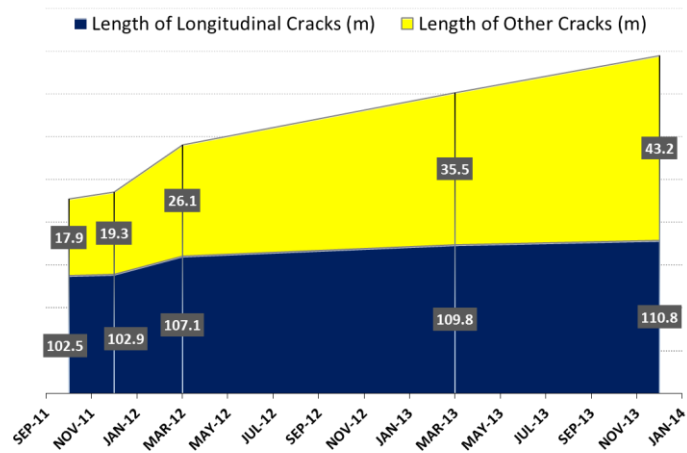
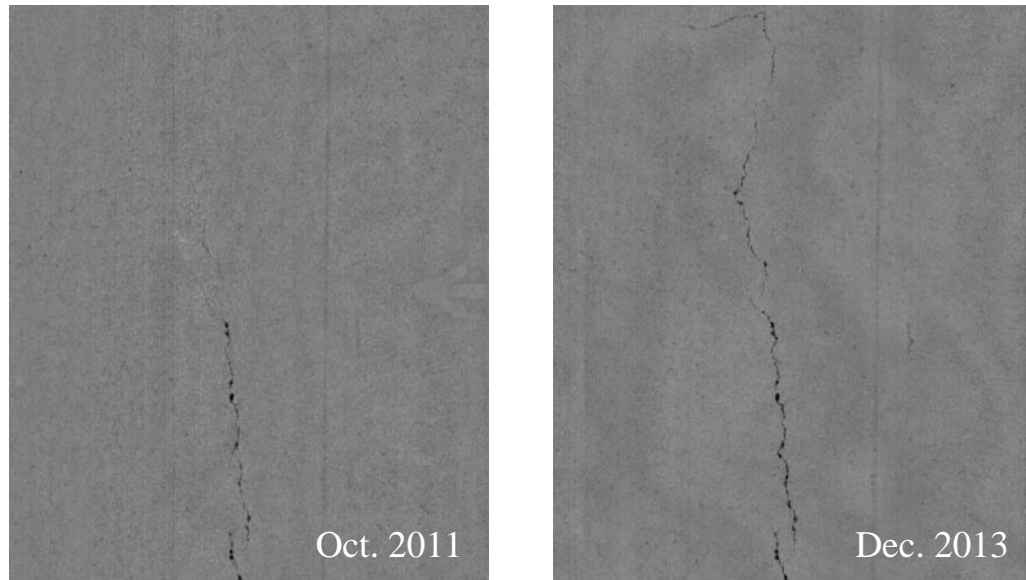
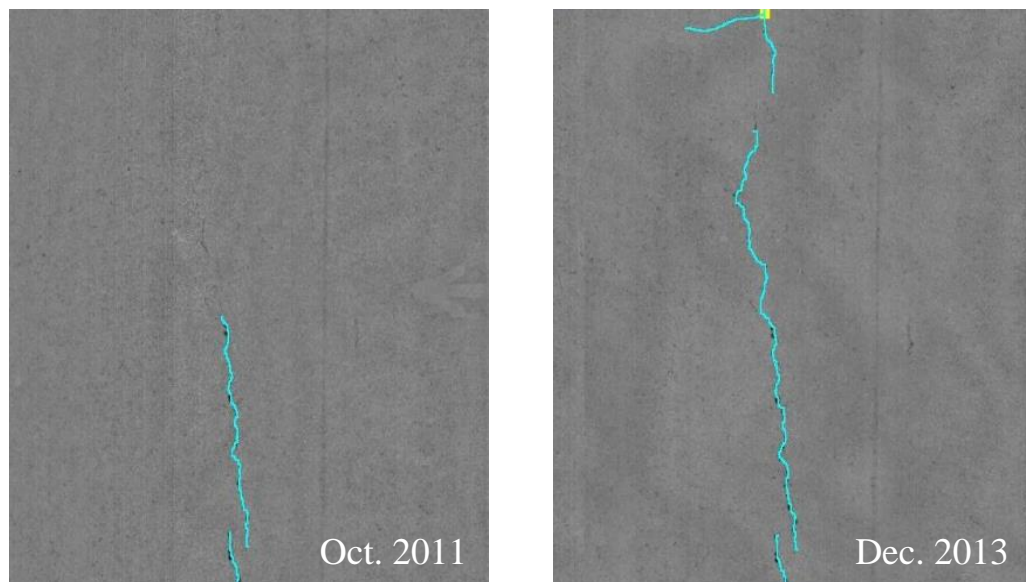


**Figure 5.17 Comparison between crack deterioration along longitudinal and other directions on the selected 200-ft. section near Milepoint 7.5**

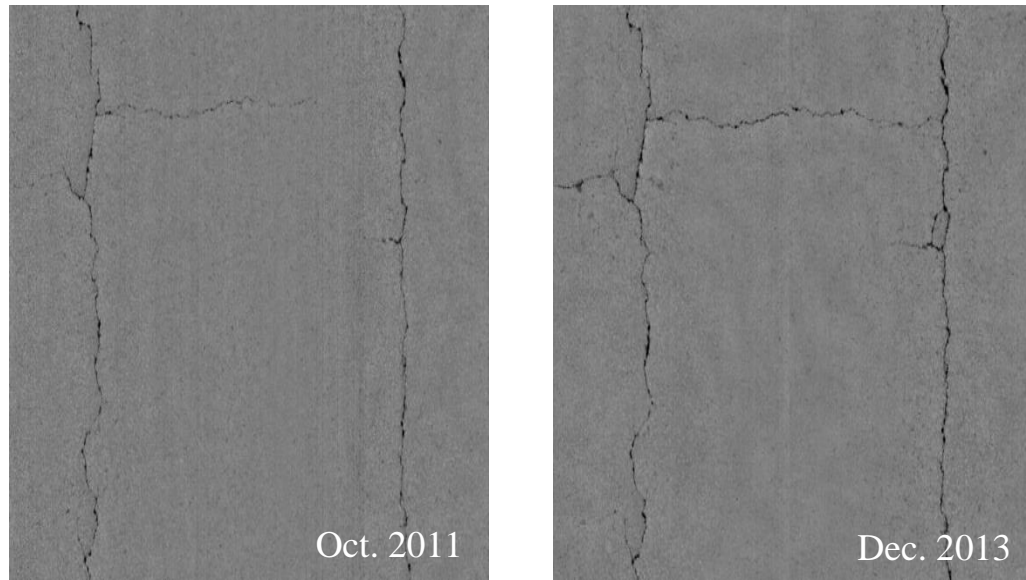


(a) Comparison between range images

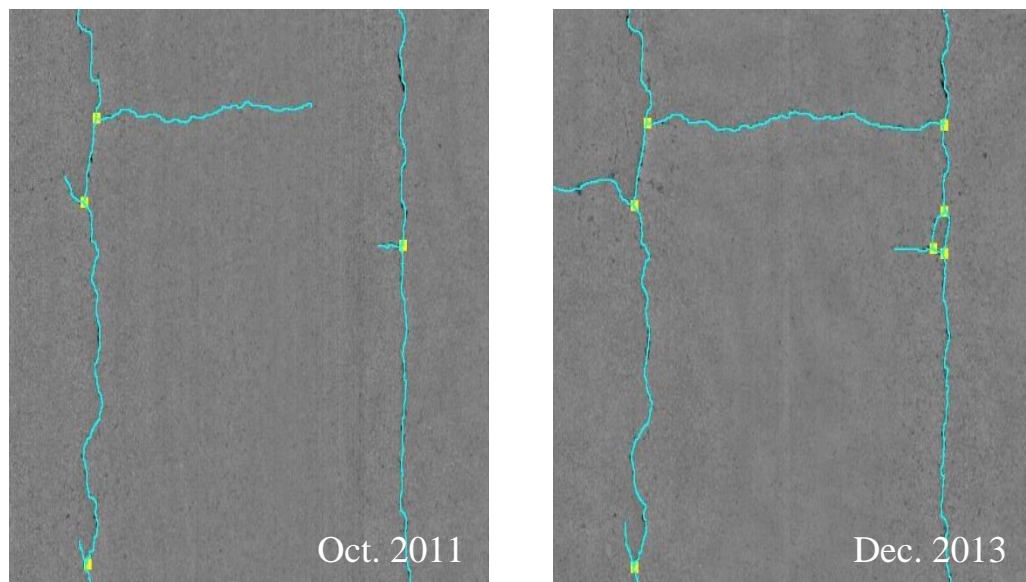


(b) Comparison between detected crack maps

**Figure 5.18 Illustration of crack deterioration along longitudinal direction on the selected section near Milepoint 7.5**



(a) Comparison between range images



(b) Comparison between detected crack maps

**Figure 5.19 Illustration of crack deterioration along transverse direction**

### **Crack Intersection**

Crack intersections locate the crossing points of the predominant crack curves. The number of crack intersections indicates the complexity of the crack pattern and the severity of the crack condition. Crack intersections are usually introduced by the branching-out or connection of existing crack curves. As shown in Figure 5.20, the number of crack intersections has increased dramatically over the two-year period, which confirms that the branching-out of existing cracks was the major crack deterioration behavior during that period of time. Figure 5.21 presents an example where crack branching-out is clearly observed.

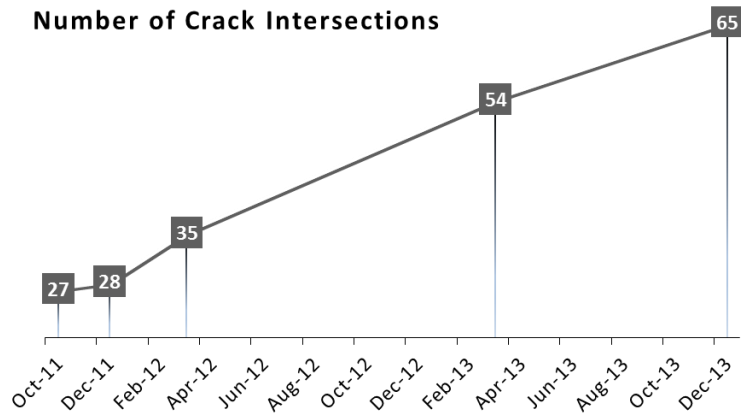
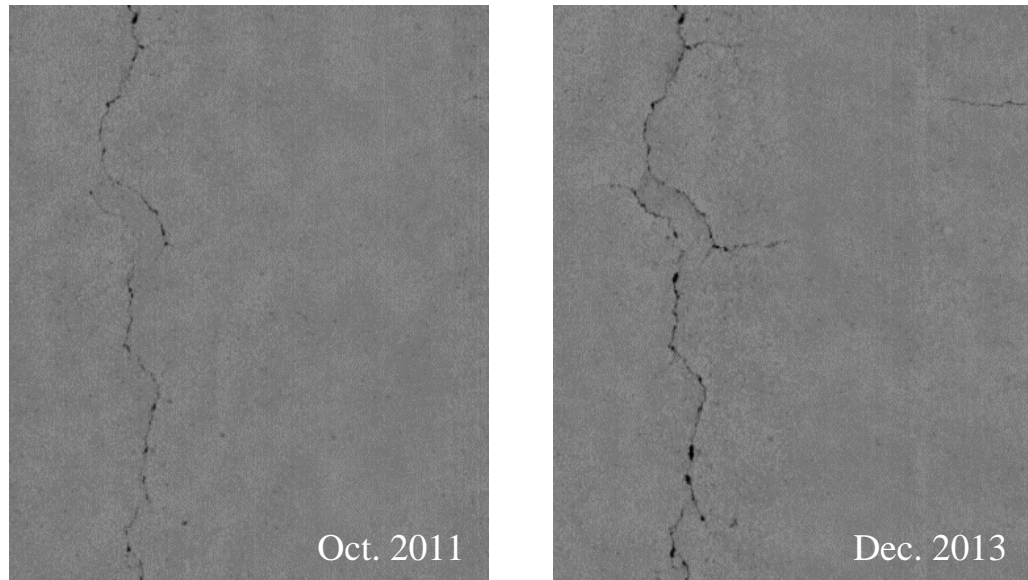
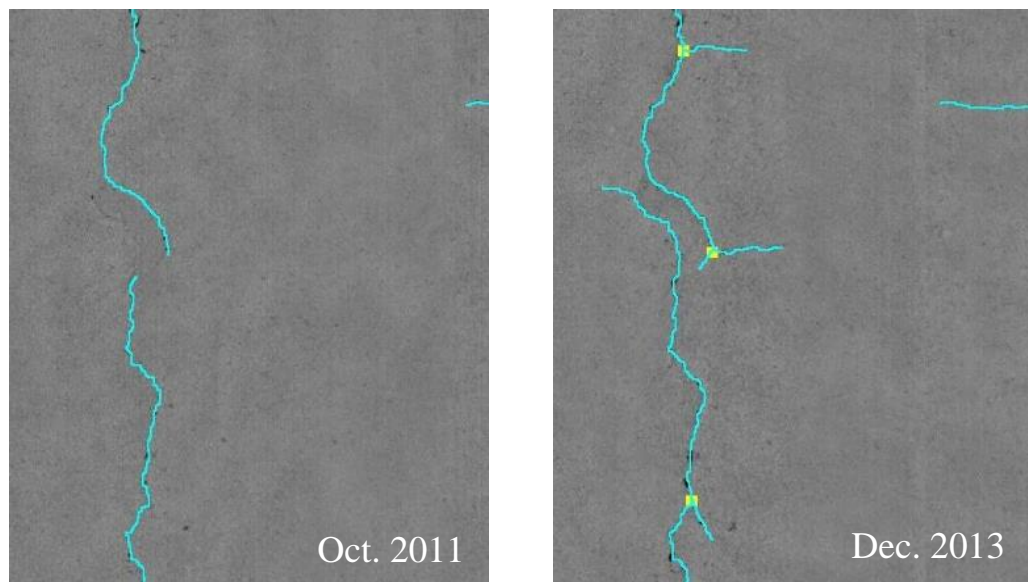


**Figure 5.20 Change in number of crack intersections across five different timestamps on the selected 200-ft. section near Milepoint 7.5**



(a) Comparison between range images



(b) Comparison between detected crack maps

**Figure 5.21 Illustration of crack branching-out (crack intersections are marked as yellow dots)**

### **Crack Polygons**

Many crack curves intersect with each other and form an enclosed piece-like area, which is referred to as a crack polygon. The number and extent of each crack polygons is an important property to differentiate crack types and severity levels. For example, an extensive existence of small crack polygons is usually referred as “alligator cracking”, which indicates high severity load-related cracking and potential structural failure. In the study, the number of crack polygons within the selected sections are counted across different timestamps (as shown in Figure 5.22). The crack polygons started to appear in the second half of the given period, but the number was still limited. A further investigation on the detected crack maps shows that these distributed polygons are isolated, so their existence doesn’t significantly impact the crack type and severity level within the selected sections. Figure 5.23 shows an example of how the crack polygons are formed through crack deterioration.

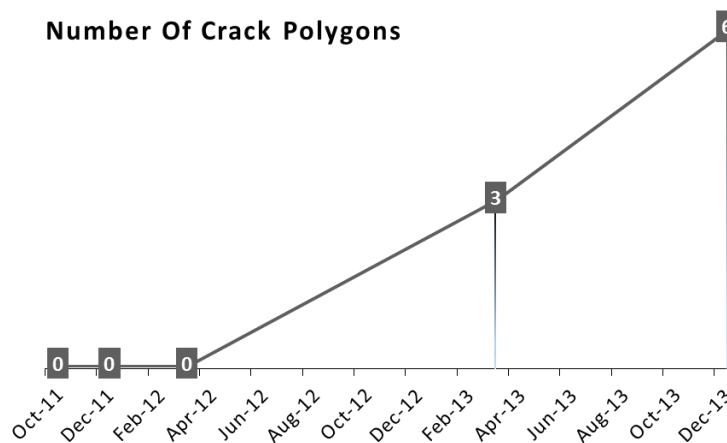
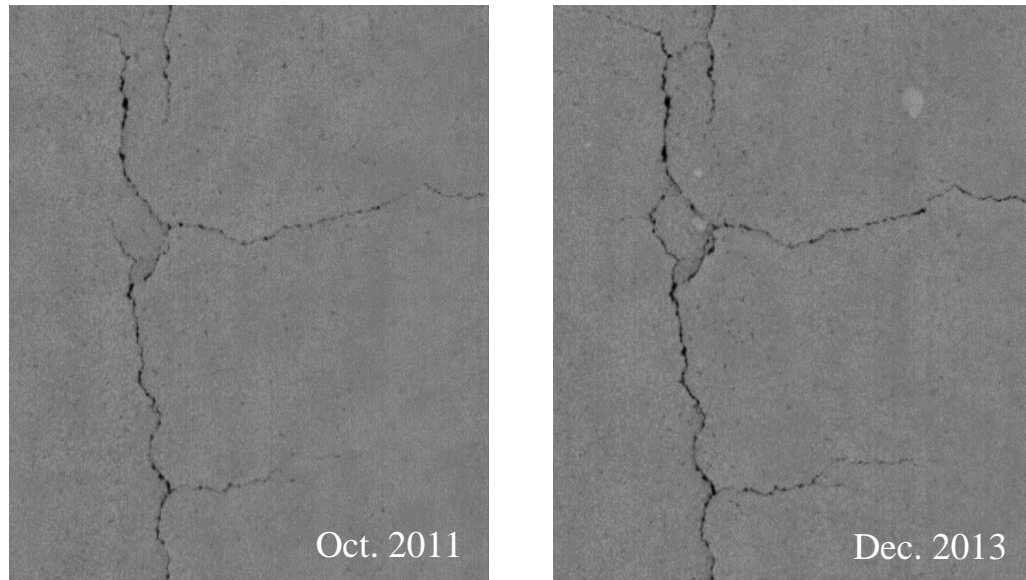
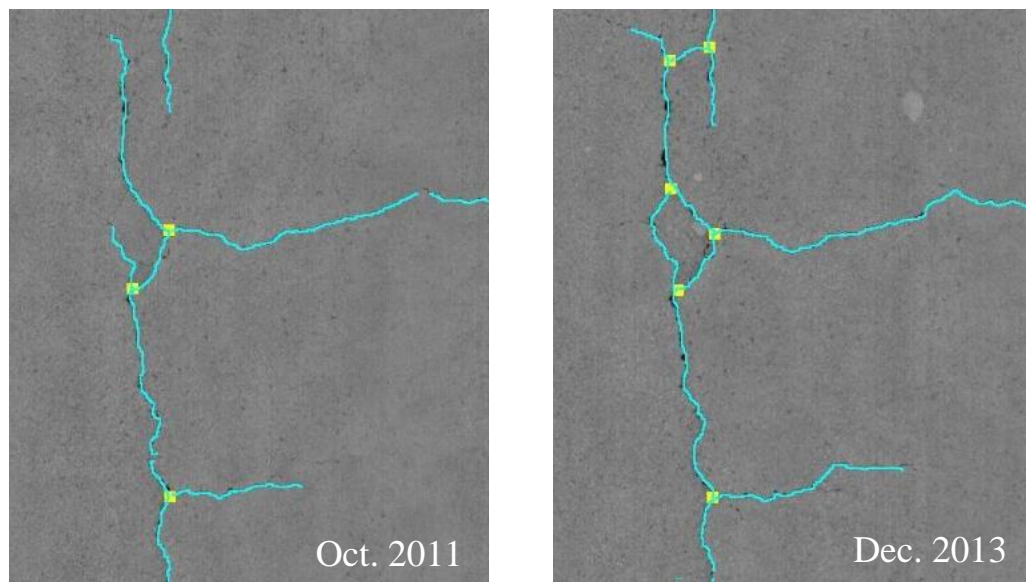


**Figure 5.22 Change in number of crack polygons across five different timestamps on the selected 200-ft. section near Milepoint 7.5**





(a) Comparison between range images



(b) Comparison between detected crack maps

**Figure 5.23 Illustration of forming crack polygons**

In summary, this section presents the potential application of monitoring pavement crack deterioration behaviors from temporal domains. The pavement cracks continuously deteriorate over time. In order to identify the critical timing to trigger pavement maintenance, the behavior of crack deterioration should be thoroughly studied.

The proposed method provides a detailed representation of crack deterioration that will reveal how infrastructures react to certain situations, such as climate change or extreme events. Pavement sections can be identified as vulnerable/sustainable based on their high/low deterioration rates, and their detailed behaviors on failing/succeeding extreme conditions and particular roadway environment can be revealed with the proposed method. While it is infeasible to comprehensively cover the entire research, this study is a concrete first step and is believed to be transformative in changing the way researchers have approached sensing based infrastructure condition monitoring and risk assessment. In addition, the existing issues and potential challenges are identified based on the experience from this study, which are expected to benefit future research in this field and listed as follows.

- First, the method for data registration between multiple timestamps needs to be developed. In this study, multiple timestamps are registered together manually based on the markers on the road. This requires markers to be painted on the road to label the terminus of the survey section before data collection. It becomes infeasible to conduct the study at a larger scale (e.g. in a state-wide survey). Automatic data registration method based on GPS and existing pavement features is needed for future research.
- Second, the data variability needs to be thoroughly evaluated. On one hand, the survey areas are not always consistent between multiple timestamps, and data completeness is always guaranteed. Most pavement data acquisition systems are able to cover one lane width, only if the vehicle is driving in the middle of the lane. However, this is difficult to guarantee in large-scale and long-span research.

Therefore, standard data collection procedures need to be developed. On the other hand, the inherent data variability needs to be studied so that it is not confused with the external crack deterioration behaviors.

- Third, research is needed to understand diverse internal and external factors of crack deterioration behavior. The study presented in this section focuses on monitoring and quantifying the changes. The next stage is to utilize these data in the pavement management applications, including forecasting deterioration behaviors and enhancing pavement design. It requires large-scale research and also depends on data availability in many other areas, such as traffic, environmental factors, design, construction and existing maintenance, etc.

## **CHAPTER 6. CONCLUSIONS AND RECOMMENDATIONS**

Pavement cracks are one of the most common pavement surface distresses; they are caused by constant overloading, asphalt aging, environmental impacts, and improper design, etc. Most state departments of transportation (DOTs) use crack data as essential information for their pavement asset management, including determining the optimal treatment method and timing, etc. State DOTs are also required to report pavement crack data as part of the annual pavement condition data through the Highway Performance Monitoring System (HPMS). Traditionally, state DOTs conduct manual pavement crack evaluations through field visual surveys, which are subjective, labor-intensive, time-consuming, and dangerous to field engineers in hazardous roadway environments. Methods have been developed to automate the pavement crack condition evaluation process, including both crack detection and classification. However, the existing crack detection algorithms haven't yet achieved the desirable performance to be fully automated. In addition, the past studies haven't yet addressed the challenging task of automatically classifying the complicated crack definitions from real-world distress protocols. This study proposes a crack detection and diagnosis methodology for automated pavement condition evaluation; it has two main focuses, one of which is to develop an accurate and robust crack detection algorithm to generate crack maps from the sensor data, and the other is to develop a generalized framework to transform the detected crack maps into engineeringly meaningful information, including crack types and severity levels, to support transportation agencies' pavement management decisions. This

chapter summarizes the major contributions and findings of this study and proposes recommendations for future research.

## 6.1 Contributions

The contributions of this research are as follows:

- **A new crack detection algorithm is developed to automatically generate crack maps from the pavement images.**
  - Built upon the active contour-based minimal path procedure, the key innovation of the proposed algorithm is that it removes the constraint of prior inputs by automatically generating key points across the image through tensor voting and crack skeleton analysis. Such automatic initialization is critical for a fully automated pavement crack evaluation method.
  - The proposed algorithm is capable of accurately detecting continuous crack curves and preserving the high-level topological information of crack patterns, which are critical inputs for the subsequent crack condition analysis, such as automatic crack type and severity level classification.
  - The noise removal and profile rectification procedure proposed in this study is generically applicable to 3D pavement surface data and can be used in the detection and analysis of other pavement surface distresses, such as raveling and rutting, etc.
- **A generalized crack diagnosis framework is proposed and developed to transform detected crack maps into useful pavement management decision**

**support information, including different crack types and severity levels and crack deterioration behaviors.** It consists of the following:

- A multi-scale crack representation based on the Crack Fundamental Element model to extract the engineeringly meaningful and rich crack properties from the detected crack maps at multiple scales. These crack properties are completely independent from the diverse distress protocols or survey practices from federal and state agencies; therefore, they provide consistent crack measures between agencies and lay a critical foundation for a standardized pavement condition measure to fulfill the MAP-21 requirements. In addition, these crack properties can be flexibly transformed into existing crack definitions in different distress protocols, thus helping to maintain the legacy of state DOTs' historical data and pavement management practices.
- A generalized method is proposed for the first time to automatically classify complicated crack types and severity levels in real-world distress protocols. It first extracts crack properties from the detected crack maps with the proposed multi-scale crack representation, and then it interprets these properties through a supervised machine learning classifier calibrated by real-world pavement data. In this study, the proposed framework has been applied to the AASHTO PP 67 standard and GDOT's PACES protocol, and it can also be extended to other complicated distress protocols. The ordered logistic regression model is used in this study and can be further replaced with more sophisticated classifiers if needed.

- A pilot study of quantifying crack deterioration behaviors in a field environment is conducted. With the emerging sensor data and the proposed methodologies, this study evaluates the feasibility of representing the quantifying crack deterioration in details on real pavements. The proposed crack deterioration study using detail-level sensor data will enable researchers to develop transformative ways to enhance infrastructure condition monitoring and risk management. It can be used to identify the vulnerable/robust pavement sections and study their detailed behaviors in failing/succeeding extreme conditions and particular roadway environments. This study also identifies the issues to address for future, large-scale data utilization and infrastructure management.

## 6.2 Findings

The findings for the proposed crack detection algorithm are as follows:

- **The proposed crack detection algorithm is fully automatic and is different than existing minimal path algorithms that require at least one prior input point for each crack curve.** Such full automation saves large amounts of time and manual effort in detecting cracks. Experimental tests compare the proposed algorithm to an existing variant of the minimal path algorithm developed by Kaul et al. (2012). The results show that to generate an accurate crack map, Kaul's algorithm needs an average of 6.6 user-input points, while the proposed algorithm is fully automatic. Thus, the proposed algorithm can produce an accurate crack map with much less effort. In addition, the detection accuracy of the proposed algorithm is significantly better on high-density cracks (e.g. alligator cracking)

than Kaul's semi-automatic algorithm, which suffers from subjective and inconsistent key point selection.

- **The proposed crack detection algorithm is robust to different pavement surface textures.** Experimental tests show that the proposed algorithm can effectively handle pavement images collected from different surface types. The experimental dataset comes from concrete surfaces of Interstate highways I-16 and I-516, asphalt open graded friction course surface from Interstate highway I-85, and asphalt dense graded surface from state route GA SR-236. The proposed algorithm achieves an average accuracy score of 91.2 (using buffered Hausdorff distance scoring method) in comparison to manual digitized ground truth crack maps, which indicates its robust performance across different pavement surface textures.
- **The proposed crack detection algorithm is robust to different crack patterns.** Experimental tests evaluate the proposed algorithm on both synthetic images and real pavement images. The synthetic images consist of three fundamental crack structures, including single curves, intersections, and polygons, and artificially added noises. Real-pavement images in the test show five different categories of cracking conditions: no cracking, longitudinal cracking, transverse cracking, the combination of longitudinal and transverse cracking, and alligator cracking. The proposed algorithm demonstrates an accuracy score of 92.6, which indicates its robust performance across different crack patterns.
- **In terms of accuracy, the proposed crack detection algorithm outperforms existing crack detection algorithms and the commonly used commercial**



**crack detection software.** The proposed algorithm is compared with other crack detection algorithms and software, including dynamic optimization (Alekseychuk 2006; Jiang and Tsai 2013); it has been documented in pertinent literature as having the best accuracy as an automatic algorithm. It is also compared to LCMS commercial software (version 4.1.1, release in March 2015) (Laurent et al. 2008). The proposed algorithm demonstrates superior performance across different pavement surface textures and different crack patterns. Its superior performance is demonstrated specifically in two aspects: 1) it has a better capability to detect fine cracks from a low-contrast pavement images because tensor voting helps enhance vague and discontinuous cracks from the image and the minimal path algorithm guarantees finding the global optimal curve as long as the input points are provided; and 2) it has fewer false positive detections on rougher or non-uniform surface textures, and it demonstrates significantly better accuracy on OGFC and concrete surfaces.

- **The proposed crack detection algorithm generates repeatable crack maps from multiple runs of data, despite the natural data variance introduced through the collection process.** Repeatability tests are conducted on two 100-ft. sections with five runs of data collected on each section. Experimental results show that the relative standard deviation of total crack length across five runs is, at most, 2.2 percent; the difference is mainly caused by the inconsistent detection of transverse cracks near image boundaries. In addition, the similarity of detected crack maps across multiple runs has a score of at least 89.8. The results show that

the proposed algorithm can be utilized in objective and reproducible automated pavement crack surveys.

The proposed crack diagnosis framework produces the following results:

- **The crack properties extracted from the proposed multi-scale crack representation are fully compatible with existing federal and state crack definitions.** The crack definitions from both the AASHTO provisional standard PP 67 and GDOT's PACES distress protocol are implemented in this study. The extracted properties have demonstrated their capability to be flexibly transformed into simple standards, as well as complicated real-world distress protocols.
- **The proposed automatic crack classification algorithm achieves high classification accuracy on load cracking, block/transverse (B/T) cracking, and their severity levels.** Experimental results show that the algorithm achieves an accuracy of 92.2% when classifying load cracking and its four severity levels on a test set of 701 images; it achieves an accuracy of 98.1% when classifying B/T cracking and its three severity levels on a test set of 368 images.
- **The proposed automatic crack classification and quantification method provides accurate survey results that compare well to the manual ground truths established in the field.** Site comparisons are conducted to compare the proposed crack classification and quantification method and manual field survey. Three 100-ft. pavement sections from GA SR-236 and one section from GA SR-275 are selected. GDOT pavement engineers help establish the ground truths in the field, and the crack extents are precisely measured using a measuring wheel. Based on the experimental results, the overall crack deducts given by the

proposed method are close to those of the field measurement, with an average absolute difference of 3.25, which is within the error tolerance ( $\pm 5$  deduct points) in GDOT's current survey practices.

The most significant benefits that the transportation agencies, e.g. state DOTs can obtain by adopting the proposed crack detection and diagnosis methodology are the improved accuracy, repeatability, and survey coverage. The reasons can be summarized into the following aspects. First of all, the methodology can improve the accuracy and reliability of the DOTs' existing practice. The current manual survey practice suffers from different issues, such as the inconsistency of human judgment and the potential bias of the sampling process. The proposed methodology can gather detailed distress information in a full-extent survey in order to determine accurate treatment methods and timing, which will further allow more reliable cost and budget planning. Second, the improved accuracy becomes critical when investigating crack deterioration over time, which will contribute to more reliable pavement deterioration modeling and forecasting. Third, the proposed methodology creates the opportunities for new operations and management practice. For example, automated, machine-guided crack sealing requires the detected crack maps to be as accurate as possible, which is very difficult to achieve in the past. Another example is that the proposed methodology can help determine localized treatments. With the limited budget, it has become more and more difficult to provide maintenance operations to the projects as a whole. Localized treatments are a cost-effective alternative, but it has to be supported by such full-extent, detailed survey results. The costs of implementing the proposed methodology may vary between different state DOTs, and will not be quantitatively evaluated here. The most important prerequisite of

adopting the proposed methodology is the availability of sensor data on highway networks, which requires initial and periodic investments. However, as more and more state DOTs have already setup similar roadway sensing systems or purchased the sensor data from vendors, the proposed methodology can be directly utilized to enhance the pavement management decision making capability.

### **6.3 Recommendations for Future Work**

For the proposed crack detection algorithm, the following recommendations are made:

- Parallel processing and GPU processing for the tensor voting framework is recommended to further speed up the algorithm. Since the voting process from each token is independent, the algorithm is compatible with potential parallel processing implementation. For practical use, cluster computing can also be considered when dealing with large-scale pavement survey tasks.
- Different methods can be used to replace adaptive thresholding to reduce the number of initial tokens for the tensor voting, in order to further reduce the computation cost.
- Establishing a mapping relationship between the pavement surface roughness and the tensor threshold  $\Gamma$  is recommended. For example, the rough surface textures for OGFC surfaces and raveled surfaces, introduce additional initial tokens for the tensor voting; therefore, the overall amplitude of the crack potential map is higher; this will require a larger tensor threshold  $\Gamma$  to avoid false positive detections.
- An algorithm to further differentiate construction joints, pavement scratches and cracks is recommended for practical implementation. They can further be

separately based on the spatial distribution of detected pixels along the predominant orientation; while crack pixels have a free-form shape and meander with a larger variance along the curve, joints and scratches are straight lines or smooth curves.

- It is recommended that 2D and 3D pavement surface data be combined to better detect sealed cracks. Limited by the data acquisition mechanism, 3D surface data is not able to capture sealed cracks because these cracks have no elevation differences or only minor elevation differences when comparing them to their neighborhood. Incorporating 2D intensity images is expected to help resolve this issue. The proposed algorithm is best tuned for 3D surface data, but it has been proved to also be applicable to 2D intensity images.

For the proposed crack diagnosis framework, the following recommendations are made:

- The proposed crack classification and quantification method should be extended to other distress protocols. The current study focuses on the AASHTO PP 67 and GDOT's PACES distress protocol (specifically on load cracking and B/T cracking). Future research can involve crack definitions from different federal and state agencies to enhance the capability of the proposed method.
- A large-scale implementation on state-wide pavement condition survey is recommended. The advantages of an automatic crack survey, including objectivity and full coverage, can be beneficial to the state DOTs' current pavement management practices.

- With the flexibility of the proposed crack classification framework, different classification models can be explored, including neural network, decision forest, etc., to further enhance the classification accuracy for different applications.
- The automatic crack survey results should be combined with other distresses, including rutting and raveling, etc., for treatment determination in a sensor-based pavement management system. A GIS-based application is recommended for visualizing and managing these automatic survey results, which will further enhance the decision-support capability.
- An automatic method for data registration between multiple timestamps of collected data should be developed so that the large-scale crack deterioration study using detail-level sensor data can be feasible. This possibly requires the use of both GPS and existing pavement features, such as lane marking and cracks, etc., that can be matched in spatial and temporal domains.

## **APPENDIX A. MINIMAL PATH AND ITS APPLICATION ON PAVEMENT CRACK DETECTION**

### **A.1 Background**

The minimal path techniques are derived from the active contour model, which was introduced by Kass et al. (1988) for boundary integration and feature extraction in the area of computer vision and image processing. The active contour (i.e. snake) model requires the users to draw an initial curve in an image; then, the curve evolves by minimizing a pre-defined energy functional to reach the goal. This energy functional contains an image-based term that is related to desired features, such as edges and boundaries; in addition, it also contains a curve-based term to keep the smoothness of the curve. One significant limitation of various active contour models is their initialization-dependent performance: spurious and isolated edges in a noisy or complex image may trap the curve evolution into a local minimum. To tackle this limitation, Cohen and Kimmel (1997) introduced a global minimal cost path approach, which allowed users to specify two end points instead of a complete initial curve and guaranteed detection of the global minimum of an active contour model's energy between two end points. The key difference between this minimal path approach based on active contour models and the minimal path estimation using graph search algorithms like the A\* (Dijkstra 1959; Sedgewick 1988) is that the graph based algorithms consider the pixels in an image as the vertices of the graph, which suffer from digitization bias due to the metrication error; the minimal path approach based on active contour models, on the other hand, deals with the continuous version of the problem as long as possible and, thus, provides higher accuracy.

Despite its advantages, the minimal path approach still requires user-input end-points for the desired curve. Studies have been conducted to relax the requirements on prior information. Benmansour and Cohen (2009) proposed a variant of the minimal path approach, which required one end-point as initial input and detected representative key points along the curve using front propagation. The algorithm terminated automatically on closed curves, but for open structures, either all the endpoints or some endpoints plus the length of the curves were still required. Kaul et al. (2012) further improved the algorithm, which only requires one arbitrary point along the desired curve. The stopping criteria are re-designed to work with both closed and open curves. However, the performance depends on the step-size of the propagation, and early termination still exists, especially on low-contrast pavement images. Other researchers have used statistical shape priors (Guo and Fei 2009; Yan and Kassim 2006) and Principal Component Analysis (PCA) (Li and Fei 2008) to detect closed contour objects with known shapes. These studies are designed for medical image processing tasks, such as extracting organ shapes, but can hardly be applied on pavement crack detection, where the crack shapes are diverse and uncertain.

The task of pavement surface condition evaluation needs to deal with millions of pavement images collected across the highway networks. The efforts of user input and interaction need to be eliminated or, at least, minimized. The motivation of the current work is to detect cracks on pavement images with completely automatic initialization. In Section A.2, the theory of minimal path techniques will be introduced. Section A.3 presents some preliminary research efforts on applying the minimal path approach on the pavement crack detection.



## A.2 Theory of Minimal Path Techniques

The minimal path techniques captures the global minimum curve between two user input endpoints based on a contour dependent energy functional. As mentioned previously, the active contour model combines an image feature term and a smoothing term in a composite energy functional:

$$E(\gamma) = \alpha \int_0^1 \|\gamma'(s)\|^2 ds + \beta \int_0^1 \|\gamma''(s)\|^2 ds + \lambda \int_0^1 \Phi(\gamma(s)) ds \quad (\text{A.1})$$

where  $\alpha$ ,  $\beta$ , and  $\lambda$  are real positive weighing constants,  $\gamma(s) \in \mathbb{R}^n$  is a curve that is parameterized with respect to arc-length  $s$ ,  $\gamma'(s)$  and  $\gamma''(s)$  are the first and second derivatives of the curve and  $\Phi$  is a potential that depends on desired image features. In the minimal path technique, a simplified energy is chosen that is given by

$$E(\gamma) = \int_{\Omega} (\Phi(\gamma(s)) + \omega) ds \quad (\text{A.2})$$

where  $E(\gamma)$  is energy computed along the curve,  $\gamma(s)$  is the curve chosen in domain  $\Omega$ , and  $\omega$  is a real constant. In this study, we assume that the potential  $\Phi$  already includes the constant  $\omega$ . A potential  $\Phi: \Omega \rightarrow \mathbb{R}^+$  is built from a given 2D or 3D image  $I: \Omega \rightarrow \mathbb{R}^+$ , where  $\Phi$  is greater than 0 and holds lower values around the desired features of the image  $I$ . The choice of the potential  $\Phi$  depends on the application. For example, the potential function  $\Phi$  for cracks can be taken to be a function of intensity value at each pixel because cracks are darker than the background. The goal is to extract a curve that minimizes the energy functional  $E: A_{p_1, p_2} \rightarrow \mathbb{R}^+$  between two user defined points  $p_1$  and  $p_2$

$$E(\gamma) = \min_{\gamma \in A_{p_1, p_2}} \int_{\gamma} \Phi(\gamma(s)) ds \quad (\text{A.3})$$

where  $A_{p_1, p_2}$  is the set of all path connecting  $p_1$  to  $p_2$  and  $s$  is the arc length parameter.

The curve connecting  $p_1$  to  $p_2$  that globally minimizes the energy  $E(\gamma)$  is called the

minimal path between  $p_1$  and  $p_2$  or the geodesic. The geodesic curve is denoted by

$C_{p_1, p_2}$ . This minimization problem can be solved through the computation of geodesic

distance map  $U_1 : \Omega \rightarrow \mathbb{R}^+$  associated with  $p_1$ . The geodesic distance map is defined as

the minimal energy integrated along a path between  $p_1$  and any point  $x$  of the domain

$\Omega$

$$\forall x \in \Omega, U_1(x) = \min_{\gamma \in A_{p_1, x}} \int_{\gamma} \Phi(\gamma(s)) ds \quad (\text{A.4})$$

The values of  $U_1$  are the arrival times of a front propagating from the source  $p_1$  with

velocity  $(1/\Phi)$  and  $U_1(p_1) = 0$ .  $U_1$  satisfies the Eikonal equation:

$$\|\nabla U_1(x)\| = \Phi(x) \quad \text{for } x \in \Omega \quad (\text{A.5})$$

This geodesic distance map calculation can be generalized to the case of multiple sources.

The minimal action map or the geodesic distance map associated with potential

$\Phi : \Omega \rightarrow \mathbb{R}^+$  with a set of  $n$  sources  $S = \{p_1, \dots, p_n\}$  is the function  $U : \Omega \rightarrow \mathbb{R}^+$ , where

$$\forall x \in \Omega, U(x) = \min_{1 \leq j \leq n} \{U_j(x)\} \quad (\text{A.6})$$

$$\text{and } U_j(x) = \min_{\gamma \in A_{p_j, x}} \int_{\gamma} \Phi(\gamma(s)) ds$$

For all  $p_j \in S$ ,  $U(p_j) = 0$  and  $U$  satisfies the Eikonal equation, as well. Another

important quantity is the Euclidean distance map. It's the function  $L : \Omega \rightarrow \mathbb{R}^+$  that

assigns the Euclidean length of the minimal geodesic between  $x$  and the source  $S$  to

every point  $x$  of the domain  $\Omega$ .

$$\forall x \in \Omega, L(x) = \int_{C_{pj,x}} ds \quad (\text{A.7})$$

where

$$C_{pj,x} = \min_{1 \leq i \leq n} C_{pi,x} \quad (\text{A.8})$$

is the minimum of all minimal paths from  $x$  to each source point  $p_i$ .  $C_{pi,x}$  is calculated using the potential  $\Phi$ . In general if  $\Phi \neq 1$  for all  $x \in \Omega$ , then the geodesic distance map  $U$  is always different from the Euclidean distance map  $L$ .

Centered finite difference schemes for solving the Eikonal equation are unstable. There are three algorithms to compute the map  $U$ , and they are all consistent with the continuous energy formulation implemented in a rectangular grid. These three algorithms utilize level set methods, shape from shading methods, and Fast Marching methods. Fast Marching methods were favored because their lower complexity compared to the other methods. Sethian (1999) proposed the Fast Marching method to solve the Eikonal equation that relies on a one-sided derivative that looks in the up-wind direction of the moving front. In the 2D case, at each point  $x = (i, j)$ , the numerical method gives the solution approximating  $U_{i,j}$

$$\left( \frac{\max \{u - U_{i-1,j}, u - U_{i+1,j}, 0\}}{\Delta x} \right)^2 + \left( \frac{\max \{u - U_{i,j-1}, u - U_{i,j+1}, 0\}}{\Delta y} \right)^2 = (\Phi(i, j))^2 \quad (\text{A.9})$$

Here  $\Delta x$  and  $\Delta y$  are the grid spacing in the  $x$  and  $y$  direction respectively. This is the 4-neighbor scheme for the Fast Marching method.

The structure of the algorithm is almost identical to Dijkstra's algorithm for computing shortest paths on graphs. In the course of the algorithm, each grid point is tagged either "Solved" (a point for which  $U$  has been computed and frozen), "Active" (a

point for which  $U$  has been estimated but not frozen) or “Unvisited” (a point for which  $U$  is unknown). The set of “Active” points form an interface between the set of grid points for which  $U$  has been frozen (the “Solved” points) and the set of other grid points, i.e. the propagation frontier, the Fast Marching algorithm helps calculate geodesic distance map  $U$  and Euclidean distance map  $L$  for every grid point. The improvement made by the Fast Marching algorithm is computationally efficient because a heap data structure can be used to quickly find the next “Solved” points at each step, which should be the points with the smallest  $U$  value among the current “Active” points. If “Active” points are ordered in a minimum heap structure, the computational complexity of the Fast Marching method is  $O(N \log N)$ , where  $N$  is the total number of grid points.

Benmansour and Cohen (2009) compute the geodesic distance map  $U$  and the Euclidean distance map  $L$ , according to the discretization scheme for the Fast Marching method given by Sethian (1999). Various improvements have been made to improve the accuracy of computing  $U$  and  $L$ , such as the 8-neighbor and 12-neighbor scheme.

After the geodesic distance map  $U$  is calculated, the geodesic between starting point and any other points in the domain can be traced using back propagation. For a single starting point  $p_1$ , the minimum of  $U$  is at the front propagation starting point  $p_1$  where  $U(p_1) = 0$ . The gradient of  $U$  is orthogonal to the propagation fronts, since these are its level sets. Therefore, the minimal path between any point  $q$  and the starting point is found by sliding back along the gradient of the map  $U$  until arriving at  $p_1$ . This back propagation procedure is a simple steepest gradient descent. It is possible to make a straightforward implementation on a rectangular grid: given a point  $q$ , the next point in

the chain connecting  $q$  to  $p_1$  is selected to be the neighbor  $p'$  of  $q$  for which  $U(p')$  is minimum.

### A.3 Preliminary Investigation on Crack Detection

In this section, we evaluate whether the minimal path techniques are applicable on pavement crack detection. We start from the simplest potential function, which is given by

$$\Phi(i, j) = I(i, j) + \varepsilon \quad (\text{A.10})$$

where  $I(i, j)$  is the image pixel value at each point  $x = (i, j)$  and  $\varepsilon = 10^{-6}$  is a constant.

Two points on an image are randomly assigned at the beginning. As described in the previous section, the algorithm starts with one input point, calculates the geodesic distance map with the given potential function until it reaches the other input point, and then uses a back propagation algorithm to generate the minimal path between these two points. The grid spacing for the discretization step was chosen to be 1. The purpose of adding a small constant  $\varepsilon$  is to avoid the back propagation's being trapped inside wide cracks with a pixel value of zero. The results on one sample image are shown in Figure A.1.

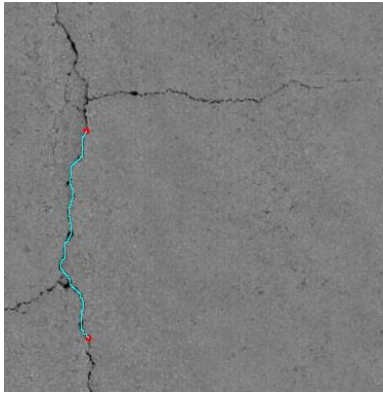
The input is a pavement range image collected through the line laser imaging system. Four different scenarios are presented with different initial point combinations. The observations can be listed:

- When the initial points are correctly located on the cracks, the minimal path procedure usually manages to detect the crack curve in between, as shown in

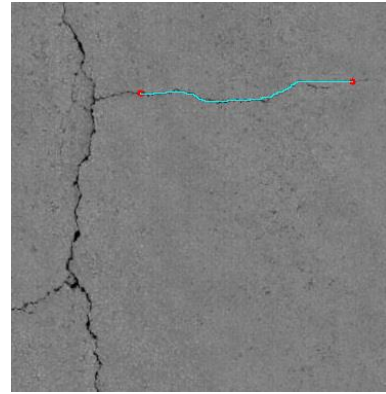
Figure A.1(a). The minimal path meanders within the cracks correctly, and this can be used for crack detection.

- When the contrast between crack and non-crack pixels are low, the minimal path procedure might fail to detect the complete crack curve, as shown in Figure A.1(b); as the external term is not significant anymore, the internal term in the energy function, which controls the smoothness of the curve, dominates the detection, and generates straight lines at some locations. This may happen around hairline cracks on the pavement, whose widths are very small. The contrast of the pavement image needs to be enhanced before being used as the potential function.
- The minimal path procedure has certain error tolerances on the initial point locations. In Figure A.1(c), one of the initial points is not exactly located on the crack curve; however, the algorithm still manages to snap to the closest curve quickly and detects the desired shortest path.
- However, the user-input initial points are still critical for the algorithm performance. Since the minimal path procedure guarantees finding the global minimum solution no matter where the input points are, misplaced inputs points will lead to false positive crack detection results, as shown in Figure A.1(d). Such prior information is still a very restrictive condition for finding correct cracks on pavement images.

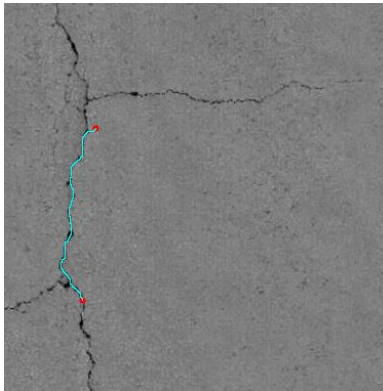
This study will further investigate how to remove the constraint of prior input points for minimal path algorithms and provide more accurate crack detection results. More details can be found in CHAPTER 3.



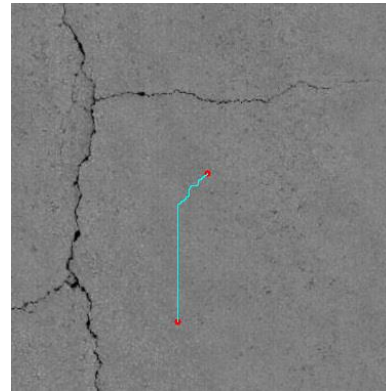
(a)



(b)



(c)



(d)

**Figure A.1 Preliminary evaluation of minimal path techniques on pavement crack detection**

## **APPENDIX B. TENSOR VOTING AND ITS APPLICATION ON PAVEMENT IMAGES**

### **B.1 Background**

The minimal path procedure described above requires the knowledge of two endpoints. In addition, it also assumes that the potential function is not very noisy and provides enough contrast (the desired feature points have a lower potential only in a local neighborhood region) that can enable the minimal path to track even convoluted, long curves along desired features. In the application of pavement crack detection in a real-world environment, these conditions are not easily met. First of all, the task of pavement surface condition survey needs to deal with thousands of images each time, which will require excessive manual effort for human to manually provide endpoint inputs. Also, the nature of pavement surface introduces fair amount of noises into the pavement images. Even with some emerging data acquisition techniques (such as the 3D line laser imaging technique), different noise sources still exist and impact the effectiveness of the potential function. Furthermore, pavement cracks usually form arbitrary patterns, including extensive branches and polygons, which introduces an extra challenge for the minimal path procedure to detect the crack pattern completely.

In this appendix, the tensor voting framework is introduced, which is used to infer curve structures from a noisy pavement image. Based on the literature review, the crack detection primarily relies on two principal assumptions: 1) Crack pixels can be distinguished from their surrounding area since they usually have a lower intensity/range value; i.e. crack pixels are usually darker/deeper than their neighborhood; and 2) crack pixels are usually continuous within a certain neighborhood; that is, crack pixels are



connected with each other to form a curve instead of being isolated. Significant cracks are not only characterized by the darker pixels, but, more importantly, the ones aligned with others form typically smooth, salient curves that encompass regions that are consistent in color or texture. We use Shashua and Ullman's definition of structural saliency (1988), which is a product of proximity and good continuation.

The tensor voting framework is introduced by Medioni et al. (Medioni et al. 2000; Mordohai and Medioni 2006), which attempts to implement Gestalt principles for perceptual organization. It was proposed to locate structured and salient information from a noisy dataset in computer vision and then further extended to perceptual grouping in 2D and 3D, shape from stereo, and motion grouping and segmentation. Each input site can be a point (with or without direction information) or a combination of both. Each site is first encoded with the second order representation (i.e. tensor representation), and then communicates its information to its neighborhood (i.e. voting). Each site collects all the votes cast at its location and encodes them into a new tensor. Through this process, the points that potentially form salient structures get enhanced, while the others are suppressed. The features of the tensor voting framework (Mordohai and Medioni 2006), including

- local,
- unsupervised,
- robust to noise, and
- amenable to a least-commitment strategy, postponing the need for hard decisions,

make it an effective approach to identify the crack-like pixels in a noisy pavement image, which can be a complement to the minimal path procedure. In the Section B.2, the theory

of the tensor voting framework will be briefly introduced. Its application on pavement images are preliminarily explored in Section B.3.

## **B.2 Theory of the Tensor Voting Framework**

### **B.2.1 2D Tensor Representation**

In this section, we use the term “token” as the generic points that are the input of the tensor voting framework. A token is a point with orientation. Intuitively, its tensor, which indicates the saliency of perceptual structure it belongs to, can be represented with an ellipse. As shown in Figure B.1(a), the axes of the ellipse are corresponding to the orientation of the token. The major axis is the preferred orientation of a potential curve that goes through the location (usually represented with normal orientation for the sake of consistency under higher dimensions), and the minor axis is the perpendicular direction. The shape of the ellipse indicates how certain the preferred orientation is; that is, an elongated ellipse represents a token with high certainty of orientation. The size of the ellipse is related to the saliency of information encoded; larger ellipses convey more salient information than smaller ones. There are apparently two extreme scenarios:

- A degenerate ellipse that is a perfectly oriented point (as shown in Figure B.1(b)), which is referred to as a stick tensor;
- A perfect circle with the same length on major and minor axes (as shown in Figure B.1(c)), which is referred as a ball tensor.

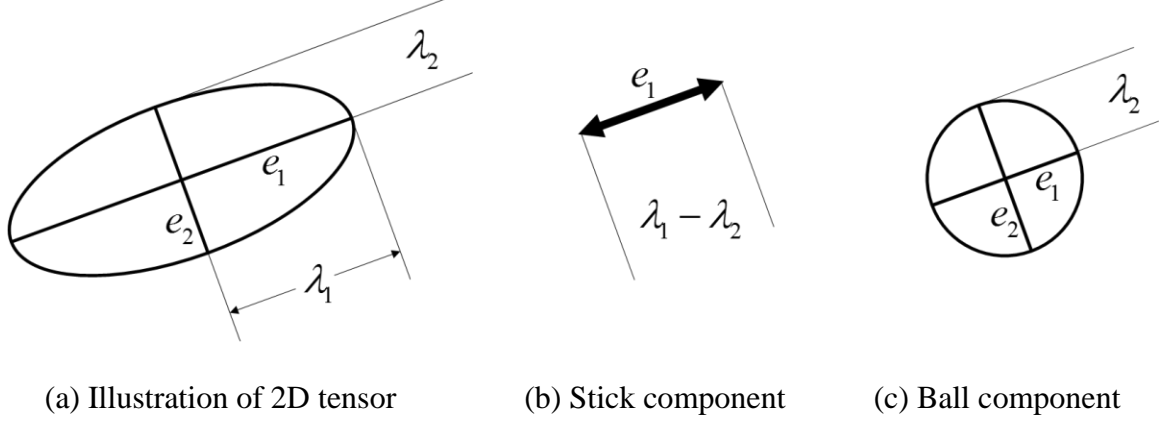


**Figure B.1 Illustration of 2D tensor and tensor decomposition**

Mathematically, this ellipse tensor, which is second order, symmetric, and non-negative definite, is equivalent to a 2x2 matrix. The axes of the ellipse are the eigenvectors of the matrix, and their aspect ratio is the ratio of the eigenvalues. An arbitrary second order, symmetric, non-negative definite tensor can be decomposed as in the following equation:

$$T = \lambda_1 \hat{e}_1 \hat{e}_1^T + \lambda_2 \hat{e}_2 \hat{e}_2^T = (\lambda_1 - \lambda_2) \hat{e}_1 \hat{e}_1^T + \lambda_2 (\hat{e}_1 \hat{e}_1^T + \hat{e}_2 \hat{e}_2^T) \quad (\text{B.1})$$

where  $\lambda_i$  are the eigenvalues in decreasing order and  $\hat{e}_i$  are the corresponding eigenvectors. Note that the eigenvalues are non-negative since the tensor is non-negative definite. As shown in the equation, an arbitrary tensor can always be decomposed into a stick component, which indicates a preferred orientation along  $\hat{e}_1$ , as shown in Figure B.1(b), and a ball component, which indicates no preference on the orientation as shown in Figure B.1(c). Correspondingly, the size of the stick component  $(\lambda_1 - \lambda_2)$  indicates curve saliency.

### B.2.2 Voting Process

After the input tokens have been encoded with tensors, the next step will be to propagate the information they contain to their neighbors. Given a token at  $O$  with normal  $\vec{N}$  and a token at  $P$  that belong to the same smooth perceptual structure, there are two parts of information that the token at  $O$  (the voter) wants to cast to the one at  $P$  (the receiver): the orientation and the magnitude. For orientation, if  $P$  shares the same perceptual structure as  $O$ , it should receive a vote along its existing preferred orientation; otherwise, it should receive a vote towards a different orientation. For magnitude, it is a function of the confidence that the voter and receiver indeed belong to the same perceptual structure.

The voting process from a stick tensor is the simplest scenario. In the absence of other information, the arc of the osculating circle (the circle that shares the same normal as a curve at the given point) at  $O$  is the most likely smooth path, since it maintains constant curvature. The second order vote is also a stick tensor and has a normal lying along the radius of the osculating circle at  $P$ . What remains to be defined is the magnitude of the vote. According to Gestalt principles, it should be a function of proximity and smooth continuation. The influence from one token to another should also attenuate curvature, to favor straight continuation over curved alternatives when both exist. Moreover, no vote is cast if the receiver is at an angle larger than 45 degrees with respect to the tangent of the osculating circle at the voter. The saliency decay function has the following form:

$$DF(s, \kappa, \sigma) = e^{-\left(\frac{s^2 + c\kappa^2}{\sigma^2}\right)} \quad (\text{B.2})$$

where  $s$  is the arc length  $OP$ ,  $\kappa$  is the curvature,  $c$  controls the degree of decay with curvature, and  $\sigma$  is the scale of voting, which determines the effective neighborhood size. The parameter  $c$  is a function of the scale and is optimized to make the extension of two orthogonal line segments to form a right angle equally likely to the completion of the contour with a rounded corner. According to Mordohai and Medioni (2006), its value is given by

$$c = \frac{-16 \log(0.1) \times (\sigma - 1)}{\pi^2} \quad (\text{B.3})$$

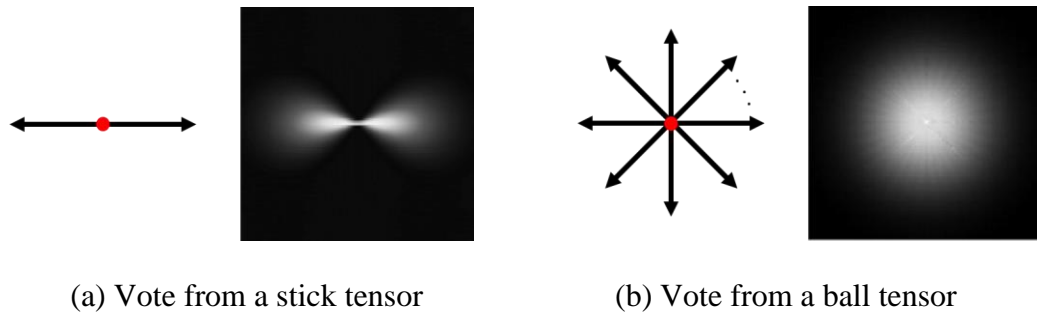


**Figure B.2 Illustration of the voting process**

The vote from a stick tensor is illustrated in Figure B.2(a). The ball tensor, which is the second elementary type of tensor in 2-D, has no preference of orientation, but still can cast meaningful information to other locations. The vote at  $P$  from a unit ball tensor at the origin  $O$  is the integration of the votes of stick tensors that span the space of all possible orientations (as shown in Figure B.2(b)). In practice, the integration is approximated by tensor addition.

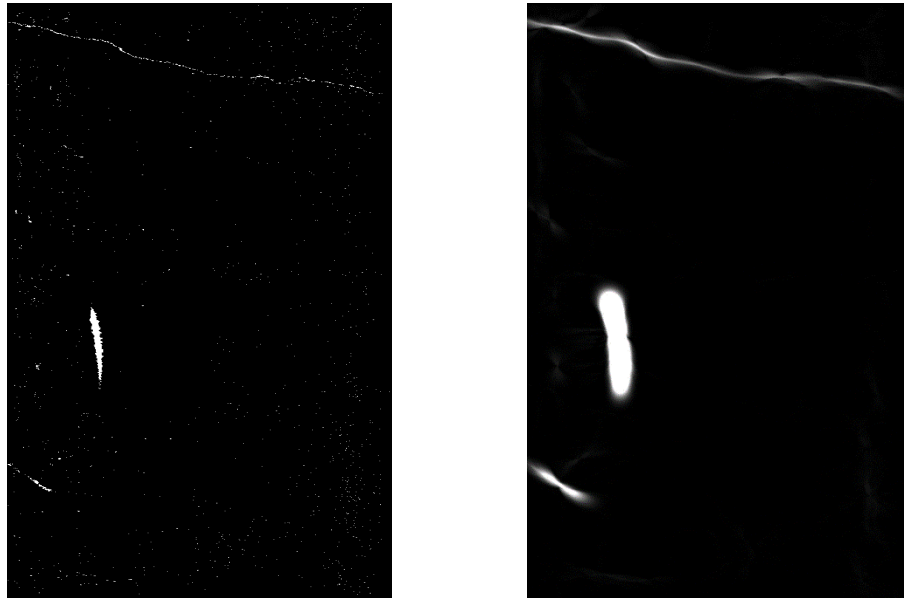
Votes are cast from token to token and accumulated by tensor addition. Analysis of the resulting second order tensors can then be performed through tensor decomposition to further identify the stick and ball component at an arbitrary location in 2-D space.

### B.3 Preliminary Investigation on Pavement Images

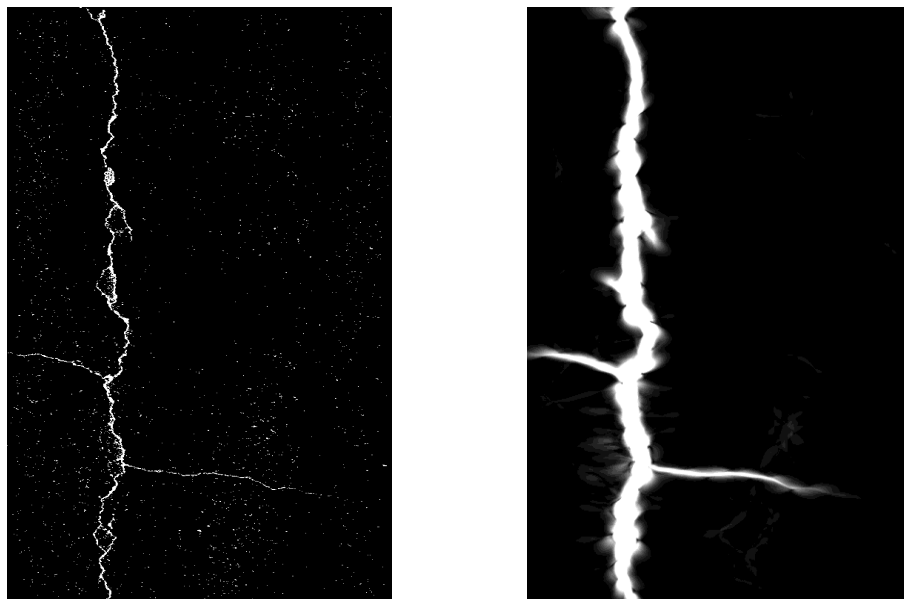
The tensor voting framework is then employed to enhance cracks in the pavement images. We use the potential crack pixels as the initial tokens and want to incorporate perceptual cues of proximity and continuity to enhance the curves. However, these crack pixels have no orientation. Therefore, we first apply a ball voting to estimate the crack-curve orientation at each crack pixel. More specifically, each detected crack pixel is initialized as a ball tensor with equal saliency and casts its votes to other crack pixels, i.e., non-crack pixels do not join this voting. After summing up the ball-voting fields from all the crack pixels, we find the principal direction at each crack pixel and set it as the orientation of the stick token at this crack pixel. We then apply stick voting by casting the votes from each stick token to all the pixels, including crack pixels and non-crack pixels. This dense stick voting will fill the gaps between the detected crack pixels to form longer crack curves.

Figure B.3 presents a couple examples of how the tensor voting framework works on pavement images. The left side images show the inputs of the tensor voting process. They are simply scatter points across the image. They can be generated efficiently through local-based thresholding or edge detection processes. However, due to the noisy nature and low contrast nature of pavement images, these results appear to contain fair amount of isolated noises, and the crack curves appear to be disjointed and fragmental. The right side images show the outputs of the tensor voting process. The pixel value at each point indicates the saliency of a potential curve structure, i.e. the existence of cracks. It can be observed that the crack features have been enhanced through this process. Especially, it connects the disjointed inputs into continuous blobs, which creates the

possibility of preserving the topology of crack shapes. The detailed information about how to utilize these outputs for the development of an automatic crack detection algorithm can be found in CHAPTER 3.



(a) Transverse cracking



(b) Combination of longitudinal and transverse cracking

**Figure B.3 Examples of tensor voting on the pavement cracks (left: input; right: output)**

## **APPENDIX C. PROFILE-BASED CRACK WIDTH MEASUREMENT**

Width is an important characteristic of pavement surface cracks. It is used by many federal and state transportation agencies to determine crack severity, such as in the LTPP protocol, the GDOT PACES protocol, and the FDOT flexible pavement survey protocol. Also, crack width information is usually used to determine the proper maintenance treatment, including estimating the optimal amount of sealant for crack sealing tasks. There is a need to automatically collect crack width information and detect the crack maps in order to support subsequent crack condition analysis and maintenance operations. In this study, a heuristic-based crack width measurement method is proposed; it requires the detected crack maps as a prerequisite, but it doesn't require any specific crack detection algorithm. This appendix is organized as follows. Section C.1 presents the details of the proposed crack detection measurement method. It is difficult to validate the accuracy of crack width measurement because it is almost impossible to establish the ground truth crack width values in the roadway environment. In this section, we evaluate the proposed method using synthetic data and lab testing. Sections C.2 and C.3 present the experimental results.

### **C.1 Proposed Crack Width Measurement Method**

Figure C.1 provides an overview of the proposed crack width measurement method. It consists of four steps: 1) form the detected crack map into linear crack segments, 2) retrieve the range profile at each pixel along the crack, 3) measure the width



of downward peak from the range profile, and 4) adjust the pixel measurement into actual crack width. The following explains these four steps in detail.

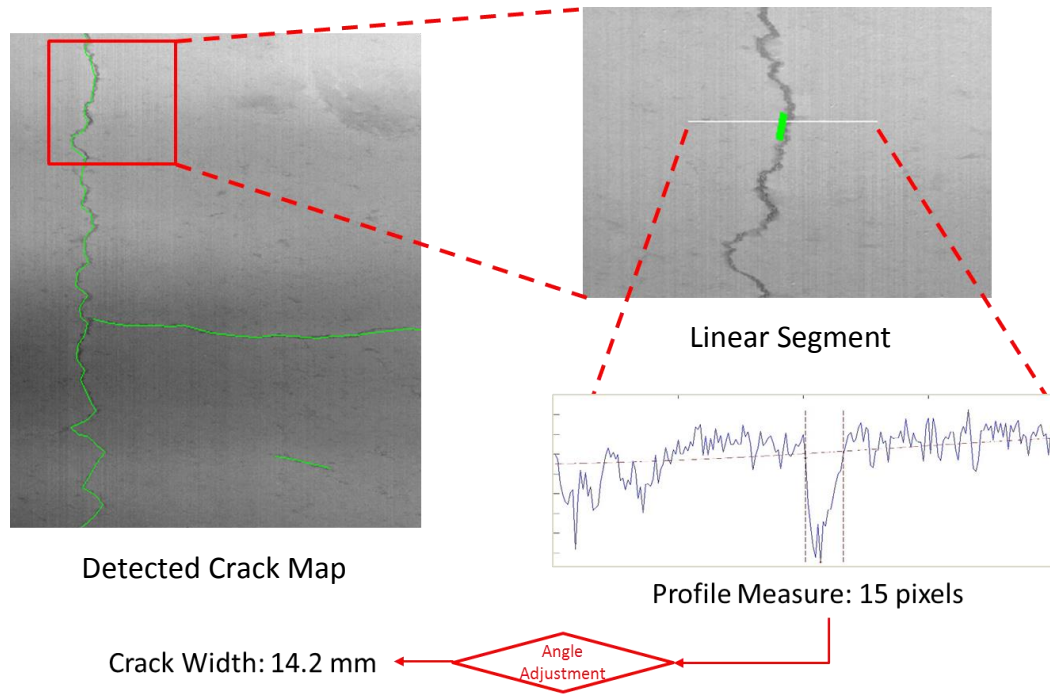


**Figure C.1 Illustration of the proposed crack width measurement method**

**Step 1: Form the detected crack map into linear crack segments**

Crack orientation needs to be known to calculate the actual crack width from the sensor data. In order to retrieve the orientation information at each point along a crack, the detected crack map is first decomposed into approximate linear crack segments. For the crack detection algorithms that produce continuous crack curves (e.g. the algorithm proposed in this study in Chapter 3), the process can be done easily. The most straightforward way is to split a crack curve into segments of equal length; a properly selected segment length will roughly create linear segments. A more complicated but accurate approach is to follow the top-down logic; we start from the entire crack curve and then split it into two segments at the point that reduces the variance the most. This process can be conducted recursively until all the segments meet a certain variance

requirement and are approximately linear. For the crack detection algorithms that produce disjointed results (like pixels or blobs), the Crack Fundamental Element model described in Section 5.2 can be used to form linear segments. Each linear segment is then assumed to have a uniform orientation that can easily be calculated.

**Step 2: Retrieve the range profile at each pixel along the crack**

The width calculation is not conducted directly on images, since the image format already loses certain information through the normalization process. Instead, we retrieve the original range profile based on the location of the crack pixels on the image. As explained previously, the range image is actually a stack of profiles; based on the Y location of each pixel, the corresponding range profile can be found. The blue line in Figure C.2 shows the original profile around the crack pixel, which is marked as the red star.

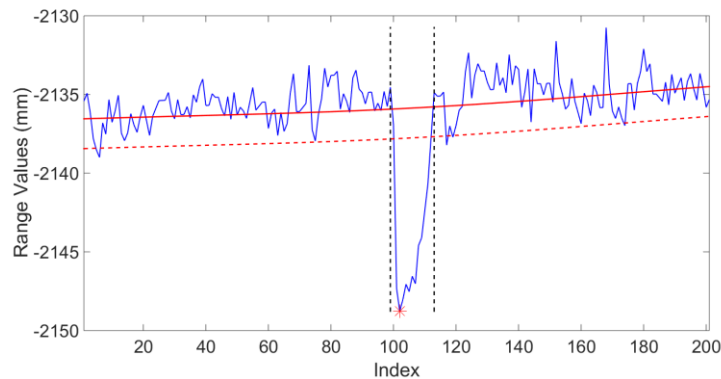


**Figure C.2 Example of measuring crack width from transverse profiles**

**Step 3: Measure the width of downward peak from the range profile**

On the original profile, the crack region appears to be a downward peak. The width of this peak corresponds to the crack width. The detected crack pixel falls into the bottom of the downward peak. In order to measure the crack width, we want to identify the two edges of the crack on the profile.

First of all, a profile smoothing process is applied in the same way as the one described in Section 3.3.2. In short, a Gaussian filter is used here as follows:

$$g(x) = \frac{1}{\sqrt{2\pi}\sigma} e^{-\frac{x^2}{2\sigma^2}} \quad (C.1)$$

The function of the Gaussian filter depends on the value of  $\sigma$ . A relatively large  $\sigma$  (in this case  $\sigma = 150$ ) is applied to smooth the entire profile and identify the cross-slope and rutting. The smoothed profile is shown as the red line in Figure C.2. It can be observed that the original range profile varies around the smoothed profile, the variance of which describes the pavement surface texture; cracks are extreme values on the profile.

Second, the standard deviation of the rectified profile is calculated by subtracting the smoothed profile from the original profile. We introduce a heuristic here, assuming that the threshold for normal pavement surface is twice this standard deviation below the smoothed profile. This threshold is shown as the red, dashed line in Figure C.2.

Finally, starting from the crack pixel, which is the bottom of the downward peak, we gradually expand two edges of the crack towards both sides. This expansion stops when the value on the original range profile goes above the threshold. For the example in Figure C.2, the two edges found are shown as black, dashed lines on both sides of the crack pixel. The gap D between the two edges corresponds to the width of the crack at this specific point.

#### **Step 4: Adjust the pixel measurement into actual crack width**

The gap measured from the profile is not exactly the actual crack width. The range profile is always collected along transverse direction, while crack orientations can be diverse. Therefore, the range profile doesn't necessarily go through the crack perpendicularly, as shown in Figure C.3. The actual crack width is calculated as follows:

$$width = D \times \sin \theta \quad (C.2)$$

where  $D$  is the gap measured on transverse profiles, and  $\theta$  is the crack orientation with respect to the transverse direction. When  $\theta$  equals to 90 degrees, i.e. the linear crack segment is perfectly longitudinal, the actual crack width equals to  $D$ .

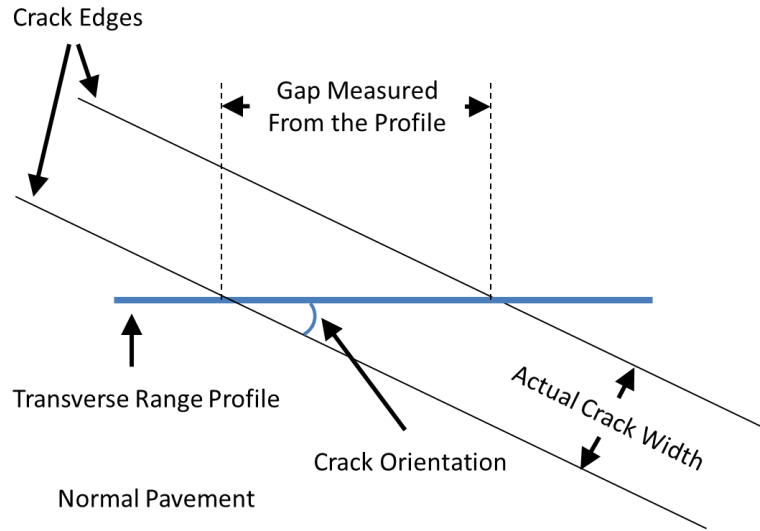


**Figure C.3 Illustration of angle adjustment**

Following this process, width can be measured at each crack pixel on the detected crack map. The information can then be aggregated and reported in proper format.

## **C.2 Validation on Synthetic Data**

Since it is very difficult to measure ground truth crack width in the field for validation purposes, this study first evaluates the proposed method using synthetic data.

The synthetic data are generated using the following procedure:

- Select a raw range image on clean pavement with no distress.
- Create a mask of this image. The majority of the mask remains black with a thin strip located in the middle. The width of this strip can be accurately controlled, and it indicates different crack widths.

- Spin the mask to a desired angle. This process simulates different crack orientations.
- Overlay the mask onto the raw range image by decreasing the range values within the strip area. The amplitude of the change indicates the crack depth. Here, this value is set to be consistently 8 mm.

In this study, synthetic images with different combinations of crack widths and orientations are generated. The crack width values include 2, 5, 10, and 20 mm. The crack orientations are selected at every 10 degrees ranging from 10 to 90 degrees. Figure C.4 shows some examples of the synthetic data.

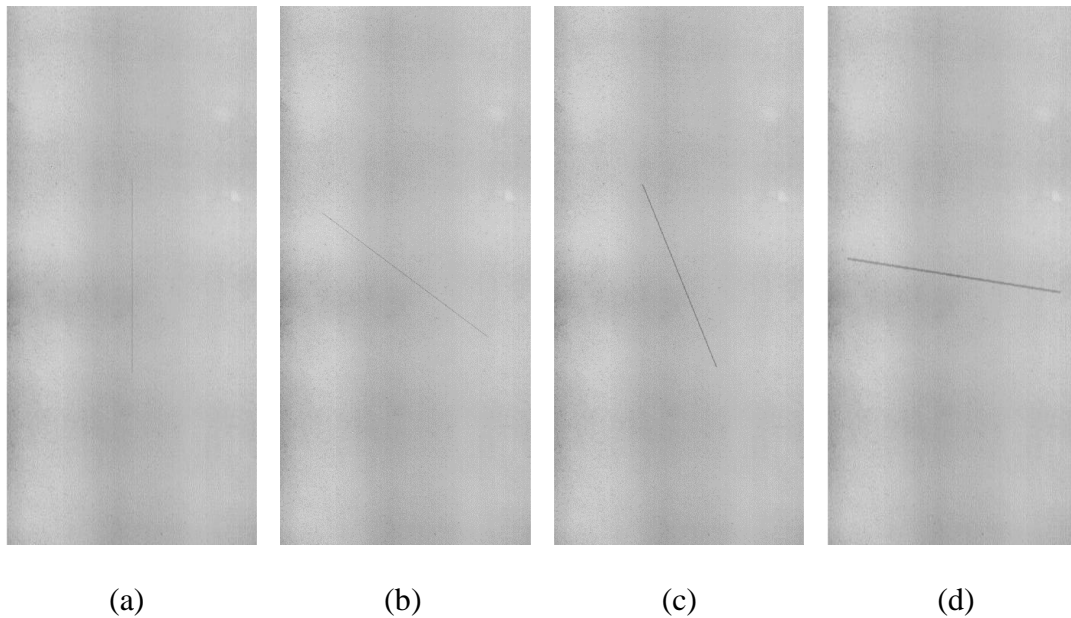


**Figure C.4 Examples of synthetic data, including different combinations of crack width and orientation: (a) 2 mm and 90 degrees, (b) 5 mm and 40 degrees, (c) 10 mm and 70 degrees, and (d) 20 mm and 10 degrees**

We then run the proposed crack detection algorithm and crack width measurement method to extract the crack map and the crack width information from the synthetic data. The crack width is measured at every pixel along the crack curve, and the

mean and standard deviations of these measurements are shown in Table C.1. First of all, we can see that at four different crack widths, the proposed algorithm's measurements are quite accurate, having a maximum offset of 0.7. Second, the measurements are slightly more accurate when the simulated cracks are wider; the measurements are more consistent at 20 mm than at 2 mm. Third, the measurements are more accurate when the simulated cracks are close to the longitudinal or transverse direction than the diagonal direction. This is possibly caused by the discretization error introduced through the image rotation. Although the simulated cracks are designed to be at certain angles, the process has to be done within the discrete domain. In the diagonal direction, the edges of the simulate cracks will be blurred after rotation, which makes it more difficult to consistently find the edges through the proposed method.

**Table C.1 Performance of crack width measurement on synthetic data (unit: mm)**

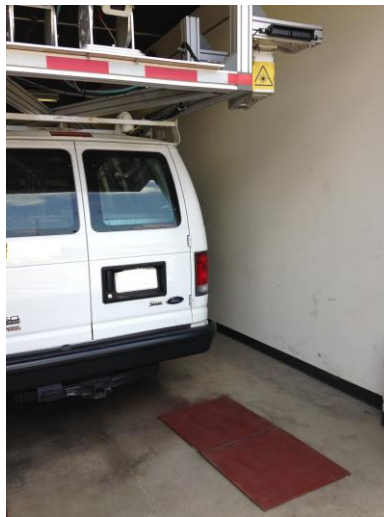
Crack Orientation	2 mm		5 mm		10 mm		20 mm	
	Mean	STD	Mean	STD	Mean	STD	Mean	STD
90 degrees	2.1	0.5	5.1	0.5	10.0	0.3	20.0	0.2
80 degrees	2.6	0.7	5.6	0.6	10.5	0.6	20.5	0.5
70 degrees	2.6	0.5	5.6	0.5	10.5	0.5	20.4	0.5
60 degrees	2.7	0.6	5.5	0.5	10.5	0.6	20.5	0.7
50 degrees	2.7	0.7	5.7	0.7	10.5	0.7	20.3	1.2
40 degrees	2.6	0.5	5.5	0.4	10.5	0.4	20.4	0.4
30 degrees	2.6	0.4	5.5	0.3	10.5	0.3	20.2	0.3
20 degrees	2.6	0.3	5.5	0.2	10.3	0.3	20.2	0.2
10 degrees	2.4	0.3	5.3	0.2	10.2	0.2	20.1	0.2

It is noted that the degree of 0 is not evaluated through this process. It is difficult to analyze cracks through transverse profiles when they are at exactly 0 degrees. Therefore, longitudinal profiles should be used to analyze the cracks close to the transverse direction, following the logic that is presented here.

### C.3 Validation through Lab Tests

Lab tests are conducted to further validate the proposed method. Figure C.5 demonstrates experimental setup. The objective is still to simulate different crack widths in a controlled environment. To simulate cracks, two steel plates are placed side by side with a thin gap between them. The vehicle travels over the plates and collects range data of the entire surface. By controlling the size of the gap, cracks with different widths are simulated. Figure C.6 shows an example of the collected range image. We set the gap to be in the transverse direction; since the sensors overhead are configured to have a certain angle in the transverse direction, the gap appears to be tilted in the collected range image.

The proposed crack width measurement method is then applied to the collected lab data. Four different crack widths are evaluated, including 2, 5, 10, and 20 mm. We measure the crack width at each point along the crack and present the mean values and standard deviations in Table C.2. The measurement accuracy is consistently good, having a maximum offset of only 1.1 mm.



(a) Overview of the setup



(b) Simulating different crack widths

**Figure C.5 Illustration of the experimental setup**

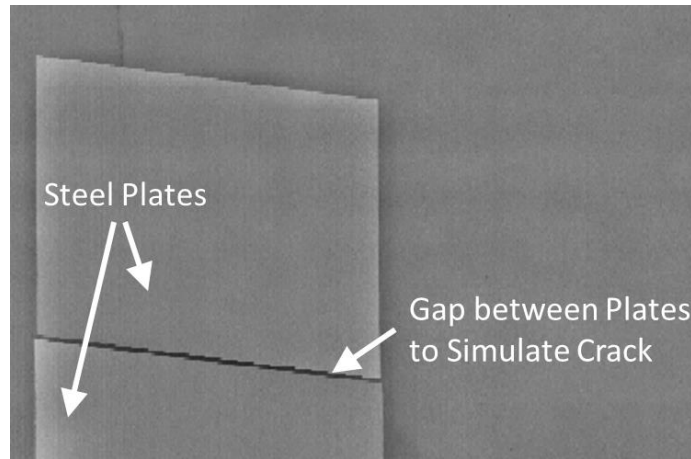


**Figure C.6 Example image of the collected lab data**

Based on the experimental results, the proposed crack width measurement method has demonstrated satisfactory performance. The extracted crack width information can be used to support the subsequent crack condition analysis. It is suggested that further validation of different orientation setups through lab tests be conducted. The proposed method utilizes 3D range data, but using similar logic, our procedures can be applied to 2D images, as well.

**Table C.2 Performance of crack width measurement in lab test**

<b>Crack Orientation</b>	<b>2 mm</b>		<b>5 mm</b>		<b>10 mm</b>		<b>20 mm</b>	
	Mean	STD	Mean	STD	Mean	STD	Mean	STD
90 degrees	2.0	0.6	5.0	0.8	10.0	0.8	20.4	0.6
60 degrees	2.4	0.4	5.2	0.4	10.8	0.3	21.1	0.5
30 degrees	1.8	0.3	5.3	0.4	10.1	0.4	20.5	0.3
0 degrees	1.9	0.4	5.2	0.4	10.0	0.5	19.5	0.1



## REFERENCES

- Adarkwa, O. A., and Attoh-Okine, N. (2013). "Pavement crack classification based on tensor factorization." *Constr. Build. Mater.*, 48, 853-857.
- Administration, F. H. (2015). "National Performance Management Measures; Assessing Pavement Condition for the National Highway Performance Program and Bridge Condition for the National Highway Performance Program." *Federal Register*, 80(2), 326 - 393.
- Ahmed, M. F., and Haas, C. (2010). "Potential of Low-Cost, Close-Range Photogrammetry Toward Unified Automatic Pavement Distress Surveying." *Transportation Research Board Annual Meeting*.
- Albitres, C. M. C., Smith, R. E., and Pendleton, O. J. (2007). "Comparison of automated pavement distress data collection procedures for local agencies in San Francisco Bay Area, California." *Transportation Research Record*(1990), 119-126.
- Alekseychuk, O. (2006). "Detection of crack-like indications in digital radiography by global optimisation of a probabilistic estimation function." *BAM-Dissertationsreihe*.
- American Association of State Highway and Transportation Officials (AASHTO) (2010). "Standard Practice for Quantifying Cracks in Asphalt Pavement Surfaces from Collected Images Utilizing Automated Methods." *AASHTO Provisional Standards PP67-10*, Washington, D.C.
- American Association of State Highway and Transportation Officials (AASHTO) (2013). "SCOPM Task Force Findings on MAP-21 Performance Measure Target-

Setting." AASHTO Standing Committee on Performance Management,  
Washington, D.C.

American Society of Civil Engineers (2013). "Report Card for America's Infrastructure."

American Society of Civil Engineers (ASCE), Reston, VA.

Amhaz, R., Chambon, S., Idier, J., and Baltazart, V. "A New Minimal Path Selection  
Algorithm for Automatic Crack Detection on Pavement Images." *Proc., the 21st  
IEEE International Conference on Image Processing*.

Avila, M., Begot, S., Duculty, F., and Nguyen, T. "2D Image Based Road Pavement  
Crack Detection by Calculating Minimal Path and Dynamic Programming."  
*Proc., the 21st IEEE International Conference on Image Processing*.

Ayenu-Prah, A., and Atttoh-Okine, N. (2008). "Evaluating Pavement Cracks with  
Bidimensional Empirical Mode Decomposition." *Journal on Advances in Signal  
Processing*, 2008.

Beauchemin, M., Thomson, K. P. B., and Edwards, G. (1998). "On the Hausdorff  
distance used for the evaluation of segmentation results." *Canadian Journal of  
Remote Sensing*, 24(1), 3-8.

Benmansour, F., and Cohen, L. D. (2009). "Fast object segmentation by growing minimal  
paths from a single point on 2D or 3D images." *Journal of Mathematical Imaging  
and Vision*, 33(2), 209 - 221.

Bray, J., Verma, B., Li, X., and He, W. (2006). "A neural network based technique for  
automatic classification of road cracks." *International Joint Conference on Neural  
Networks*, IEEE, 907-912.

- Canny, J. (1986). " A computational approach to edge detection." *IEEE Transactions on Pattern Analysis and Machine Intelligence* 8(6), 679 - 698
- Capuruç, R. A. C., Tighe, S. L., Ningyuan, L., and Kazmierowski, T. (2006).  
 "Performance evaluation of sensor- And image-based technologies for automated pavement condition surveys." *Transportation Research Record*(1968), 47-52.
- Cheng, H., Jiang, X., Li, J., and Glazier, C. (1999). "Automated Real-Time Pavement Distress Analysis." *Transportation Research Record:Journal of the Transportation Research Board*, 55-64.
- Cheng, H., Wang, J., Hu, Y., Glazier, C., Shi, X., and Chen, X. (2001). "Novel Approach to Pavement Cracking Detection Based on Neural Network." *Transportation Research Record:Journal of the Transportation Research Board*, 119-127.
- Cheng, H. D., Chen, J.-R., Glazier, C., and Hu, Y. G. (1999). "Novel approach to pavement cracking detection based on fuzzy set theory." *Journal of Computing in Civil Engineering*, 13(4), 270-280.
- Cheng, H. D., and Miyojim, M. (1998). "Automatic pavement distress detection system." *Information sciences*, 108(1-4), 219-240.
- Cheng, H. D., Shi, X. J., and Glazier, C. (2003). "Real-Time Image Thresholding Based on Sample Space Reduction and Interpolation Approach." *Journal of Computing in Civil Engineering*, 17(4), 264-272.
- Cohen, L. D., and Kimmel, R. (1997). "Global minimum for active contour models: a minimal path approach." *International Journal of Computer Vision*, 24(1), 57-78.

- Cuhadar, A., Shalaby, K., and Tasdoken, S. "Automatic segmentation of pavement condition data using wavelet transform." *Proc., IEEE Canadian Conference on Electrical and Computer Engineering*, 1009-1014 vol.1002.
- Davis, E. R. (2005). *Machine Vision: theory, algorithms, practicalities*, Morgan Hanfmann Publishers, CA, USA.
- Dijkstra, E. W. (1959). "A note on two problems in connection with graphs." *Numerische Mathematic*, 1, 269 - 271.
- El-Korchi, T., Gennert, M. A., Ward, M. O., and Wittels, N. (1991). "Lighting design for automated pavement surface distress evaluation." *Transportation Research Record:Journal of the Transportation Research Board*, 144-148.
- Federal Highway Administration (FHWA) (2013). "Highway Performance Monitoring System Field Manual." Federal Highway Administration (FHWA).
- Federal Highway Administration (FHWA) (2015). "National Performance Management Measures; Assessing Pavement Condition for the National Highway Performance Program and Bridge Condition for the National Highway Performance Program." *Federal Register*, 80(2), 326 - 393.
- Fu, P., Harvey, J. T., Lee, J. N., and Vacura, P. (2011). "New Method for Classifying and Quantifying Cracking of Flexible Pavements in Automated Pavement Condition Survey." *Transportation Research Record: Journal of the Transportation Research Board*(2225), 99-108.
- Georgia Department of Transportation (GDOT) (2007). "Pavement Condition Evaluaiton System." GDOT Office of Maintenance, Atlanta, GA.

- Georgopoulos, A., Loizos, A., and Flouda, A. (1995). "Digital image processing as a tool for pavement distress evaluation." *ISPRS Journal of Photogrammetry and Remote Sensing*, 50(1), 23.
- Goodman, S. N. (2001). "Assessing Variability of Surface Distress Surveys in Canadian Long-Term Pavement Performance Program." *Transportation Research Record: Journal of the Transportation Research Board*(1764), 112-118.
- Guo, S., and Fei, B. "A minimal path searching approach for active shape model (ASM)-based segmentation of the lung." *Proc., the SPIE - The International Society for Optical Engineering*, 4B 1 - 8.
- Haas, C. (1996). "Evolution of an automated crack sealer: a study in construction technology development." *Automation in Construction*, 4(4), 293-305.
- Haas, C., and Hendrickson, C. (1990). "Computer-based Model of Pavement Surfaces." *Transportation Research Record*(1260), 91-98.
- Hassani, A., and Tehrani, H. G. "Crack detection and classification in asphalt pavement using image processing." *Proc., RILEM International Conference on Cracking in Pavements*, 891-896.
- Hou, Z., Wang, K. C. P., and Gong, W. "Experimentation of 3D pavement imaging through stereovision." *Proc., International Conference on Transportation Engineering*, American Society of Civil Engineers, Reston, VA 20191-4400, United States, 376-381.
- Huang, J., Liu, W., and Sun, X. (2014). "A Pavement Crack Detection Method Combining 2D with 3D Information Based on Dempster-Shafer Theory." *Computer-Aided Civil & Infrastructure Engineering*, 29(4), 299 - 313.

- Huang, Y., and Tsai, Y. (2011). "Enhanced pavement distress segmentation algorithm using dynamic programming and connected component analysis." *Transportation Research Record: Journal of the Transportation Research Board*(2973), 89-98.
- Huang, Y., and Xu, B. (2006). "Automatic inspection of pavement cracking distress." *Journal of Electronic Imaging*, 15(1), 013017-013016.
- Jahanshahi, M., Jazizadeh, F., Masri, S., and Becerik-Gerber, B. (2013). "Unsupervised Approach for Autonomous Pavement-Defect Detection and Quantification Using an Inexpensive Depth Sensor." *Journal of Computing in Civil Engineering*, 27(6), 743 - 754.
- Jiang, C., and Tsai, Y. (2013). "Enhanced Crack Segmentation Algorithm Using Three-Dimensional Pavement Data." *Transportation Research Board Annual Meeting*, National Academy of Science, Washington, D.C.
- Kass, M., Witkin, A., and Terzopoulos, D. (1988). "Snakes: active contour models." *International Journal of Computer Vision*, 1(4), 321 - 331.
- Kaul, V., Tsai, Y., and Mersereau, R. (2009). "A Quantitative Performance Evaluation of Pavement Distress Segmentation Algorithms." *Transportation Research Record: Journal of the Transportation Research Board*(2153), 106-113.
- Kaul, V., Yezzi, A., and Tsai, Y. (2012). "Detecting Curves with Unknown Endpoints and Arbitrary Topology Using Minimal Paths." *IEEE Transactions on Pattern Analysis and Machine Intelligence*, 34(10), 1952 - 1965.
- Kerekes, J. (2008). "Receiver operating characteristic curve confidence intervals and regions." *IEEE Geoscience and Remote Sensing Letters*, 5(2), 251-255.

- Kim, Y.-S., and Haas, C. T. (2002). "A manmachine balanced rapid object model for automation of pavement crack sealing and maintenance." *Canadian Journal of Civil Engineering*, 29(3), 459-474.
- Kim, Y.-S., Haas, C. T., and Greer, R. (1998). "Path Planning for Machine Vision Assisted, Teleoperated Pavement Crack Sealer." *Journal of Transportation Engineering*, 124(2), 137-143.
- Kirschke, K. R., and Velinsky, S. A. (1992). "Histogram-Based Approach for Automated Pavement-Crack Sensing." *Journal of Transportation Engineering*, 118(5), 700-710.
- Koutsopoulos, H. N., and Downey, A. B. (1993). "Primitive-Based Classification of Pavement Cracking Images." *Journal of Transportation Engineering*, 119(3), 402-418.
- Koutsopoulos, H. N., El Sanhoury, I., and Downey, A. B. (1993). "Analysis of Segmentation Algorithms for Pavement Distress Images." *Journal of Transportation Engineering*, 119(6), 868-888.
- Laurent, J., Lefebvre, D., and Samson, E. (2008). "Development of a New 3D Transverse Laser Profiling System for the Automatic Measurement of Road Cracks." *SURF 2008*.
- Lee, B. J., and Lee, H. D. (2004). "Position-invariant neural network for digital pavement crack analysis." *Computer-Aided Civil and Infrastructure Engineering*, 19(2), 105-118.

- Lee, B. J., and Lee, H. D. (2010). "Improved Crack Type Classification Neural Network based on Square Sub-images of Pavement Surface." *Innovations in Computing Sciences and Software Engineering*, 607-610.
- Lee, H. "Standardization of distress measurements for the network-level pavement management system." Publ by ASTM, 424-436.
- Lee, H., and Kim, J. (2005). "Development of a crack type index." *Transportation Research Record: Journal of the Transportation Research Board*(1940), 99-109.
- Lee, H., and Kim, J. (2006). "Analysis of Error in Pavement Ground Truth Indicators for Evaluating the Accuracy of Automated Image Collection and Analysis System." *Journal of ASTM International*, 3(5).
- Lee, H., and Oshima, H. (1994). "New Crack-Imaging Procedure Using Spatial Autocorrelation Function." *Journal of Transportation Engineering*, 120(2), 206-228.
- Lettsome, C. A., Tsai, Y., and Kaul, V. (2012). "Enhanced adaptive filter-bank-based automated pavement crack detection and segmentation system." *Journal of Electronic Imaging*, 21(4).
- Li, K., and Fei, B. (2008). "A new 3D model-based minimal path segmentation method for kidney MR images." *2nd International Conference on Bioinformatics and Biomedical Engineering*, Shanghai, China, 2342 - 2344.
- Li, Q., Yao, M., Yao, X., and Xu, B. (2010). "A real-time 3D scanning system for pavement distortion inspection." *Measurement Science and Technology*, 21(1), 1-8.



- Li, Q., Zou, Q., and Liu, X. (2011). "Pavement Crack Classification via Spatial Distribution Features." *EURASIP Journal on Advances in Signal Processing*, 2011.
- Mallat, S., and Zhong, S. (1992). "Characterization of signals from multiscale edges." *Pattern Analysis and Machine Intelligence, IEEE Transactions on*, 14(7), 710-732.
- Medioni, G., Lee, M.-S., and Tang, C.-K. (2000). *A Computational Framework for Segmentation and Grouping*, Elsevier.
- Mordohai, P., and Medioni, G. (2006). *Tensor Voting: A Perceptual Organization Approach to Computer Vision and Machine Learning*, Morgan and Claypool Publishers.
- Nazef, A., Mraz, A., Gunaratne, M., and Choubane, B. (2006). "Experimental evaluation of a pavement imaging system: Florida Department of Transportation's multipurpose survey vehicle." *Transportation Research Record: Journal of the Transportation Research Board*, National Research Council, Washington, DC. , 97-106.
- Nejad, F. M., and Zakeri, H. (2011). "An optimum feature extraction method based on Wavelet-Radon Transform and Dynamic Neural Network for pavement distress classification." *Expert Syst. Appl.*, 38(8), 9442-9460.
- Nguyen, T., Begot, S., Duculty, F., and Avila, M. "Free-form Anisotropy: A New Method for Crack Detection on Pavement Surface Images." *Proc., the 18th IEEE International Conference on Image Processing*.

- Oh, H., Garrick, N. W., and Achenie, L. E. K. "Segmentation Algorithm Using Iterated Clipping for Processing Noisy Pavement Images." *Proc., Imaging Technologies: Techniques and Applications in Civil Engineering: Proceedings of the 2nd International Conference*, 138-147.
- Oliveira, H., and Correia, P. L. (2013). "Automatic Road Crack Detection and Characterization." *IEEE Trans. Intell. Transp. Syst.*, 14(1), 155-168.
- Ouyang, A. G., and Wang, Y. P. (2012). "Edge Detection In Pavement Crack Image With Beamlet Transform." *Proceedings of the 2nd International Conference on Electronic & Mechanical Engineering and Information Technology*, B. Wu, ed., Atlantis Press, Paris.
- Rada, G. R., Bhandari, R. K., Elkins, G. E., and Bellinger, W. Y. (1997). "Assessment of Long-Term Pavement Performance Program Manual Distress Data Variability: Bias and Precision." *Transportation Research Record: Journal of the Transportation Research Board*(1592), 151-168.
- Saar, T., and Talvik, O. "Automatic asphalt pavement crack detection and classification using neural networks." *Proc., Proceedings of the 12th Biennial Baltic Electronics Conference*, 345-348.
- Salari, E., and Bao, G. "Pavement distress detection and classification using feature mapping." *Proc., IEEE International Conference on Electro/Information Technology*.
- Salari, E., and Bao, G. (2011). "Pavement Distress Detection and Severity Analysis." *Image Processing: Machine Vision Applications Iv*, 7877.

- Santhi, B., KRISHNAMURTHY, G., SIDDHARTH, S., and RAMAKRISHNAN, P. K. (2012). "Automatic Detection of Cracks in Pavements Using Edge Detection Operator." *Journal of Theoretical and Applied Information Technology*, 36(2), 199-205.
- Sedgewick, R. (1988). *Algorithms*, Addison-Wesley.
- Sethian, J. A. (1999). "Fast marching methods." *SIAM Review*, 41(2), 199 - 235.
- Shashua, A., and Ullman, S. (1988). "Structural saliency: The detection of globally salient structures using a locally connected network." *International Conference on Computer Vision*, 321 - 327.
- Song, X., Pogue, B. W., Dehghani, H., Jiang, S., Paulsen, K. D., and Tosteson, T. D. (2007). "Receiver operating characteristic and location analysis of simulated near-infrared tomography images." *Journal of Biomedical Optics*, 12(5), 054013-054011.
- Su, Y. S., Kang, S. C., Chang, J. R., and Hsieh, S. H. (2013). "Dual-Light Inspection Method for Automatic Pavement Surveys." *Journal of Computing in Civil Engineering*, 27(5), 534-543.
- Sun, Y., Salari, E., and Chou, E. "Automated pavement distress detection using advanced image processing techniques." *Proc., Proceedings of 2009 IEEE International Conference on Electro/Information Technology*, 373-377.
- Tighe, S. L., Li, N., and Kazmierowski, T. (2008). "Evaluation of semiautomated and automated pavement distress collection for network-level pavement management." *Transportation Research Record: Journal of the Transportation Research Board*(2084), 11-17.

- Tsai, J., Kaul, V., and Mersereau, R. (2010). "Critical Assessment of Pavement Distress Segmentation Methods." *ASCE Journal of Transportation Engineering* 136, 11-19.
- Tsai, Y., Jiang, C., and Huang, Y. (2014). "Multiscale Crack Fundamental Element Model for Real-World Pavement Crack Classification." *Journal of Computing in Civil Engineering*, 28(4).
- Tsai, Y., Jiang, C., and Wang, Z. "Implementation of Automatic Crack Evaluation Using Crack Fundamental Element." *Proc., the 2014 IEEE International Conference on Image Processing (ICIP)*, 773 - 777.
- Tsai, Y., Kaul, V., and Yezzi, A. (2013). "Automating the crack map detection process for machine operated crack sealer." *Automation in Construction*, 31, 10-18.
- Tsai, Y., and Li, F. (2012). "Critical Assessment of Detecting Asphalt Pavement Cracks under Different Lighting and Low Intensity Contrast Conditions Using Emerging 3D Laser Technology." *J. Transp. Eng.-ASCE*, 138(5), 649-656.
- U.S. Army Corps of Engineers (1989). "Micro Paver User's Guide, Version 2.1." U.S. Army Corps of Engineers, Construction Engineering Research Laboratory.
- U.S. Department of Transportation Federal Highway Administration (2003). "Distress Identification Manual for the Long-Term Pavement Performance Program." *FHWA-RD-03-031*, Washington, D.C.
- Wang, H., Zhu, N., and Wang, Q. (2007). "Segmentation of pavement cracks using differential box-counting approach." *Journal of the Harbin Institute of Technology*, 39(1), 142-144.

- Wang, K. C. P. (2000). "Designs and Implementations of Automated Systems for Pavement Surface Distress Survey." *Journal of Infrastructure Systems*, 6(1), 24-32.
- Wang, K. C. P. (2011). "Automated Pavement Surface Imaging Model 4096 (APSI-4096)." *WayLink System Corporation*.
- Wang, K. C. P., and Gong, W. "Real-time automated survey of pavement surface distress." *Proc., Proceedings of the International Conference on Applications of Advanced Technologies in Transportation Engineering*, American Society of Civil Engineers, 465-472.
- Wang, K. C. P., and Gong, W. (2005). "Real-time automated survey system of pavement cracking in parallel environment." *Journal of Infrastructure Systems*, 11(3), 154-164.
- Wang, K. C. P., Li, Q., and Gong, W. (2007). "Wavelet-based pavement distress image edge detection with a trous algorithm." *Transportation Research Record*(2024), 73-81.
- Wang, Y. (2002). "Image matching based on robust Hausdorff distance." *Journal of Computer Aided Design & Computer Graphics*, 14(3), 238-241.
- Xu, B. (2005). "Artificial Lighting for the Automated Pavement Distress Rating System." The University of Texas at Austin, Austin, Texas.
- Yan, P., and Kassim, A. A. (2006). "Medical image segmentation using minimal path deformable models with implicit shape priors." *IEEE Transactions on Information Technology in Biomedicine*, 10(4), 677 - 684.

- Yao, M., Zhao, Z., Yao, X., and Xu, B. (2015). "Fusing complementary images for pavement cracking measurements." *Measurement Science and Technology*, 26(2), 025005.
- Ying, L., and Salari, E. (2010). "Beamlet Transform-Based Technique for Pavement Crack Detection and Classification." *Computer-Aided Civil and Infrastructure Engineering*, 25(8), 572-580.
- Zalama, E., Gomez-Garcia-Bermejo, J., Medina, R., and Llamas, J. (2014). "Road Crack Detection Using Visual Features Extracted by Gabor Filters." *Computer-Aided Civil & Infrastructure Engineering*, 29(5), 342 - 358.
- Zhang, A., Li, Q., Wang, K. C. P., and Qiu, S. (2013). "Matched Filtering Algorithm for Pavement Cracking Detection." *Transportation Research Record*(2367), 30-42.
- Zhou, J., Huang, P., and Chiang, F.-P. (2005). "Wavelet-based pavement distress classification." *Transportation Research Record*(1940), 89-98.
- Zhou, J., Huang, P. S., and Chiang, F.-P. (2006). "Wavelet-based pavement distress detection and evaluation." *Optical Engineering*, 45(2).
- Zou, Q., Cao, Y., Li, Q. Q., Mao, Q. Z., and Wang, S. (2012). "Crack Tree: Automatic crack detection from pavement images." *Pattern Recognit. Lett.*, 33(3), 227-238.